CA'FOSCARI UNIVERSITY

DEPARTMENT OF MOLECULAR SCIENCES AND NANOSYSTEMS

Master Degree in Science and Technology of Bio and Nanomaterials (LM53)

Università Ca'Foscari Venezia

Swansea University Prifysgol Abertawe

RESEARCH THESIS

Pluronic copolymer nanoparticles as an exemplar for Epidrug delivery in Endometrial Cancer

Graduant: **Veronica Feltracco**

Supervisor: Prof./Doct **Patrizia Canton**

Co-supervisor: Prof./Doct **Lewis Francis**

ANNO ACCADEMICO: 2018/2019

SUMMARY

Endometrial Cancer (EC) is the fifth most common cancer in women, affecting 318,000 women per year globally (Morice et al. 2015). There is, therefore, the need for new improved therapeutic approaches. Aberrant epigenetic mechanisms that lead to chromatin modification and gene in/activation represent important features for cancer cells.

Epigenetic drugs offer a therapeutic possibility of reversing the cancer cell phenotype, using inhibiting enzymes to induce molecular scale alterations which in turn lead to cancer cell differentiation toward a normal phenotype or apoptosis. Saha, suberoylanilide hydroxamic acid (SAHA), is an epidrug which belongs to the histone deacetylase (HDAC) inhibitor class, which is already being used in the clinic for selected cancer types (Sharfstein et al. 2011).

The Reproductive Biology and Gynaecological Oncology (RBGO) Research Group in Swansea is a multidisciplinary team focused on female infertility and uterine cancer, translating fundamental research to patient benefit through novel diagnostic and therapeutic mechanisms. An established research project has tested and optimized the efficacy of SAHA enabled HDAC inhibition in Type I and Type II Endometrial Cancer Cell Models. Together with the differential expression levels of proteins involved in cell cycle regulation and apoptosis, the molecular mechanism of action signatures has been shown to correlate with cellular phenotype mapping suggestive of increased therapeutic index. The targeted delivery mechanism is continuously being explored, to increase specific tumor tissue delivery.

This project focuses on the study of a polymer nanoparticle (NP) approach using polymeric block copolymers, to encapsulate an epigenetic drug for EC treatment. Following successful encapsulation of the SAHA epidrug in specific delivery vectors, a full analysis of associated improvements in therapeutic efficacy was assessed using an in vitro model of type I and II EC cell lines. Thanks to their bioavailability and biodegradability characteristics, pluronic block copolymers were chosen as polymers vesicles (Howard et al. 2016; Prabhu et al. 2015). Two nanoparticle formulations were used, one made with Pluronic F127, the other one made with HA-SH and Pluronic S-S pyridyl kindly provided by Swedish collaborators in Uppsala. Following fabrication, the nanoparticles were characterized for size distribution, surface zeta-potential, shape, and encapsulation efficiency. Cell cytotoxicity studies were performed on Type I (Ishikawa) and Type II (Hec50) EC cell lines using empty and encapsulated nanoparticles at increasing concentrations and time-points, and the

results compared with the free drug formulations. To assess the mechanisms of action of the encapsulated SAHA and its effect on apoptosis, cell-cycle and phenotype, Western Blot experiments were performed. The results helped in the understanding of the drug influence on cellular phenotype and differentiation mechanisms.

Using a multidisciplinary approach, a comprehensive analysis of epidrug delivery methods on cell tumor models was conducted, by driving early research progress toward new better therapeutic results. The project will directly influence the development of therapeutics for Uterine Cancers within Swansea University laboratories, with all collaborative partners.

RIASSUNTO

Il tumore all'endometrio (EC) è il quinto tumore più comune nelle donne, colpendo globalmente 318.000 donne all'anno (Morice et al., 2015). Risulta quindi necessario trovare nuovi e migliori approcci terapeutici. I meccanismi epigenetici aberranti che portano alla modificazione della cromatina e all'attivazione del gene rappresentano importanti caratteristiche per le cellule tumorali. Sono stati sviluppati dei farmaci epigenetici che offrono la possibilità di invertire gli effetti causati dalle aberrazioni epigenetiche, facendo uso di molecole inibenti che inducono il differenziamento o l'apoptosi delle cellule tumorali. SAHA, acido idrossamico suberoilanilide (SAHA), è un farmaco epiqgenetico appartenente alla classe degli inibitori dell'istone deacetilasi (HDAC), che è già in uso nella clinica per diversi tipi di cancro (Sharfstein et al. 2011a).

Il gruppo di ricerca sulla biologia riproduttiva e la ginecologia oncologica (RBGO) di Swansea è un gruppo multidisciplinare incentrato sull'infertilità femminile e sul cancro uterino, con l'obiettivo di tradurre la ricerca di base in un concreto beneficio per il paziente attraverso nuovi meccanismi diagnostici e terapeutici. I ricercatori di questo gruppo hanno già testato l'efficacia di SAHA nell'indurre inibizione delle HDACs in modelli di cellule tumorali endometriali di tipo I e tipo II. Hanno inoltre valutato il suo effetto nell'alterare i livelli di espressione proteica coinvolti nella regolazione del ciclo cellulare e dell'apoptosi, che correlano con un aumento dell'indice terapeutico. Il meccanismo di distribuzione mirata del farmaco rimane sotto studio con l'obiettivo di aumentare la consegna specifica del tessuto tumorale.

Questo progetto si concentra sullo studio di un approccio di nanoparticelle polimeriche (NP) usando copolimeri a blocchi polimerici, per incapsulare un farmaco epigenetico per il trattamento del tumore all'endometrio. In seguito al successo dell'incapsulamento dell'epidrug SAHA in specifici vettori di somministrazione, è stata eseguita un'analisi completa utilizzando un modello in vitro di due linee cellulari rappresentanti il tumore all'endometrio di tipi I e di tipo II. I copolimeri a blocchi pluronici sono stati scelti come vescicole polimeriche grazie alle loro caratteristiche di biodisponibilità e biodegradabilità (Howard et al. 2016;, Prabhu et al., 2015). Sono state utilizzate due formulazioni di nanoparticelle, una realizzata con Pluronic F127, l'altra realizzata con HA-SH e il Pluronic S-S piridile gentilmente forniti da collaboratori svedesi con sede ad Uppsala.

Dopo la fabbricazione, le nanoparticelle sono state caratterizzate per la loro dimensione, potenziale zeta superficiale, forma ed efficienza di incapsulamento. Gli studi di citotossicità cellulare sono stati condotti su linee cellulari di tipo I (Ishikawa) e di tipo II (Hec50) usando differenti concentrazioni e time-points di nanoparticelle vuote ed incapsulate col farmaco, che sono poi state comparate con il farmaco libero. Per valutare i meccanismi di azione del farmaco incapsulato e il suo effetto sull'apoptosi, ciclo cellulare e fenotipo, sono stati eseguiti esperimenti Western Blot, esperimenti di analisi proteica su cellule Ishikawa ed Hec50 trattate con nanoparticelle incapsulate per 48 ore a diverse concentrazioni.
I risultati ottenuti si sono rivelati utili nella comprensione dell'influenza del farmaco sui meccanismi cellulari fisiologici ed aberranti.

Utilizzando un approccio multidisciplinare, è stata condotta un'analisi complessiva del "drug delivery method" applicato a modelli cellulari tumorali portando i primi progressi della ricerca verso nuovi migliori risultati terapeutici. Il progetto influenzerà direttamente lo sviluppo di terapie per i tumori uterini nei laboratori dell'Università di Swansea, con tutti i partner collaborativi.

INDEX

1. INTRODUCTION

1.1 Solid tumor introduction

The Emperor of all maladies affects human lives of all ages. Cancer lives silently in our countries and there were 14.1 million new cancer cases, 8.2 million cancer deaths, and 32.6 million people living with cancer worldwide only in 2012 (Ferlay et al. 2015).

Cancer is a disease characterized by unregulated cell growth and the invasion and spread of cells from the site of origin to the other sites in the body. There are over 100 types of cancer, for this reason, cancer is well defined as a group of diseases. The classification depends on the tissue of origin. Carcinomas occur in epithelial cells, sarcomas in mesoderm cells (bone, muscles) and adenocarcinomas in glandular tissue (breast). The unregulated development of cell growth leads to the distinction between a benign tumour and a malignant tumour. The second one, as opposed to the first, metastasizes showing features of invasion. Cancer can be considered a genetic disease resulting in an alteration of the DNA sequence from point mutations to deletions and chromosomal translocations. Carcinogens, agents that cause cancer, alter the DNA sequence or cause mutations that represent a multi-step process in carcinogenesis. There is an increased risk of cancer with age explained by the accumulation of mutations that lead cancer to become more present in human life over the centuries. These mutations are transmitted to daughter cells after the cellular division, thus they cannot be passed on to the next generation of offspring. Only germline mutations, alteration in the DNA of sperm or egg cells, can be inherited. Cancer is in fact defined as a genetic disease at the cellular level. Moreover, is worth noting that germline mutations usually cannot cause cancer immediately but represents an increased risk of developing the disease. It's important to underline that cells are ever-changing for the adaptation to the environment resulting in genetic mutations that occur mainly for the cell's defence mechanisms. Some factors with an important role in carcinogenesis are diet, reproductive life, smoking and environment with epigenetic phenomena (discussed later). Cell division (cell proliferation), apoptosis and differentiation regulate cell growth and the cell number. They can be affected by an oncogene, a gene mutated that produces a higher quantity of protein causing a tumour formation or by the loss of function of tumour suppressor genes that inhibit tumour formation. (Gilbert, 2000) (Peto, 2001).

1.1.1 Gynecological cancer

Gynecological cancers are five and involve cervix, uterus, ovaries, vagina and vulva. These malignancies are responsible for almost half a million deaths annually. The gynecological cancer impact is alarming and new treatments are required to improve patients outcomes. Thanks to nanomedicine, it will be possible to swing statistics in favor of survival women by improving cancers treatments (Howard et al. 2016).

Human papilloma virus (HPV) is responsible for cervical cancer that results the fourth most common cancer among women globally. Routine screening is needed for early detection and

cervical cancer is preventable by immunization against HPV. Also vaginal and vulvar cancers can be attributed to HPV, not always, and fortunately they are more rare than cervical cancer (Howard et al. 2016). Ovarian cancer symptoms are often non-specific, for this reason this disease is called "silent killer". Over 70% of cases are diagnosed at an advanced stage (Gajjar et al. 2012). It is classified as the seventh most common cancer-related death and the eight most common type of cancer in the world (Jemal et al. 2011).
Among the gynecological cancers, ovarian cancer is one of the biggest killer, only 25% of late stage patients survive the 5-year (Ferlay et al. 2015). Endometrial cancer, or uterine, is the fifth most commonly diagnosed cancer in the developed world and the most prevalent gynaecological cancer among women (Morice et al. 2015). This disease is fortunately diagnosed at early stage and can have a good prognosis (Howlader et al. 2011).

1.2 Endometrial Cancer

Endometrial cancer (EC) is the most common gynecological malignancy in Europe and North America (Murali et al. 2014). It is traditionally classified in type I (estrogen-dependent) and type II (estrogen independent) and is responsible for about 6% of new cancer cases and 3% of cancer death per year (Cancer Research UK. 2014). Around 75% of women with endometrial cancer are diagnosed in the early stages (stages I or II), and 5-year overall survival is 74–91%. Has been reported that for patients at late stage disease (stage III or IV), 5-year overall survival is respectively, of 57–66% and 20–26% (Murali et al. 2014). The American Cancer Society estimates 47,130 new cases and 8,010 deaths only in 2012 (Sorosky, 2012).

Endometrial cancer has increased 21% in incidence since 2008, and the death rate has increased more than 100% over the past two decades. The mean age for endometrial adenocarcinoma is 61 years, with most cases diagnosed in women between the ages of 50 and 60 years. 90% of cases occur in women older than 50 years and approximately 20% of women have diagnoses before menopause and approximately 5% of women will have development of disease before age 40 years. Moreover, approximately 72% of endometrial cancers are stage I, 12% are stage II, 13% are stage III, and 3% are stage IV (Sorosky, 2012).

EC begins in the uterus, in the layer of cells that form the lining of the uterus (endometrium). Signs and symptoms of endometrial cancer may include vaginal bleeding after menopause, bleeding between periods, an abnormal, watery or blood-tinged discharge from the vagina and pelvic pain (Clinic, 2018). Endometrial cancer occurs after a genetic mutation turning healthy cells into abnormal cells that grow and multiply out of control and a tumor mass is formed. Subsequently, cells invade nearby tissues and can metastasize, spread in the biological environment of the body (Clinic, 2018). EC is composed of four stages. In stage I, there is the disease only in the uterus and this stage can be subdivided into stages IA and IB, depending on how far cancer has spread. In stage IA, cancer is in the endometrium only or less than halfway through the myometrium (muscle layer of the uterus), in stage IB, cancer has spread into the myometrium as it is shown in the figure below. Subsequently, in stage II, EC has reached the connective tissue of the cervix, continuing in stage III,

beyond the uterus and cervix. More precisely, in stages IIIA, cancer has spread to the outer layer of the uterus and/or to the fallopian tubes, ovaries, and ligaments of the uterus, while in stage IIIB, it has reached the vagina and/or to the parametrium (connective tissue and fat around the uterus), and

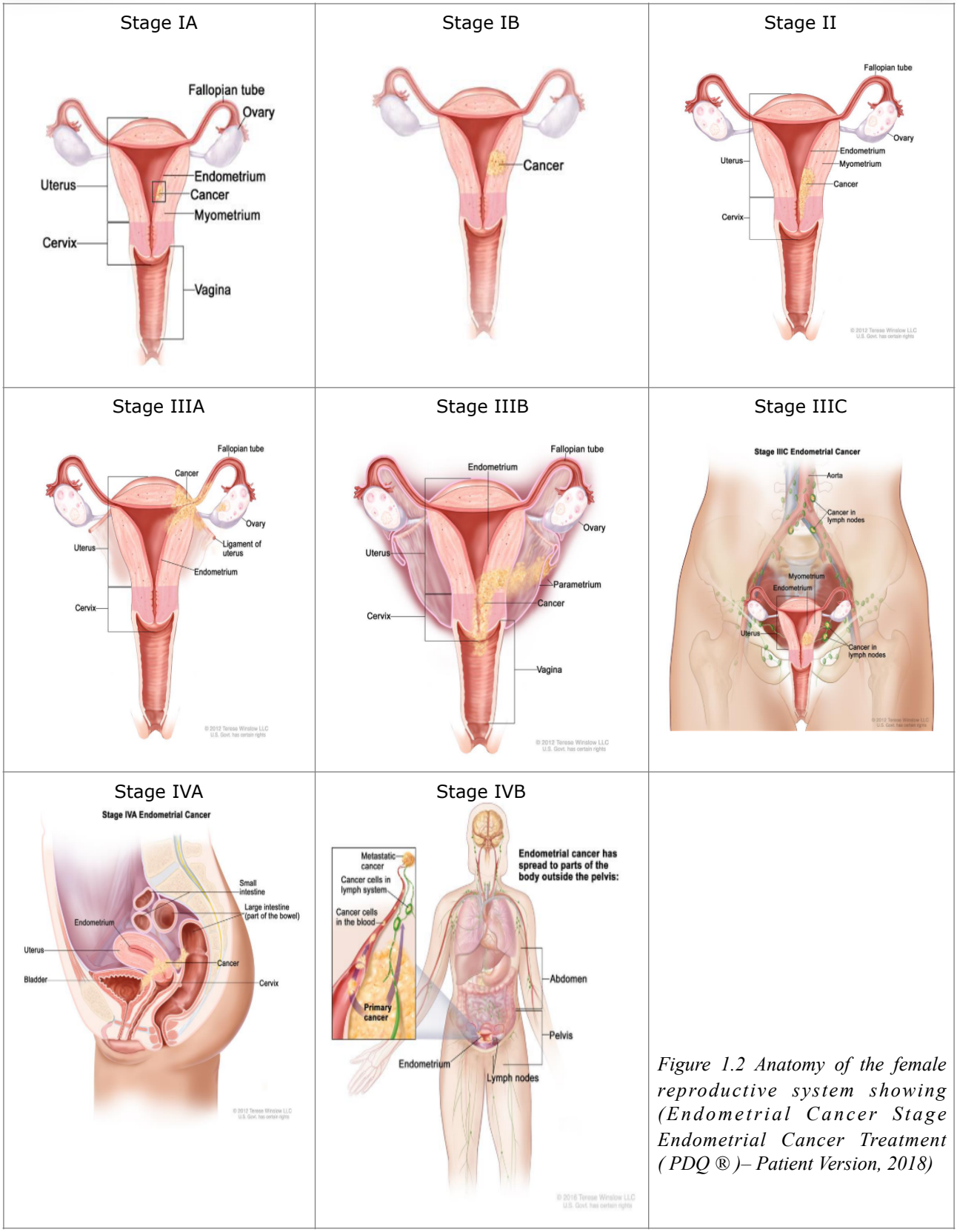

Figure 1.2 Anatomy of the female reproductive system showing (Endometrial Cancer Stage Endometrial Cancer Treatment (PDQ ®)– Patient Version, 2018)

then in stage IIIC, the disease arrives at lymph nodes in the pelvis and/or around the aorta (the largest artery in the body, which carries blood away from the heart). In the last stage (IV), cancer is

located beyond the pelvis, in stage IVA, in the bladder and/or bowel wall and, in stage IVB, the disease has spread to other parts of the body beyond the pelvis, including the abdomen and lymph nodes in the groin (NHI National Cancer Institute. 2018). The cancer can spread and form a tumor in another part of the body (metastasis) through the lymph system or the blood, traveling through the lymph vessels or the blood vessels.

EC can have a familial association or can be associated to the Lynch syndrome, hereditary non polyposis colorectal cancer (Sorosky, 2012). Different studies show that EC development is strongly correlated to lifestyle and excess weight, the major risk factors that cause up to half of all endometrial cancer cases worldwide (Cust et al. 2007). The biologic mechanism through which endometrial cancer occurs is still under investigation as there are always new factors that contribute to the change of cells life behavior.

1.2.1 Sub-types ECs: Type I vs Type II

Endometrial cancer has commonly been classified into two types, type I and type II, based on clinical, metabolic, and endocrine characteristics (Bokhman, 1983). EC classification is summarized in *Table 1.2.1*. Type I tumor is associated with estrogen excess, hormone-receptor positivity, and endometrial hyperplasia and occurs most frequently in younger, obese, or peri-menopausal women. It has favorable outcomes differently from Type II EC that has less favorable outcomes. Type II tumors usually occur in non-obese women and in the absence of endocrine and metabolic disturbances. They are poorly differentiated contrary to Type I tumors and it represents high-grade tumor differently from Type I EC (Murali et al. 2014). Type I EC is an endometrioid, low grade, HR (Hormone Receptor) positive carcinoma. It is originated by a typical sequence of hyperplastic changes of the endometrium and is followed by endometrial hyperplasia. Type II EC, a high grade, is HR-negative and is non-endometrioid carcinoma, with a poor survival rate (Morice et al. 2015). It occurs in the atrophic endometrium of elderly women and once diagnosed it appears with myometrial invasion and metastases. Studies explain that the starting molecular event for the development of Type II tumor is a mutation of p53 leading to an aggressive metastatic (Gründker et al. 2008).

	Type I	Type II
Associated clinical features	Metabolic syndrome: obesity, hyperlipidemia, and increased estrogen concentrations	None
Grade	Low	High
Hormone receptor expression	Positive	Negative
Histology	Endometriod	Non-endometrioid (serous, clear-cell carcinoma)
p53 mutation	No	Yes
Prognosis	Good (overall survival 85% at 5 years)	Poor (overall survival 55% at 5 years)

Table 1.2.1 Dualistic classification of endometrial cancers, by Bokhman subtype (Murali et al.2014).

Type I and II ECs present typical patterns of genetic modification and morphological differences. Inactivation of PTEN characterized Type I EC (Risinger et al. 1997) followed by mutation of K-ras

(Mutter et al. 1999), b-catenin genes (Fukuchi et al. 1998). Genetic changes present in type II ECs are mutations in the p-53 gene, it's the most common genetic defect (Gründker et al. 2008). Loss of E-cadherin expression and HER-2/erb-B2 gene mutations have also been shown to be present at differing rates and should determine the transition from the epithelial to the mesenchymal phenotype observed in malignant cells (Morice et al. 2015).

Endometrial cancer comprises a range of diseases with specific genetic and molecular characteristics and other analyses focusing on the diseases's heterogeneity are identifying new distinct molecular subgroups (Body et al. 2016). This is crucial to improve the prognostic value and the clinical decision-making algorithms.

1.2.2 Aetiology and Risks Factors

Endometrial cancer (EC) is the fifth most common cancer in women in developed countries, accounting for 4.8% of new cancers and 2.1% of cancer deaths. The highest incidence rates in 2012 were estimated to be 19.1 and 15.6 per 100,000 in North America and Western Europe respectively, attributed to the greater overall prevalence of obesity and metabolic syndromes in these regions (Clark et al. 2016, Colombo et al. 2016). Established non-genetic risk factors for EC include age and exposure to exogenous estrogens, or endogenous estrogens associated with, early age at menarche, late-onset menopause and obesity (Rauh-Hain et al. 2015). On the other hand, a role for genetic factors in EC susceptibility is supported by the fact that a family history of EC is associated with a ~2–3-fold increased risk of EC (Troung et al.2005).
Therefore, many factors predispose women to EC such as: obesity, inactivity, being over 50 (post-menopausal), use of hormone replacement, a history of polycystic ovaries, early menarche, late menopause, diabetes, endometriosis and a family history of colo cancer (Booth et a. 2012). The development of the EC is strongly linked to lifestyle factors and excess weight is one of the major risk (Kaaks et al. 2002). Therefor, the biologic mechanism through which obesity occurs, increases risk of developing EC. In fact, insulin resistance, hyperinsulina and diabetes are implicated in the etiology of EC (Fader et al. 2009). Moreover, the administration of estrogen for replacing therapies to alleviate the symptoms of menopause predispose women to developing the cancer. The increase of the levels of bioavailable of estrogens and the reduction of the progesterone levels, lead to increased mitotic activity of endometrial cells (Altman et al, 2015). Interestingly, use of Tamoxifen, a selective oestrogen receptor modulator prescribed for breast cancer, has also been associated with EC by increasing the risk of developing EC by 6 to 8-fold. It can bind to the estrogen receptor in the endometrial lining, promoting an opposite effect leading to an uncontrolled cell proliferation and in breast cancer, inhibits the proliferation of the cells (Amant et al. 2005; Beral et al, 2003).

1.2.3 Diagnosis and Treatments

Endometrial cancer prognosis depends largely on the stage of the disease at the time of diagnosis (Michail & Michael 2015). Although EC commonly occurs after the age of 50, thus is conventionally thought to be a cancer of the postmenopausal period, a percentage of sick women is in premenopausal and is younger than 40 years (Body et al. 2016). Current diagnosis and treatment of EC are being challenged by a desire to maintain fertility with younger patients. Studies that evaluate the frequency of diagnosing, state that other epidemiological factors could be older age, higher mean BMI (body mass index), late menopausal status, prolonged bleeding, and multiple

episodes of PMB (postmenopausal bleeding) (Salman et al. 2013). In Salman et al. study, has been investigated that 23% of women with recurrent bleeding had EC, instead, only 1.4% of women with single bleeding episode had a final diagnosis of EC (Michail & Michael 2015). Preoperative staging has the role to establish cervical invasion and lymph node metastasis of EC in order to define the surgical management. The best imaging technique used in preoperative staging is MRI (magnetic resonance imaging), as is has a high inter-observer concordance. Transvaginal ultrasonography can be used to diagnose myometrial and cervical invasion but is unable to determine lymph node status (Body et al. 2016). In general, the detection of lymph node and metastases represents an important limitation of the imaging technique. F-fluorodeoxyglucose PET-CT has high accuracy. Moreover, PET/MRI are examples of emerging molecular imaging techniques that can improve diagnostic results thanks to superior image acquisition and soft tissue contrast (Chicklore et al. 2013).

Surgery was the earliest therapeutic strategy used to remove cancer, but it results in a non-precise at the level of the metastasized cells. Therefore, chemotherapy and radiotherapy have been used to eradicate metastasized cells. The aim with all drugs is to prevent proliferation and to kill the cancer cells achieving an effective result with the minimum side-effects, indicated by the therapeutic index (Morice et al. 2015). It is proven that chemotherapies that target DNA, RNA and protein and distrust cell cycle, continue to defeat cancers extending lives. Doxorubicin, platinum agents and Paclitaxel, are the most common treatment used, but there are continuous studies focus on the research of new drugs with higher efficiency and less debilitating side-effects in order to prevent surgery and to swing statistic in favor of survival (Hill & Dizon 2012). For example, other studies demonstrated that metformin, a famous diabetes drug, could be used as a new pharmaceutical for treating gynecological cancers (Febbraro et al. 2014). Furthermore, different trials show combined treatments (Nogami et al. 2013). Interestingly, another therapeutic option is the hormonal therapy, in fact, a study showed a percentage of treatment-responsive patients of up to 75% on 81 patients (Ramirez et al. 2004).

1.2.4 Gene regulation

It is demonstrated that the human genome is composed of 30.000-40.000 protein-coding genes (Consortium 2001). Different regulatory mechanism occurs cellular levels such as DNA replication, the transcription, the translation, gene regulation and protein expression (Brown 2002). Aberrant gene regulation and alteration of the RNA transcriptome can lead to a modification or loss of protein function. Therefore, multiple mechanisms at multiple levels occur involving gene mutations (Brown 2002). It worth noting that epigenetics is an essential phenomenon involved in the regulation of gene expression, a key role in this research project.

1.4 Epigenetic Revolution

“In addition to changes in genetic sequence” is the literal meaning of “epigenetic” word, it represents any gene activity alteration without changing the DNA sequence *(Figure 1.4)*. Epigenetic mechanisms are natural and essential processes in many organism activities, but they can be adverse health and behavioral effect when they occur improperly (Goldgerb et al. 2007). There is a change in gene activity, but changes in the nucleotide sequence are not shown. Gene expression is controlled by nucleotide residues and chromatin structure alterations or translated messenger RNA degradation (Cramer et al. 2015). The mechanisms for epigenetic have been classified in DNA methylation, histone modification (chromatin remodeling), small interfering RNA (siRNA) and

micro RNA (miRNA)-mediated gene regulation (Goldberg et al. 2007).

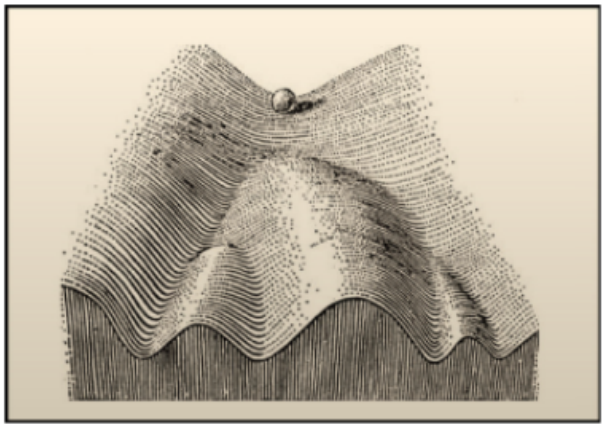

Figure 1.4 Waddington's Classical Epigenetic Landscape. The concept of an epigenetic landscape was proposed by Conrad Waddington in 1957. At various points in this dynamic visual metaphor, the cell, represented by ball, can take specific permitted trajectories, leading to different outcomes or cell fates (Goldberg et al. 2007).

Cancers of all type, cognitive dysfunction, reproductive, cardiovascular, respiratory, autoimmune and neurobehavioral illness, seem to be linked with epigenetic mechanisms. Many agents could be responsible for epigenetic processes, including heavy metals, tobacco smoke, diesel exhaust, pesticides, polycyclic aromatic hydrocarbons, viruses and bacteria, radioactivity and nutrient with additives (Riehemann et al. 2014). Epigenetics and epigenomics, the genome-wide distribution of epigenetic changes, are crucial to the understanding of all genetic mechanisms and evolution.
Among all the epigenetics research conducted so far, the most extensively studied disease is cancer.

1.4.1 Epigenetic in EC

Epigenetics has a critical role in endometrial cancer, as epigenetic mechanisms are implicated in the initiation and development of cancer and other illness such as multiple sclerosis, asthma, neurological disorders and depression (Cramer et al. 2015). Is has been studied that multiple genes were silenced due to DNA hypermethilation of, for example, E-cadherin (Muraki et al. 2009). Methylation is an important factor for the malignant transformation of endometrium in EC, HDAC expression in the endometrium has been demonstrated, it leads to a poor outcome (Weichert et al. 2008).

Cancer heterogeneity is associated with resistance development to drug treatments, for these reasons it potentially represents a big issue for cancer therapy. The mechanism by which tumors develop resistance has still not been totally clarified, and the processes are different. A most important issue is that drug resistance can be driven by epigenetic mechanisms that may be reversible (Lackner et al. 2012; Fisher et al. 2013). With these premises, the study and development of new, targeted therapies are needed.

1.4.1.1 DNA methylation in EC

DNA methylation consist in the addition or removal of a methyl group (CH3), and it has since been observed in many diseases and health conditions. This reaction, that is catalyzed by DNA methyltransferases, a specific enzyme, occurs in the DNA sequence at level of 5-position (C5) of cytosine nucleotides, next to a guanine nucleotide (Dupont et al. 2009).

Cytosin, Adenine and guanine methylation has been observed. Gene transcription can occur when transcription factors and the transcription initiation complex are able to see DNA codon, as there is no methylation in the DNA region of interest. Otherwise, transcription cannot initiate in presence of DNA methylation and DNA binding proteins are not able to bind to the promoter elements (Dupont et al. 20019). Cytosin methylation is the major epigenetic modification in mammalian, and the active DNA cytokine methyltransferase enzymes have the role to transfer a methyl group to C5 of cytosine mediating the epigenetic process (Asadollahi et al. 2010). CpG islands, regions that present the targeted cytosine residues, are located in promoter sections of genes where inhibit gene expression (Kwon & Shin 2011). Preclinical data suggests that combining SAHA with DNMT inhibitors can lead to the re-expression of DNA methylated genes (Chen et al. 2011).

1.4.1.2 Histone Modifications in EC

There are multiple types of histone modifications which are catalyzed by a number of enzyme families, acetylation and methylation are the most well characterized. These modifications alter the DNA-protein interactions in order to determine the ability of a gene to be transcribed and expressed. Therefore, the organization of chromatin structure and the regulation of gene transcription can be modified by acetyl groups added or removed from lysine amino acids (Goldberg et al. 2007). The post-translational modifications are classified in acetylation, methylation, ubiquitination, and phosphorylation (Strahl & Allis 2000). Acetylation and deacetylation of lysine residues represent the best characterize histone modifications and are located at the amino-terminal tail domains of histones H3 and H4. Histone acetyltransferase enzymes (HATs) and histone deacetylase enzymes (HDACs) are responsible for these catalytic reactions (Egger et al. 2004). The HDACs are subdivided into classes I-IV (Cramer et al. 2005). Acetylation is performed by histone acetyltransferases (HATs) which add an acetyl group to lysine amino acids and remove the positive charges of lysine residues and decreasing electrostatic interactions with the negatively charged bases of DNA. The consequence is the conversion of heterochromatin to euchromatin reducing the affinity of the histone for the DNA. The transcriptional activity is increased, therefore histone acetylation activates binding of transcription factors with DNA. On the other hand, deacetylation leads to transcriptional inhibition. Methylation can occur on lysine or arginine amino acids and can occur in mono-, di- or tri-methylation events by histone methyltransferases. This mark does not substantially alter the charge of amino acids and can be associated with both gene activation and inactivation (Cramer et al. 2005).

1.4.2 Epigenetic drugs

Epigenetic drugs (“Epidrugs”) are the key to target aberrant epigenetic mechanisms in EC disease, since DNA methylation and histone modifications are both reversible. it may be possible to reverse abnormal modifications or potentially add beneficial modifications to change gene expression profiles in different diseases, especially cancer and neurological disorders (Cramer et al. 2015).

1.4.2.1 DNMTs & HDACs

DNA methylation and histone acetylation aberrations have been treated with engineered DNMTs and HDACs inhibitors respectively. The first epidrug used was 5-azacytidine, a DNMT inhibitor

with the role to block DNA methylation and involved for the alteration of gene expression and phenotypes in fibroblastic cells (Taylor & Jones 1979). 5-azacytidine covalently link with DNA methyltransferases (DNMT) and has also been studied in endometrial cancer demonstrating the results improving of the disease is treated with the drug (Hu et al. 2012). Thanks to their fundamental role in cancer, inhibitors targeting HDAC proteins have been developed, as they are able to reduce proliferation and metastasis promoting apoptosis in cancer. In the Figure is shown four HDAC inhibitors for cancer treatment approved by FDA (Negmeldin & Pflum 2017). Saha and Belinostat and Belinostat, two HDACs, were studied and used for T-cell lymphoma treatment (Prince & Dickinson 2012) and Panobinostat for multiple myeloma treatment (San-miguel et al. 2015). HDAC inhibitors, as figure shows, have a similar chemical structure constituted by a capping group, a linker region and a metal binding group (*Figure 1.4.2.1)*. The linker region connect the capping group, that interacts with solvent-exposed residues of the HDAC active site, and the metal binding group that has the ability to bind with the catalytic metal located and buried in the active site (Negmeldin & Pflum 2017).

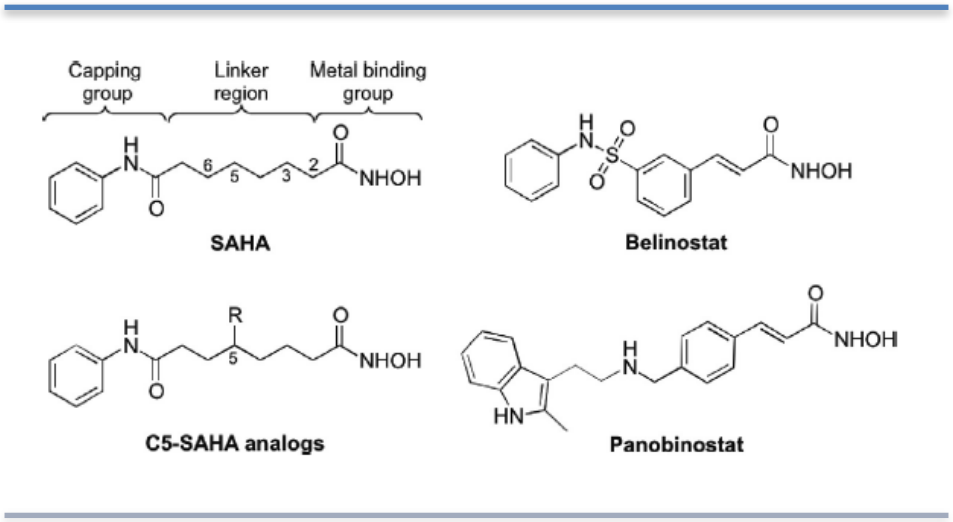

Figure 1.4.2.1 Chemical structures of the FDA-approved drugs SAHA, Belinostat, and Panobinostat, along with the C5-modified SAHA analogs reported here (Negmeldin & Pflum 2017).

Panobinostat constitutes the deacetylase inhibitors class (DACs) and it has been approved by FDA and EMA for multiple myeloma treatments. It can be used in combination with other drug for example Bortezomib, as this regulate the acetylation of around 1,750 proteins responsible of several biological processes (San-miguel et al. 2015).
HDACs are well tolerated and effective in early stage of cancer disease. Future trials of HDACs combinations with other agents, like DNA methylation agents, proteasome inhibitors, immunomodulatory agents, will studied to improve treatment efficacy (Prince & Dickinson 2012).

1.4.2.2 SAHA (suberanilohydroxamic acid)

SAHA is a histone deacetylase inhibitor used in many treatment diseases.Vorinostat also called as suberanilohydroxamic acid (SAHA) represents an inhibitor of Histone deacetylases (HDACs) that are enzymes used as a target as they are involved in the expression of suppressor genes in the tumor (Mohamed et al. 2016). It acts as a chelator of zinc ions located in the active site of the enzyme. Vorinostat is a small-molecular-weight compound formed by linear hydroxamic acid. The empirical

formula for Vorinostat is C14H20N2O3 *(Figure1.4.2.2)* with a molecular weight of 264.32 g/mol and a pKa around 9.
SAHA binds to the zinc atom of the catalytic site of the HDAC enzyme and the phenyl ring is projected out of the catalytic domain localizing it onto the surface of the HDAC enzyme. This mechanism leads to an accumulation of acetylated proteins including histones, whit the consequence that the histones manifest in multiple cellular effects. Saha has a rapid metabolism, a predominant route of elimination due to its short half-life. Two metabolic via are involved in its metabolism, glucuronidation hydrolyzes and β-oxidation, where, a vorinostat glucuronide and a vorinostat hydrolysis metabolite, inactive metabolites, that are excreted in the urine (Mohamed et al. 2016). Currently, the mechanism of action of these drugs is not entirely understood, as there is a limited understanding of the specificity of epigenetic changes in much complex illness. Specific researches in enzymes involved in epigenetic processes, more effective therapies will be used for a wide range of diseases including cancer (Yoo and Jones, 2006). Moreover, Vorinostat results completely soluble in dimethyl sulfoxide and slightly soluble in water, alcohol, isopropanol, and acetone. Therapeutic potential of Vorinostat is valid, but having a poor aqueous solubility (0.2mg/ml), development novel formulations of the drug for oral and parenteral administrations are needed in order to improve solubility (Mohamed et al. 2016).

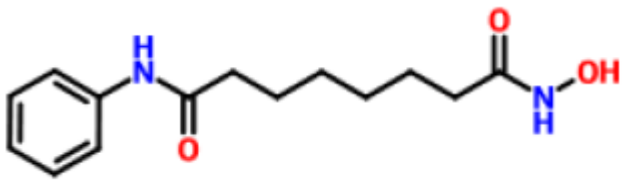

Figure 1.4.2.2 Molecular structure of Vorinostat (Mohamed et al. 2016)

Currently, the mechanism of action of these drugs is not entirely understood, as there is a limited understanding of the specificity of epigenetic changes in much complex illness. Specific researches in enzymes involved in epigenetic processes, more effective therapies will be used for a wide range of diseases including cancer (Yoo and Jones, 2006). Moreover, Vorinostat results completely soluble in dimethyl sulfoxide and slightly soluble in water, alcohol, isopropanol, and acetone. Therapeutic potential of Vorinostat is valid, but having a poor aqueous solubility (0.2mg/ml), development novel formulations of the drug for oral and parenteral administrations are needed in order to improve solubility (Mohamed et al. 2016).

1.5. Nanomedicine: the Frontier of Cancer Treatment

Multidisciplinary developments have led to an explosion of Nanomedicine applications, as this organic evolution has enabled the positives of nanomedical approaches to be appreciated in multiple fields, each of which are required to deliver bespoke future medicines *(Figure 1.5.1)*. From 1959, when Richard Feynman at the annual meeting of the American Physical Society explain the desire of manipulating and controlling small scale things, nanoscience and nanotechnology developed so far showing new opportunities in different fields, from engineering to medicine (San-miguel et al. 2015).

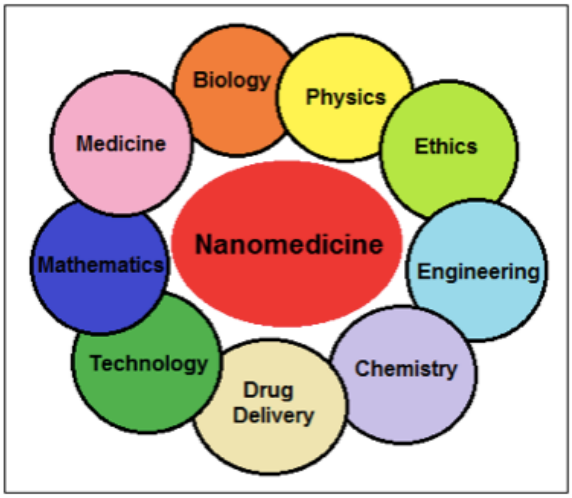

Figure 1.5.1 Nanomedicine is a connection among several fields

The field of medicine had a societal and ethical change *(Figure1.5.2)*, and "nanomedicine", applying nanotechnology to medicine, was the term started to use. Nanomedicine started to smarter decisions to kill specific cells and repair them using a better control system, drug release is an example. Instead, the goal of conventional therapies, like surgery, radiation, and chemotherapies, was to remove disease cells faster than healthy cells (Silva et al. 2019).

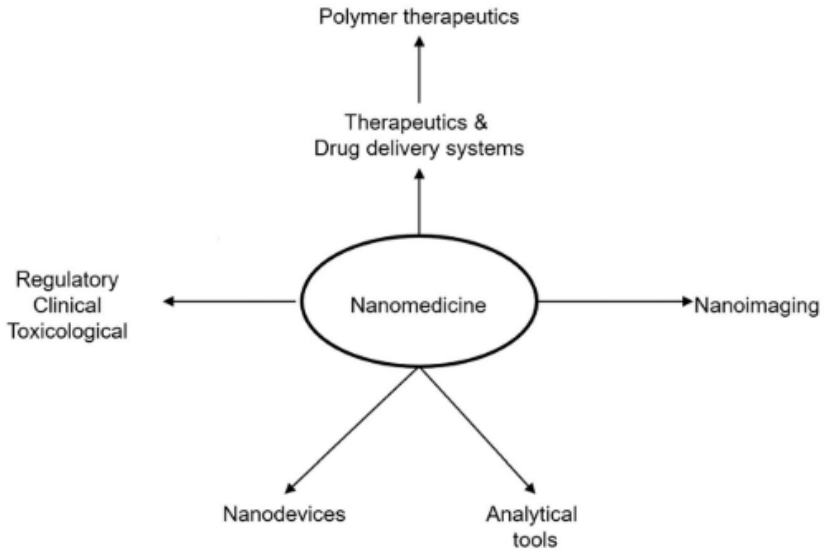

Figure 1.5.2 The five main subdisciplines of medicine (Azzopardi et al. 2016)

In the 1960s, phospholipid-based liposomes and polymer-based nanoparticles were the first nano-sized agents to be investigated for clinical applications. Since then, numerous other types of nanomedicine agents have been under evaluation including iron-oxide and gold-nanoparticle, albumin-drug conjugates, solid lipid nanoparticles, carbon nanostructure and antibody-drug conjugates (ADCs) (Falco et al. 2015).

To date, nanomedicine's biggest contribution to medicine has come for the formulation of drug delivery systems (DDS) such as liposomes, nanoparticles, and ADCs. The packaging of drugs in DDS can lead to their prolonged circulation at therapeutic levels by reducing renal clearance. Their increased cellular permeability can significantly enhance cellular uptake of hydrophilic drugs, as well as facilitating their transport across the blood-brain barrier. Furthermore, DDS can serve to target their payloads to particular tissues and in the case of ACDs to selectively target diseased cells, thus reducing the off-target toxicities associated with many free drugs (Howard et al. 2016).

Nanomedicine has also been applied to diagnostic, such as the use of nanomaterials in the detection of disease biomarkers and disease-related genetic mutations, and as imaging agents for tumor detection. Additionally, the third set of nano-agents called theranostics, combine therapeutic and diagnostic capabilities, delivering a mixture of drugs and imaging agents to a tumor site, or radiolabelled antitumor antibodies which provide radiotherapy as well as imaging (Howard et al 2016). Finally, nanomedicine has also been employed successfully in vaccinology, where nanoparticles are used as antigen delivery systems and/or adjuvants (Howard et al 2016).

1.5.2 Nanomedicine targeting

A distinct capacity to target tumors is essential in the success of cancer treatment. Increased site specificity and internalization can improve the efficacy of treatment and decrease the possibility of the serious side effects that cancer patients often experience. Nanoscale cancer therapy shows two main mechanisms on tumor targeting for their efficacy: passive and active. Nanomedicines are passively targeted to the tumor sites thanks to the enhanced and permeability and retention (EPR) effect which sets pathophysiological differences between solid tumors and normal tissue.
EPR effect is the main mechanism for nanomedicines to be passionately targeted to the tumor site. When blood vessels of the tumor are devoid of smooth muscle resulting in highly permeable. Cancer cells produce high levels of vascular permeability factors causing a perpetually dilated state and allowing for the uptake of oxygen and nutrients required for tumor cell growth. Instead, retention occurs through tissue dressage when the diseased lymphatic vessels prevent loss of macromolecules (Howard et al. 2016). This crucial mechanism allows for the accumulation of the anticancer drug. Active targeting involves the interaction between ligands of nanomedicines leaning toward tumor and tumor cell surface enhancing cellular uptake. Receptor-mediated endocytosis is the main example of active targeting allowing the binding of the antitumor drug to its target antigen. For this reason, tumor antigen characteristics are crucial and should be highly expressed on the tumor cell surface (Chen et al.2018).

1.5.2 Nanoparticle options and Pluronic polymer type

Nanomedicine has performed several advantages using nanoparticles technologies such as liposomes, polymer micelles, dendrimers and, nanoparticle functionalized *(Figure 1.5.2.1)*. Each of them presents a specific design in order to overcome numerous biological barriers in drug delivery (Pitt-barry et al. 2014). Every year new approaches for nanoparticles development are engineered (Mg et al 2015). Nanostructures can be modified in order to allow them to achieve tumor cells site and deliver properly the active principle that they carry more efficiently than the free drug formulation alone.

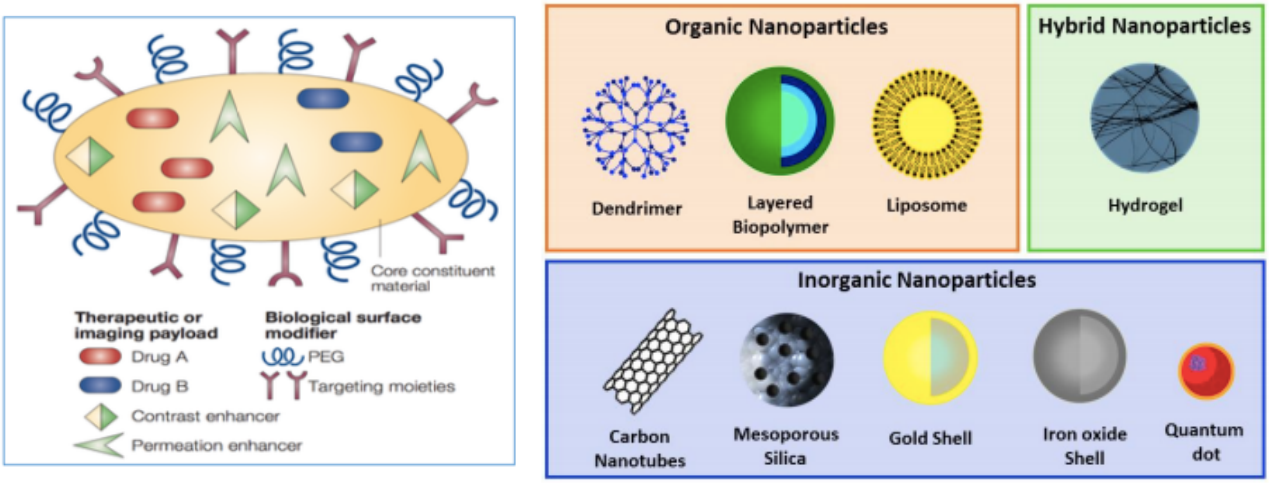

Figure 1.5.2.1 On the left, Multifunctional nanoparticle (Ferrari et al. 2015). On the right Schematic representation of different types of nanoparticles (NPs) divided into organic, hybrid and inorganic categories (Silva et al. 2019).

Professor Conlan S. and coworkers have provided an overview of polymer therapeutics used in oncological surgery (Azzopardi et al 2016). Nanoparticles can be engineered for different purposes, imaging, therapy, bio-sensing (Silva et al. 2019) For cancer treatment, vectors, that efficiently target the drug to the site of interest and with no toxic characteristic have to be designed. Polymeric nanoparticles demonstrated to be bioavailability, having a short half-lives and controlled release (Prabhu et al. 2015). A great variety of polymers have been used, but for the aim of this thesis project Pluronic-based nanostructure was used. As illustrated in *(Figure 1.5.2.2)*, Pluronic is a trig-block copolymers formed by polyethylene oxide (PEO) and alternated by polypropylene oxide (PPO).

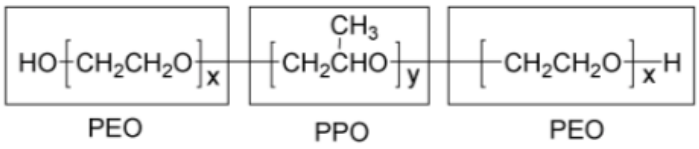

Figure 1.5.2.2 General tori-block copolymer structure of pluronics.

Pluronics have the capacity of arranging themselves forming micelles and the hydrophobic part (PPO) stuck internally, while the hydrophilic part (PEO) bound outside that remain in contact with solvent. Pluronic F127, used in this work, was fabricated in Swansea University laboratories using the thin film technology (Zhang et al. 2011; Zhang et al. 1996), and Pluronic F108 was kindly provided by a Swedish laboratory in Uppsala, a close collaborator of the Reproductive biology and Gynecological Oncology Group in Swansea. Both the polymers have been proven to be non-toxic and biodegradable for biological applications (Liu et al. 2012). A variety of methods polymeric nano system creation can be employed and they should be classified based on the material they are made taking advantage of either the highly charged nature of some of these materials or their amphiphilic properties (Pinto Reis et al. 2006) (Sundar et al. 2010).

1.5.3 Nanoparticle encapsulation methods

For this project, the Saha epidrug was loaded inside Pluronic nanoparticles (Zhang et al. 2011). Encapsulation a drug into a nanocarrier avoid multiple issues related to its side effects. The hydrophobic nature of Saha enables the drug to bind the hydrophobic polymer chains forming micelles of plutonic with Saha present in the internal part (Figure 1.5.3).
The encapsulation efficiency calculation is needed to understand drug efficacy measuring the amount of drug well encapsulated. Furthermore, the release profile of the drug from nano carriers give a good indication of the rate and timing at which nanoparticles discharge their content. This is an help for the researches to define a protocol for this specific formulation clinical use (Huang & Brazel 2001) (Xiong et al. 2005) (Yeo & Park 2004).
The nanopartcle systems has to be characterized after the fabrication process. This stage is essential to determine the system acceptability in the biological environment.
Generally nanoparticles are studied for their shape, size, surface charge and drug encapsulation efficiency (Cho et al. 2013).

1.5.3.1 Liposome systems

Liposomes are nano vectors used in nanotechnology and have a critical role in cancer therapy. Figure 1.5.3.1a summarizes a their classification. They are used in cancer treatment as they reduce side effaces to normal tissues and have several specific characteristics that differ from other therapeutic delivery systems. Liposomes are biocompatible, no immunogenic and present ability for self-assembly and for carrying large drug payloads giving them a protection from external environment. Other important features in liposome are the capacity to load both hydrophilic and hydrophobic agents improving their solubility and the ability to reduce the toxicity of the drugs (Zununi et al. 2017). Liposomes have a spheric structure constituted in one or more concentric lipid bilayers surrounding aqueous spaces and could be sorted with polyethylene glycol (PEG), an inert polymer which allow them to be easily charged by phagocytic cells of the reticuloendothelial system (RES) in blood circulation (Zununi et al. 2017) .

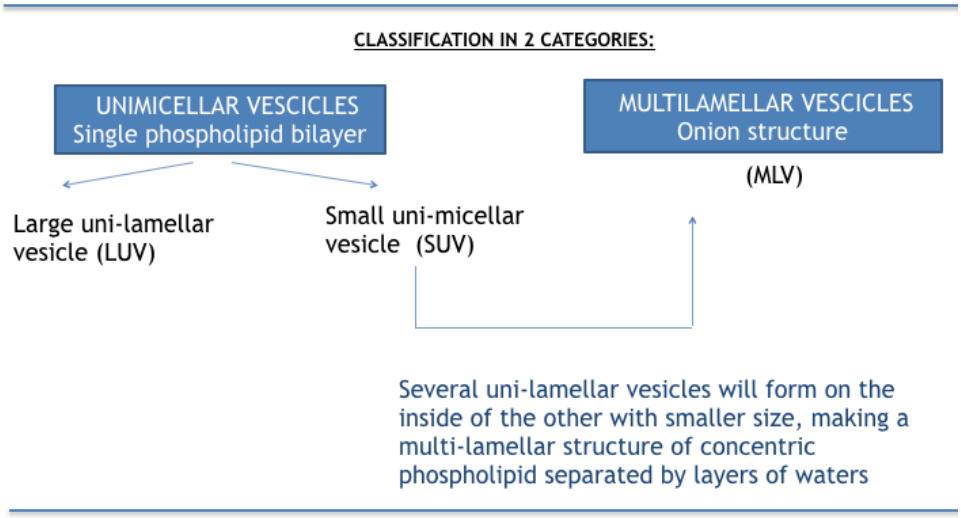

Figure 1.5.3.1a Liposomes classification (adapted from Zununi et al.2017)

Moreover, liposome-based combinatorial therapeutics system can improve the exist systems and overcome the limitations. A recent study shows that Doxorubucin, a drug used for cancer treatment, has been encapsulated in a PEGylated liposome increasing the circulation time with little leakage (Collier et al. 2017) *(Figure 1.5.3.1b)*.

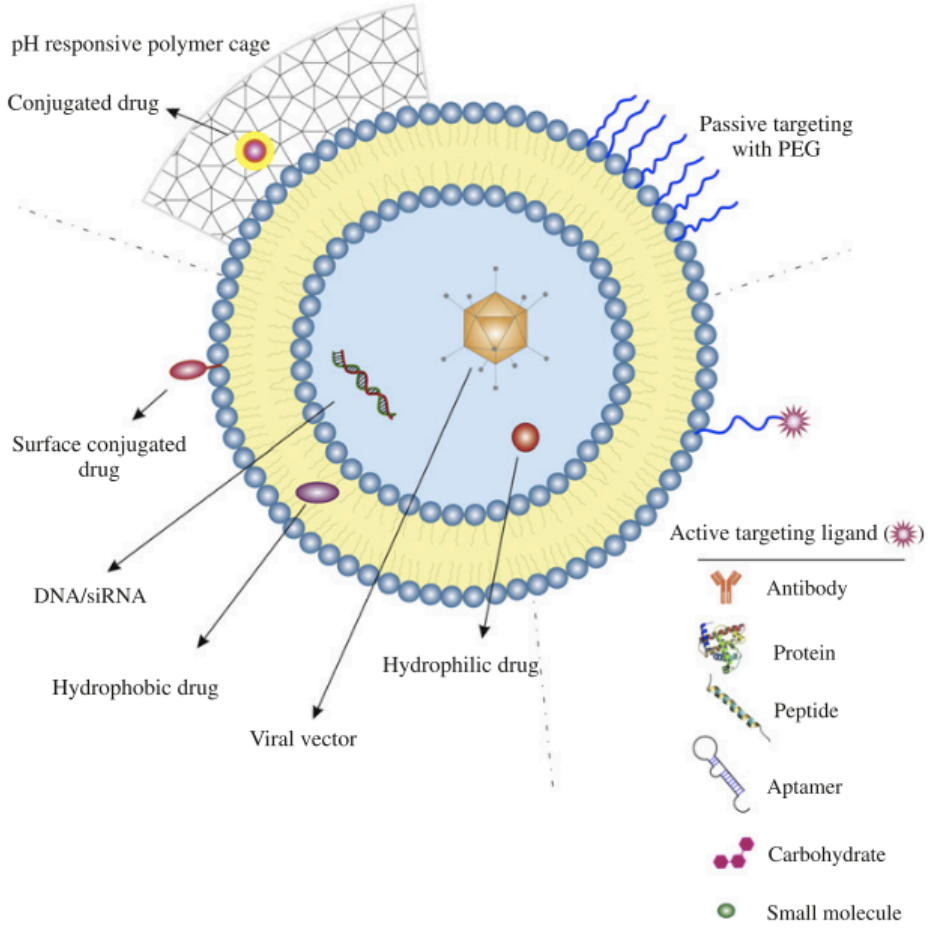

Figure 1.5.3.1b Structural and design considerations for liposome systems (Zununi et al.2017)

There are different methods for liposomes preparation, one method is the reverse-phase evaporation that was described in a scientific work combining detergent dialysis and solvent evaporation in order to obtain a high aqueous space-to-lipid ratio (Szoka 1978). *Figure 1.5.3.1c* summarizes the four principal steps for liposomes preparations and the different techniques. Liposomes represent an ideal carrier system and can be applied in several fields such as in food, cosmetics, pharmaceutics, and tissue engineering. Some researches reported that they could improve drug up-take into cells and bioactivity of curcumin (Zununi et al.2017).

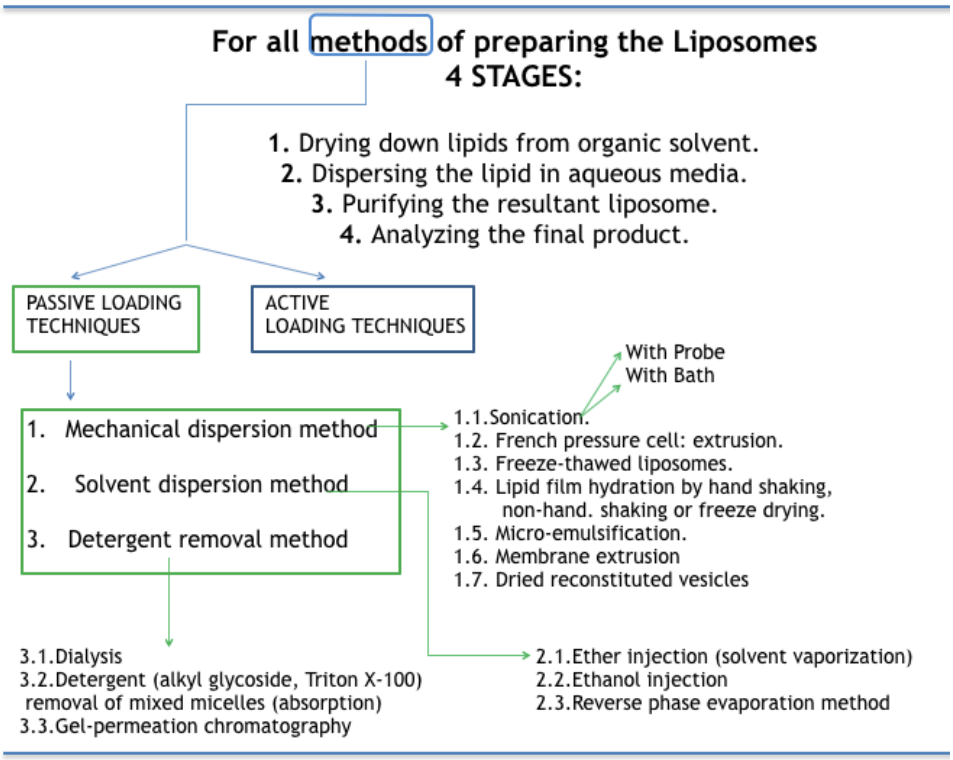

Figure 1.5.3.1c liposome preparation and summery of liposome techniques (adapted from Zununi et al.2017)

1.6 Improved Epidrug Efficiency

Tumors represent an aberration of the biological system that is an extremely complex environment organized to over-defend from any external enemy. Nanoparticles design is projected to create nanoparticles that can avoid the physiological defense and take advantage of the tumor aberrations mechanisms. Endocytosis is the process which encloses within vesicles nanoparticles that achieve the site of interest and can be classified through different mechanisms like phagocytosis, pinocytosis and receptor-regulated endocytosis (Oh & Park 2014). In this context, the way a nonmaterial interacts with cells has to study during the nanoparticles system project design in order to achieve positive clinical evaluations.

1.6.1 Size and Shape of nanoparticles

The EPR effect has been proven to permit nanoparticles be passionately targeted within the cancer vessels, thus is an important factor that has to be considered for the nanoparticles design (Torchilin 2011). There is a connection between nanoparticle size and and its capacity to undergo the EPR effect. A size smaller than 100nm can positively enter the tumor interstitial space (Cabral et al. 2011). Nanoparticle's cellular uptake is also demonstrated to be influenced by size NP activating the specific membrane receptors (Jiang et al. 2008).
Moreover, the shape of NPs are considered on of the best compromise for drug delivery and targeting system. Ferrari and co-workers showed that particles can travel in different ways through the blood vessel and their geometry is essential to reach tumor site (Decuzzi et al. 2009). Spherical

and quasi-spherical NPs flow distant from the cell wall, differently from discoidal ones that marginate to vessel walls in a major rate oscillating from one wall to the other (Blanco et al. 2015). From different studies, it has been illustrated that many factors influence the interaction of Np with a specific cell, including the ligand density when it presents (Albanese et al. 2012).

1.6.2 Surface charge and cell-nanoparticle interactions -tesi pisano

Researches demonstrate that np internalization occurs depending on the different surface properties and endocytosis mechanism (He et al. 2010). Negatively and positively charged nanoparticles are both internalized by cells and the first one can also be endocytosed even if there is repulsion coming from the negative charge of the membrane phospholipid bilayer (Verma & Stellaci 2010). Thus the parameter by which is possible to determine the charge of the nanoparticle is the Zeta-potential. This depends on the pH solution and gives information about the colloid stability. More precisely, Nps are considered stable if they have a Zeta potential more positive than +30mV or more negative than -30mV (Malvern instruments 2004).

1.6.3 Tumour biomarkers_CD44

CD44 is a complex of transmembrane glycoprotein and it is also called Hermes antigen, homing cell adhesion molecule (Liu 2015). This glycoprotein complex is encoded by the CD44 gene located on chromosome 11 that is constituted by 20 exons. CD44 standard isoform (CD44s) and CD44 variant isoform (CD44v) are functionally isoforms coming from transcription for the CD44 gene that undergoes alternating splicing (Liu 2015). The first is found in most cells and the second one is expressed on tumor cells and during inflammations. CD44 proteins are mainly formed by three elements, a short C-terminal cytoplasmic domain, a transmembrane domain, and seven extracellular domains which contains a stem region and an N-terminal HA-binding link-homology module, as *Figure 1.6.3* shows.

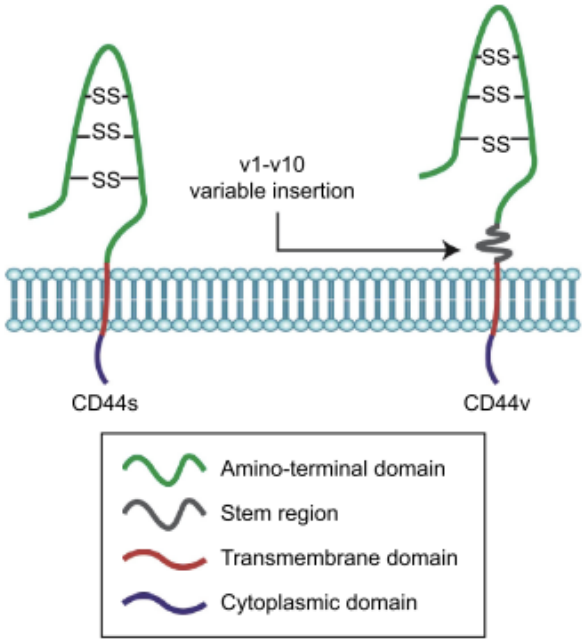

Figure 1.6.3 Key domains of CD44 (Liu 2015)

The transmembrane receptor protein CD44 belongs to the family of adhesion molecules, thus are involved in interactions between cell and cell-matrix. Lymphocytes functions are mediated by CD44, the same occurs for cell activation, motility, adhesion to the extracellular matrix and to stromal cells and, cell division (c).

The role of CD44 expression and its isoforms is essential for better understanding of nanosystem fabrication, as they represent possible markers and a potential target for tumor cells (Zhao et al 2016). CD44 has been also studied to have a role in the Epithelial-to-mesenchymal transition (EMT) process (Ponta et al. 2003). Recently, the potential role of CD44 variant isoforms has been studied. Various human malignancies are linked with this factor, for example, neoplasms,

carcinomas of the stomach, colon, breast and uterine cervix (Ross et al 2001). CD44 isoforms, such as CD44v6, have been associated with EC disease. The expression pattern of CD44 depends on the menstrual cycle and Type I EC cells expresse low amounts of CD44 while type II E cells show significantly increased expression. It has been argued that CD44 may play a functional role in normal endometrium and is also expressed in endometrial carcinomas (Tempferl et al.1998).

1.6.4 Nanoparticles functionalization

Nanoparticles represent a real advantage for drug delivery and have several biological applications. They have many roles. The first is to enhance the stability of therapeutic agents throughout their chemical and physical properties, then they permit the release of encapsulated anti-tumor drug increasing the hydrophobic drug solubility. NPS also need to increase drug concentration to target the tumor site because of EPR (Enhanced Permeation and Retention) (Kumar et al. 2017). For all these reasons, “nude” nanoparticles can encounter issues entering the biological environment due to the presence of different defensive mechanisms of the host. Functionalization is a useful technique that reduces these possible problems. Mononuclear phagocyte system (MPS) or Reticulo Endothelial system (RES) is one of the major obstacles for drug delivery which nanoparticles are sequestered. A formation of a protein corona can be formed around the NPS (opsonization), in order to avoid that a sufficient amount of NPS reaches the target. It can happen immediately after injection (Blanco et al. 2015). Poly-ethylene glycol (PEG) is a polymer used in order to avoid RES action. Is has been demonstrated that PEG decreases the uptake from phagocytes (Jokers et al. 2011) (Farace et al. 2016). Moreover, is known that endometrial cancer has an increased surface concentration of CD44 which bind to hyaluronic acid (HA) receptor leading the connection with the extracellular matrix (Wojciechowsky et al. 2014). It’s suggested to use HA to functionalize the nanoparticles achieving a better target of CD44-overexpressing tumors (Huang et al. 2016). HA is a non-sulfated glycosaminoglycan constituted by repeating disaccharide units D-glucuronic acid and N-acetyl-D-glucosamine, is present in the tissue matrix and fluids maintaining the hydration status and the osmotic balance. In many tumors there are high levels of HA, these can be a diagnostic or prognostic marker based on the cancer type. The targeting trough sulfated-HA inhibits tumor growth and angiogenesis in prostate cancer (Subtypes 2013).

2. AIM OF THE THESIS

Endometrial cancer (EC) is the most common gynecological disease in developed countries and female patients have poor outcome presenting a mortality rate of around 25% at five years (Daby et al. 2017). Given the low prognosis of gynecological cancers; specifically, Endometrial and Ovarian cancer, the need for innovative efficient treatment techniques is critical. New nanomedicine systems, approved in the clinical use can target to the tumor tissues and based on the enhanced permeability and retention (EPR) effect, can have unique medical effects (Chen et al. 2018).

The aim of this thesis was to develop a nanoparticle delivery system using an in vitro Endometrial Cancer cell line model (Hec50 and Ishikawa). The nanoparticle system was fabricated using Pluronic polymer (Pluronic F127 and Pluronic S-S pyridyl) to encapsulate successfully a hydrophobic epidrug (SAHA) and to enhance efficacy through targeted delivery in a solid tumor cancer type. In the last years, the use of Pluronic triblock copolymer as a biomaterial has been widely investigated, due to its particular physicochemical characteristics, which include thermo-responsiveness, easy chemical functionalization, and relatively good biocompatibility. In order to improve drug delivery to the site of interest, SS Pluronic was functionalized with hyaluronic acid (HA). Nanoparticles were characterized using Dynamic Light Scattering, Scanning Electron Microscopy (SEM), Confocal Microscopy and were encapsulated with PI (Propidium iodide) dye in order to study their stability and cell penetration. In order to give a comprehensive characterization, the release profile was also studied. Furthermore, the biological effect was investigated in an in vitro model involving endometrial cancer cells (Type I EC and Type II EC). The viability and toxicity in EC cell lines were evaluated using the Real-Time Glo assay. Cell-cycle and phenotype were analyzed thanks to western blotting experiments and biomarkers such as p53, p21, E and N cadherin were studied.

This project, carried out in Centre for Nano Health laboratories (Swansea University Medical School), demonstrated that nanoparticle systems, thanks to their size, shape, surface morphology, surface charge, encapsulation efficiency, and release profile, are a valid therapeutic approach for gynecological cancers such as endometrial cancer. In order to test this hypothesis, an in vitro model of type I and II EC was performed, using cell lines Ishikawa and Hec50 respectively. Pluronic nanoparticles were fabricated in the presence and absence of SAHA, an epigenetic drug, and their therapeutic effects on EC cells were demonstrated. Furthermore, particles were functionalized with HA (hyaluronic acid) conjugation in order to assess increased drug delivery through targeted binding. The effect of particle toxicity following HA functionalization was assessed. Considering CD44 expression which is an important tumor biomarker in Ishikawa (Type I EC cells) and Hech50 (type II EC cells), an in vitro model for both type EC cell lines was performed and analyzed with the different treatments previously mentioned.

3. MATERIALS AND METHODS

3.1 Nanoparticles Fabrication

The nanoparticles were fabricated with and without the drug encapsulated prior to full material characterization (size, charge and shape) and then used in an adopted *in vitro* model of EC.

NP NAME	CONCENTRATION μM
F 127 Saha	2.5 – 5
F127 Empty	2.5
F 127-SS-Saha	1 – 1.25 – 2.5
F 127-SS-Empty	2.5
F 127-SS-HA-Saha	1 – 1.25 – 2.5
F 127-SS-HA-Empty	2.5

Table 3.1 Nanoparticles fabricated. This table summarize the nanoparticles fabricated with Pluronic F127 and functionalized at different concentrations.

3.1.1 Fabrication of Pluronic F 127 Nanoparticles

The fabrication of Pluronic F 127 Nanoparticles was done using the Thin Film Method, method widely used for fabrication of different nanoparticle formulations (Moghimipour & Handali 2012; Ai et al. 2014). In this work, 300mg of Pluronic F 127 (Sigma UK®) and 4.2mg Saha drug (Sigma, UK®) were weighed and put into a single-neck round bottom flask (50ml, Sigma UK®) that was connected to a Rotary Evaporator, shown in *Figure 3.1.1,* for 5 minutes at minimum rate (speed 6 on the rota) to mix the powders. Following the addition of 10ml of of 99.8% acetonitrile (Sigma UK®), the solution was kept at 60°C under vacuum at maximum speed (speed 12 on the rota) for one hour. The round bottom flask was then placed in the vacuum machine (vacuum gas pump, VWR™) overnight in order to allow the solvent to evaporate and the solution to dry. The following day the flask was connected to the rotary evaporator for one hour and the copolymer matrix was pre-heated in a warm water bath (SUB Aqua Plus, GRANT) at 65°C to create a transparent gel-like film. A volume of 10ml of PBS (GIBCO™) was added to the gel and the solution mixture was stirred with the Rotary Evaporator (speed 9 on the rota) for 30 minutes to obtain a clear micellar solution and allow the stabilization of the nanoparticles in the PBS. Once hydrated, the aggregates were removed during the filter sterilization process by

passing the solution through 0.22μm filters (MILLEX®, Millipore). The final product was kept at room temperature.

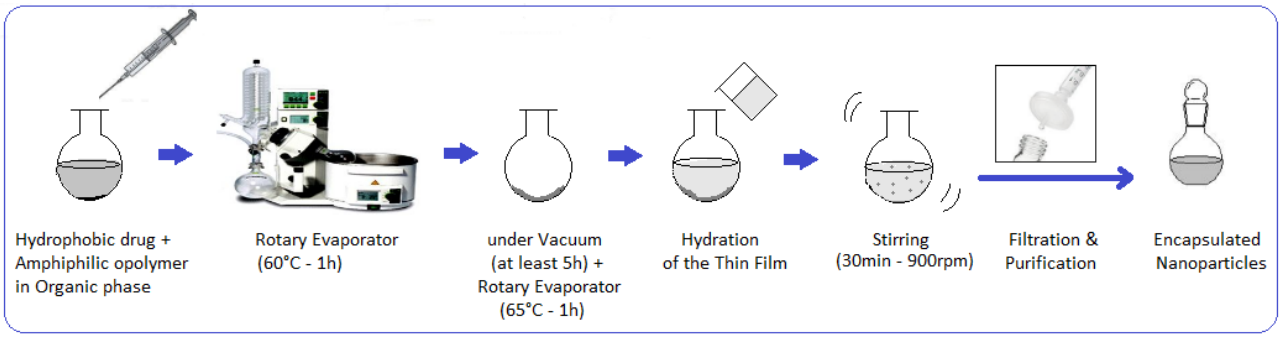

Figure 3.1.1 Schematic diagram of the preparation of Nanoparticleswith Saha encapsulated via Thin Film Hydration Method. The thin film formed in the round-bottomed flask was hydrated with PBS and the suspension was agitated for 30min before the filtration.

Saha-encapsulated nanoparticles, were fabricated using the Thin Film Method (Moghimipour, & Eskandar 2012). Briefly, 0-10 mg Saha and 300 mg Pluronic F 127 were dissolved in 10 mL acetonitrile.

3.1.2 SS functionalization & SS-HA functionalization of F-127 Nanoparticles

F 127 SS modified Pluronic was sent to our laboratory by our Swedish collaborators in Uppsala University research centre (see acknowledgements). Briefly, the protocol used for fabrication in Uppsala was the following: two grams of Pluronic were first dissolved in 6 mL of chloroform, and this solution was slowly added to a stirred solution of 4-nitrophenyl chloroformate in 6 mL of chloroform in order to activate the OH- groups. After 24 hours of shaking, the reaction product was precipitated, recovered by filtration, and re-dissolved in chloroform. The final SS Pluronic product was finally recovered by evaporation of the remaining solvent under vacuum overnight.

F 127 SS-HA nanoparticles, were fabricated just adding a calculated amount of hyaluronic acid (HA) to the nanoparticle solution previously prepared and the followed ratio was 1:1 respectively Pluronic S-S pyridil : HA-SH. Before putting the hyaluronic acid in the mixture, it was kept under UV lights for 30 minutes in order to purity it. Subsequently the mixture was mixed for at least 30 minutes (speed 9 on the rota) using the rotary evaporator. The aggregates were finally removed thanks to the filtration process through a 0.22 μm filters (MILLEXR, Millipore).

3.2 NPs characterization

Pluronic nanoparticles were characterized using a suite of physical/analytical techniques within the Centre for Nanohealth, Swansea. Nanoparticle dimensions were investigated in terms of size, shape and charge to understand their interactions with cell membranes (Blanco et al. 2015).

3.2.1 Size Anlalysis with Dynamic Light Scattering

The Zetasizer Nano range of instruments provides the ability to measure three characteristics of particles or molecules in a liquid medium. These three fundamental parameters are particle size, zeta potential and molecular weight. By using the unique technology with the Zetasizer system these parameters can be measured over a wide range of concentrations (*Figure 3.2.1a).*

Figure 3.2.1a An image of the Zetasizer Nano ZSTM machine (Malvern)

Nanoparticle size was determined measuring the Brownian motion of the particles which is the random movement of small particles due to collisions caused by bombardment by the solvent molecules that surround them. It is known that small particles move quickly in a liquid and large particles move slowly. Using this knowledge and the relationship between diffusion speed and size (defined in the Stokes-Einstein equation), the size can be determined defined in the Stokes-Einstein equation:

$$D = \frac{kT}{3\pi\eta D_H}$$

Where D=Diffusion speed, k=Boltzmann's constant, T=absolute temperature, n=viscosity and DH= hydrodynamic radius. The relationship shows how size can be determined from diffusion speed provided that the temperature and continuous phase viscosity of the sample are known.

The Brownian motion is determined by illuminating the particles with a laser and analyzing the intensity fluctuations in the scattered light. If a small is illuminated by a light source such as a laser, the particle will scatter the light in all directions. If a screen is held close to the particle, the screen will be illuminated by the scattered light of that particle or of many particles if there are many particles. The speckle pattern will consist of bright and dark areas. In the diagram is shown the propagated waves from the light scattered by the particles. The bright areas of light are where the light scattered by the particles arrives at the screen with the same phase and interferes constructively to form a bright patch *(Figure 3.2.1b)*.

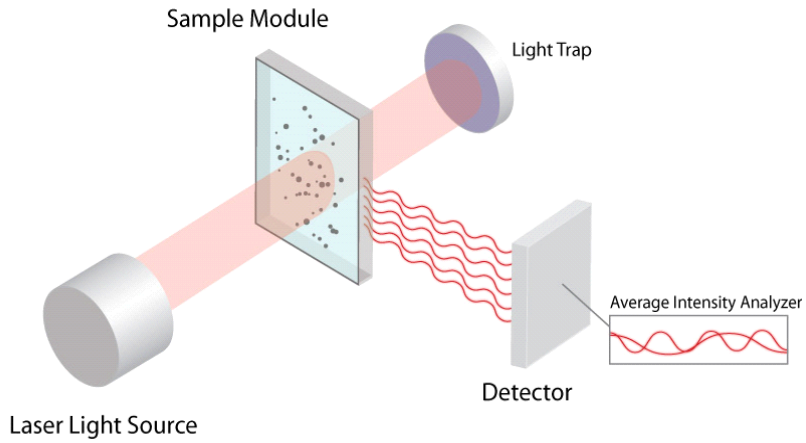

Figure 3.2.1b The scattered light falling on the detector (Malvern)

As the particle are constantly in motion the speckle pattern will also appear to move. As the particle move around, the constructive and destructive phase addition of the scattered light will cause the bright and dark areas to grow and diminish in intensity, or the intensity at any particular point appears to fluctuate. The Zetasizer Nano system measures the rate of the intensity fluctuation and then uses this to calculate the size of the particles.

Procedure for NPs characterization using Zetasizer Nano

1ml of nanoparticle stock solution was resuspended in PBS (GIBCOT was pipetted to a disposable plastic cuvette (Sigma, UK), extra caution were taken to avoid the formation of any bubbles. For each sample, 3 different sets of 10 measurement runs (10s) were performed – each set providing an average value of Zeta average and a value of polydispersity index (**PdI)**. Each nanoparticle preparation was characterized for size distribution prior to downstream applications, and only nanoparticles with a good size quality report after size measurement were taken into consideration. Average and standard deviation were performed for all data, with a minimum of three independent biological repeats. Pair-wise comparisons were done using a 2 tailed T test.

3.2.2 Zeta potential and Electrophoresis

Most of liquids contain ions; these can be negatively and positively charged atoms called cations and anions respectively. When a charged particle is suspended in a liquid ions of an opposite charge will be attracted to the surface of the suspended particle. A negatively charged sample attracts positive ions from the liquid and conversely a positive charged sample attracts negative ions from the liquid. Ions close to the surface of the particle, will be strongly bound while ions that are further away will be loosely bound forming what is called a Diffuse layer. Within the diffuse layer there is a notional boundary and any ions within this boundary will move the particle when it moves in the liquid; but any ions outside the boundary will stay where they are; this boundary is called the Slipping plane. A potential exists between the particle surface and the dispersing liquid which varies according to the distance from the particle surface; this potential at the slipping plane is called the zeta potential. Zeta potential is measured using a combination of the measurement techniques: Electrophoresis and Laser Doppler Velocimetry (Laser Doppler Electrophoresis). This method measures how fast a particle moves in a liquid when an electrical field is applied, its velocity and determines whether the particles within a liquid tends to flocculate or not (*Figure 3.2.2a).*

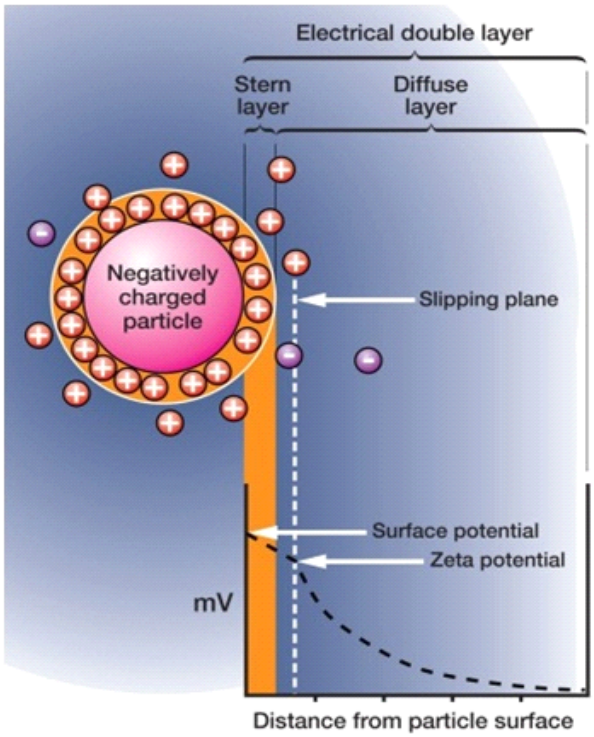

Figure 3.2.2a Mechanism of zeta potential and electrophoresis (Malvern)

The magnitude of the zeta potential gives an indication of the potential stability of the colloidal system, when one of the three states of matter: gas liquid or solid, is finely dispersed in one of the others. If all the particles in suspension have a large negative or positive zeta potential then they will tend to repel each other and there is no tendency to flocculate. However, if the particles have low zeta potential values then there is no force to prevent the particles coming together and flocculating. The general dividing line between stable and unstable suspensions is generally taken at either +30mV or -30mV. Particles with zeta potentials more positive than +30mV or more negative then -30mV are normally considered stable.

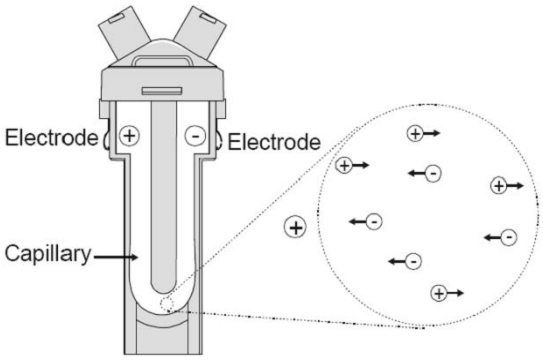

Figure 3.2.2b Cuvette used for zeta potential anlyses (Malvern)

Procedure for NPs characterization using Zeta potential

1ml of the stock solution of empty and SAHA encapsulated nanoparticles resuspended in milliQ water (Millipore) was pipetted to a folded capillary cell (Malvern) taking care to avoid the formation of any bubbles (*Figure 3.2.2b)*. Nanoparticles were suspended in milliQ water because PBS could affect charge properties. For each sample, 3 different sets of 10 measurement runs (10s) were performed. A series of data indicating zeta-potential and quality report were outputted for one or more peaks identified during the reading. Average and standard deviation were performed for all data, with a minimum of three independent biological repeats. Pair-wise comparisons were done using a 2 tailed T test.

3.2.3 Encapsulation Efficiency Analysis with HPLC

Reverse-phase high-performance liquid chromatography (RP-HPLC) is an analytical technique employed to identify and quantify different components of a mixture, separating them according to their hydrophobicity (*Figure 3.2.3a)*. Each unit of the sample interacts slightly differently with the adsorbent material of the stationary phase, causing different flow rates for different components. This brings to the partition of the components as they flow out the column, so that they will elute at different times (retention time).

Figure 3.2.3a Agilent 1100 Series HPLC

The sample is loaded onto a column containing a stationary phase having an absorbent material. Through it the mobile phase, a pure liquid or a mixture of liquids, flows. The various components of the sample, being chemically different, interact slightly differently with the stationary phase and consequently are held back in it. The mobile phase then elute them along the column, from entry to exit, at different times (retention time), making the technique selective and causing different flow rates for different components.
For these experiments, an Agilent 1100 Series HPLC equipped with a Zorbax Eclipse XDB-C18 4.5 x 150mm 5μm column (stationary phase) and an UV detector (UV 1575, Jasco) was used for the determination of the encapsulation efficiency of SAHA in different nanoparticle formulations.

Procedure for HPLC analysis

Samples were eluted in acetonitrile – 0.1% formic acid in MilliQ water (22:78 v/v). The flow rate, injection volume and detection wavelength were set at 0.8 mL/min, 10 μL and 241 nm, respectively. Chromatograms were acquired and analysed with Agilent Chemstation software. Prior to the loading measurements, known concentrations of SAHA dissolved in a solution of dimethyl sulfoxide (DMSO, an important polar solvent that dissolves both polar and nonpolar compounds and is miscible in a wide range of organic solvents) were injected, and the area of each peak (retention time = 8.34 minutes) was used to build a calibration curve. The latter was linear (R^2 = 0.9993) in the investigated range (1–100 μM). From this curve the values of the samples of interest could be extracted. Sample solutions were dissolved in DMSO and vigorously vortexed to obtain a clear solution before doing the measurements.

The general formula used to obtain the encapsulation efficiency (EE%) of SAHA inside the nanoparticles was the following:

%EE = [(Drug added - Free "unentrapped drug")/Drug added] *100

3.2.4 Topography analysis with AFM (Atomic Force Microscope)

Atomic Force Microscopy (AFM) technique was employed to assess nanoparticles topography. AFM is a surface-sensitive technique first developed by Binnig and coworkers in 1986, based on the detection of attractive and repulsive forces experienced by the proximity of a sharp tip to a sample (Binnig et al. 1986). In this technique, a tip positioned at the free end of a flexible cantilever responds in the z direction to local changes in the force environment, as the sample is scanned under the tip in the x- and y-directions. A laser beam is directed onto the free end of the cantilever and is reflected onto a photodiode. The variation in force between the tip and the surface, most commonly as a result of the surface topography, causes a change in the deflection of the cantilever, and thus the laser beam is displaced to a different area in the photodiode (*Figure 3.2.4a*). In feedback- controlled modes, these changes are detected and the initial deflection of the cantilever is restored by

the feedback electronics via the piezoelectric scanner, which is vertically moved to minimize the changes in the bending (Contact mode CM) or amplitude (Tapping mode TM) of the cantilever, and these vertical displacements are then recorded to reconstruct the 3-D topography of the sample (Hansma et al. 1989).

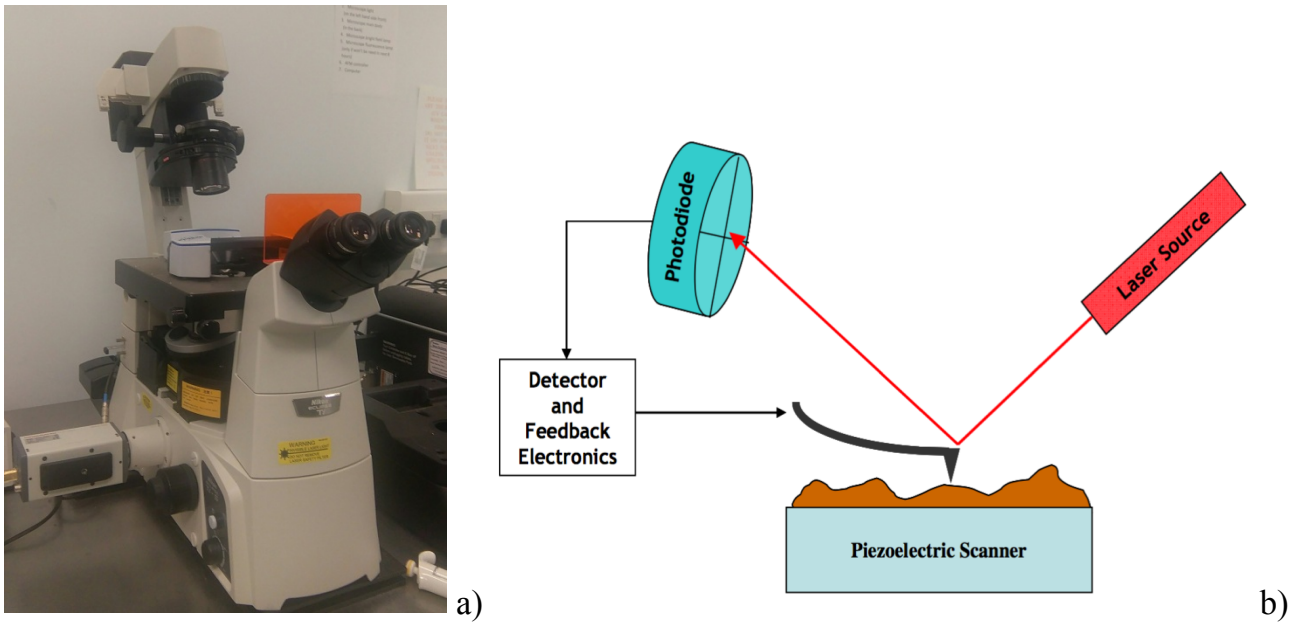

a) b)

Figure 3.2.4a Atomic Force Microscopy (AFM), a) Image of an Atomic Force Microscope, Bruker BioScope Catalyst (Bruker Instruments, Santa Barbara, California, USA). b) Schematic mechanism of functioning of an AFM instrument (Binnig et al. 1986)

According to Hooke's Law:

$$F = -kd$$

where k is the cantilever spring constant and d is the cantilever deflection. Through the knowledge of the deflection of the cantilever and of the spring constant it is possible to calculate the tip-sample interaction force, F. Of the different imaging modes used in AFM, in Tapping Mode (TM), the cantilever oscillates and touches the surface at the lower end of its oscillation cycle and a reduction of the free amplitude of the cantilever is produced. As differences in the local topography lead to differences in the oscillation amplitude, the feedback loop changes the vertical probe-sample distance in order to restore the initial oscillation amplitude and, in this way, a topographic image of the sample is obtained. Oscillating the cantilever in tapping mode means that lateral forces are virtually eliminated. This AFM technique is often more suitable than the Contact Mode (CM) for biological applications since the lateral friction force is highly reduced and a less damage of the sample is produced (Moller et al. 1999).

Peak Force Tapping (PFT) Mode was employed in these experiments. PFT is one of the last scanning techniques introduced by Bruker Instruments (USA), in which the cantilever oscillates in a sinusoidal mode over the sample surfaces at low frequencies (between 0.25-1 Hz), and creates loads of force curves in every pixel of the image.

This technique allows for a better surface tracking of rough samples, coupled with a better control of the force applied during scanning. AFM lateral resolution is the minimal discernible distance by which two objects may be discriminated. This distance is determined by the following equation (Gan 2009);

$$d = \sqrt{2R}\left(\sqrt{\Delta Z} + \sqrt{\Delta Z + \Delta h}\ \right)$$

where d, the minimum distance, depends on the radius of curvature of the tip, R, the vertical resolution, ΔZ, and the relative height of the two objects, Δh.

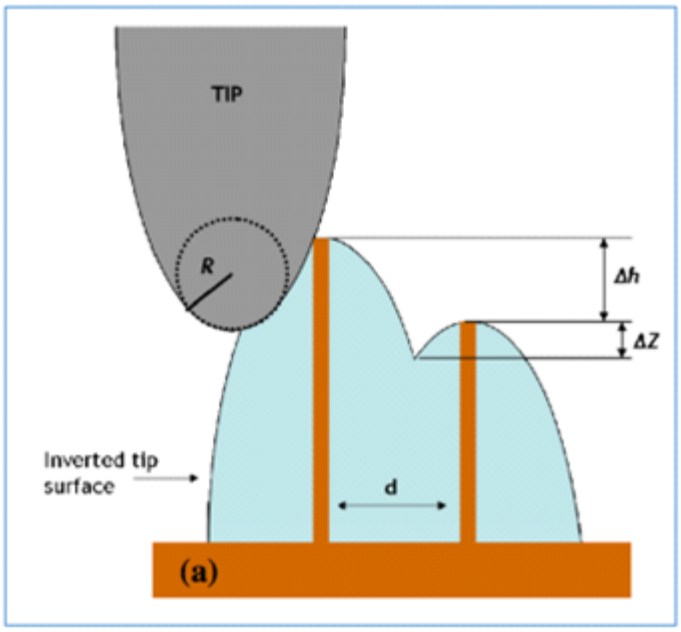

Figure 3.2.4b Image (a) modified after Gan 2009

According to this equation, the tip radius is an important factor that determines the lateral resolution: the sharper the tip, the higher will be the lateral resolution. A lateral resolution at the Angstrom level necessary to yield atomic resolution has been reported in several studies. Due to the finite dimension of the tip, the apparent width of small protruded features is larger than the true value, as illustrated in *Figure 3.2.4b.* This phenomenon is called the tip convolution effect. When imaging small protruding features, these can be contacted by a section of the tip other than the apex and an alteration of the feature shape is produced. Since the effect is governed by the width of the tip, the use of ultra-sharp tips is important to maximize resolution and obtain as true an image of the surface as possible. Although the dimensions of the tip affect the measured x- and y-dimensions of small objects, the measurement of the height of protruding features is not influenced by the tip dimension as only the tip apex interacts with the object. Therefore, to obtain proper measurements of objects, it is more reliable to measure their heights instead of their contours (Abu-Lail & Camesano 2003; Gelinas & Vidal 2010). This is what has been done in this case, and height values were measured.

Procedure for Nps characterization with AFM

10µL aliquots of 1:100 dilutions of 30µg/µL empty F127 nanoparticles in milliQ water (Millipore) were spotted on mica substrates (AGG250-1, Agar Scientific, UK) and let dry at Room Temperature. Topography of the samples was obtained in air using an Atomic Force Microscope, Bruker BioScope Catalyst (Bruker Instruments, Santa Barbara, California, USA). Bruker ScanAsyst-Air cantilevers were used, with a nominal spring constant of 0.4 N/m and a nominal resonant frequency of 70 kHz. All imaging was conducted using Peak Force Tapping (PFT) in ScanAsyst Mode. When the ScanAsyst Mode is activated, the PFT scanning is fully automatized and requires minimum user intervention.
Images were processed with first-order flattening and planefit using Bruker Nanoscope Analysis 1.5, the height of the particles was calculated using the freeware AFM software WsXM 5.0 (Horcas et al. 2007).

3.2.5 Topography analyses with SEM (Scanning Emission Microscopy)

Scanning electron microscopy (SEM) *(Figure 3.2.5a)* can be used to characterize NPs after drug encapsulation (Ven et al. 2012). SEM is an instrument capable of examining relatively thick (so called bulk) specimens by using a narrow electron-beam and offering the advantage of high resolution, high-magnification images of backscattered electrons emitted from sample surfaces. The obtaining images have a high depth-of-field thanks to the narrowness of the excitation beam and can be used to understand nanoparticles topography (Ven et al. 2012).
The beam scans across the sample's surface and different type of electron signals come from the interactions of the electron beam with the sample. The image of the specimen's surface topography is formed by these electronic signals that are processed and translated as pixels on a monitor (Reading & Chapter 2015). Electrons can be reflected (backscattered) from a bulk specimen or can be released as secondary electrons after they supply energy to the atomic electrons of the sample. A scanning principle is used: primary electrons are focused into a smaller-diameter probe that is scanned across the specimen and its direction of travel can be changed thanks to an electrostatic and magnetic field applied to the beam. The scanning occurs simultaneously in two perpendicular directions in order to cover a rectangular area (so called raster) forming an image by collecting secondary electrons from each point on the specimen (Physical principles of electron microscopy).

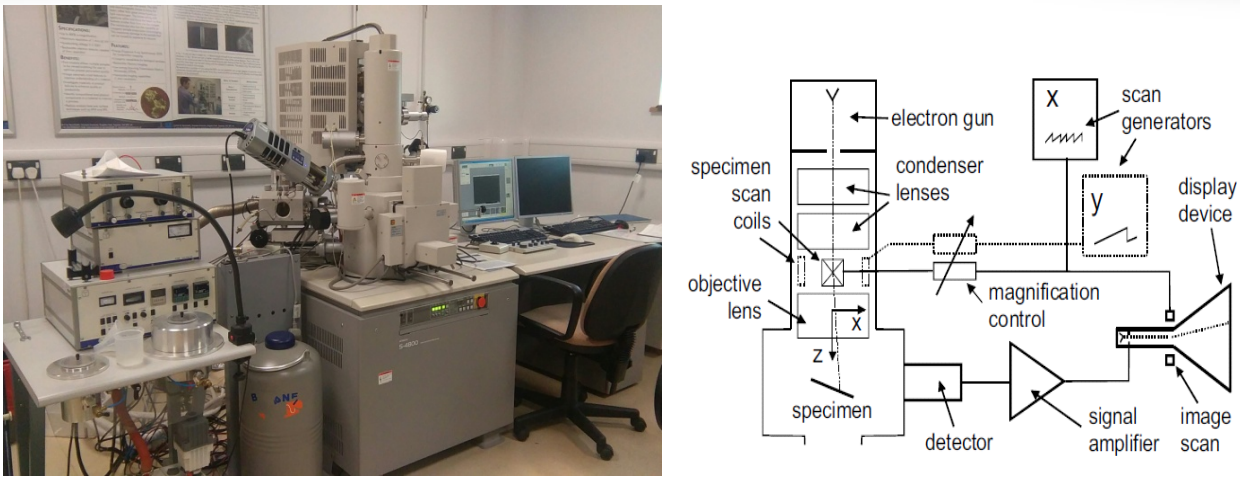

Fig.3.2.5a. Scanning Emission Microscope. An image of the SEM Hitachi S-4800 (on the left), a schematic diagram of a scanning electron microscope with a CRT display (on the right) (Ray F. Egerton).

Elastic or inelastic scattering occur when accelerated electrons enter a solid due to electrostatic interaction with atomic nuclei and with atomic electrons. A small part of primary electrons are elastically backscattered (deflection angle more than 90°) with small loss of energy. These electrons can leave the specimen thanks to their high kinetic energy and re-enter the surrounding vacuum where they are collected as backscattered-electron (BSE) signal. Inelastic scattering (deflection angle less than 90°) contribute little to the BSE signal.

The penetration depth (or electron range *R)* for electrons is given by the following approximate formula:

$$\rho R \approx a E_0^r$$

where *E*0 is the incident energy of the electrons, ρ is the density of the specimen, and a ≈ 10 ug/cm^2. Electron range R is inversely proportional to Z (atomic number), it decreases with Z, as the densities of solids tend to increase with atomic number. Therefore, the interaction volume, volume of sample containing scattered electrons, is bigger for materials with smaller atomic number and becomes small at low incident energy (Figure 3.2.5.c).

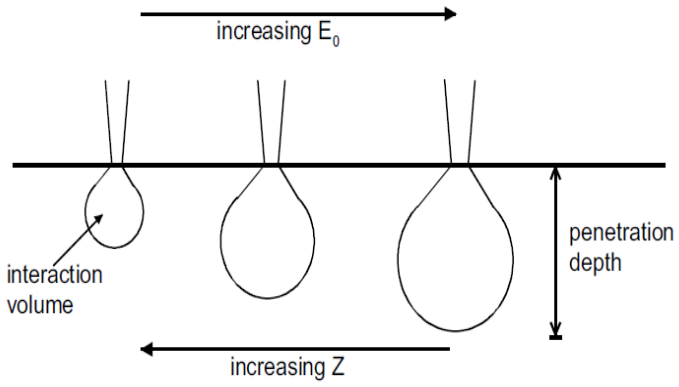

Fig3.2.5.c Schematic dependence of the interaction volume and penetration depth as a function of incident energy E0 and atomic number Z of the incident (primary) electrons (Ray F. Egerton).

Procedure for NPs characterization with SEM

50 µL of nanoparticles solution was deposit on a small piece of monocrystalline silicon and left it to evaporate for two days in a petri dish. The following day, the alluminium stub with a bioadhesive carbon tape, that is conductive, was prepared and the monocrystalline silicon piece with the nanoparticle solution evaporated was placed on it. Before the SEM analyses, the samples were placed in the vent chamber in order to realize the vacuum, and then covered with Chromium (5nm of thickness) for 10 minutes at a pressure of about 3 Bar (0-4 Bar). For nanoparticles characterization of this project was used SEM Hitachi S-4800.

3.2.6 Confocal Microscopy analysis

Confocal microscopes were developed in 1957 by Marvin Minsky who was working for neural network computing and artificial intelligence at Harvard University. This revolutionized the face of research facilitating investigations on molecules, NPs, cells, tissues and solved the problem related to the conventional wide-field fluorescence optics as bright fluorescent signals from objects outside the focal plane increase the background and give low-contrast images. In confocal microscopes the specimen is illuminated with a focused scanning laser beam and a pinhole aperture is placed in the image plane in front of an electronic proton detector *(Figure 3.2.6a)*.

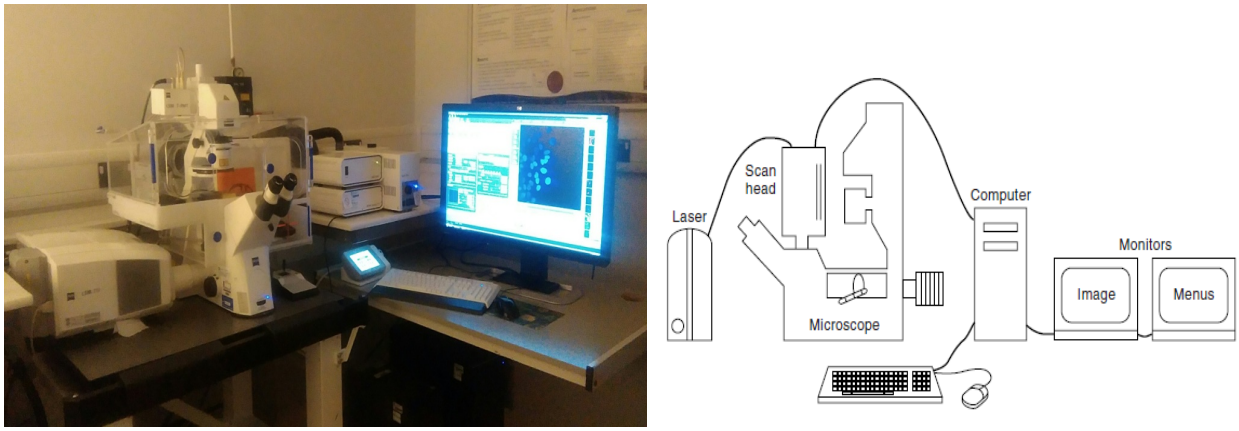

Figure 3.2.6a Confocal Microscope. An image of the Confocal Microscope Zeiss LSM 710 (on the left), basic components of a confocal laser scanning microscope (CLSM) (on the right) (Douglas B. Murphy).

The scan head generates the photon signals required to create the confocal image, it contains the following devices: inputs from one or more external laser light sources, fluorescence filter sets, a galvanometer-based raster scanning mechanism, one or more variable pinhole apertures for generating the confocal image, a photomultiplier tube (PMT) detectors for different fluorescent wavelengths (Dougals 2001).

The pinhole aperture is the crucial part of the confocal optics, which accepts fluorescent photons from the illuminated focused spot in the raster excluding fluorescence signals from objects above and below the focal plane. The pinhole eliminates much of the stray light in the optical system and is essential for producing the confocal image. In *Figure 3.2.6b,* it is reported the optical pathway in a confocal scan head. A laser beam is reflected by a dichroic mirror onto components of the scan-control mechanism that sweeps the beam in a raster back and forth across the specimen. The fluorescent light is collected by objective lens and is scanned at the scan control, transmitted through the dichroic mirror and emission (barrier) filter, and passed through the pinhole to a photomultiplier tube.
The excitation wavelengths from a laser point source are confocal with a scanning point in the specimen. Fluorescent wavelengths emitted from a point in the specimen are focused as a confocal point at the detector pinhole. Fluorescent light emitted at points above and below the plane of focus of the objective lens is not confocal with the pinhole and forms extended disks in the plane of the pinhole. Since only a small fraction of light from out-of-focus locations is delivered to the detector, out-of-focus information is largely excluded from the detector and final image. The dichroic mirror and barrier filter performs the same functions as in a wide-field epifluorescence microscope (Douglas 2001).

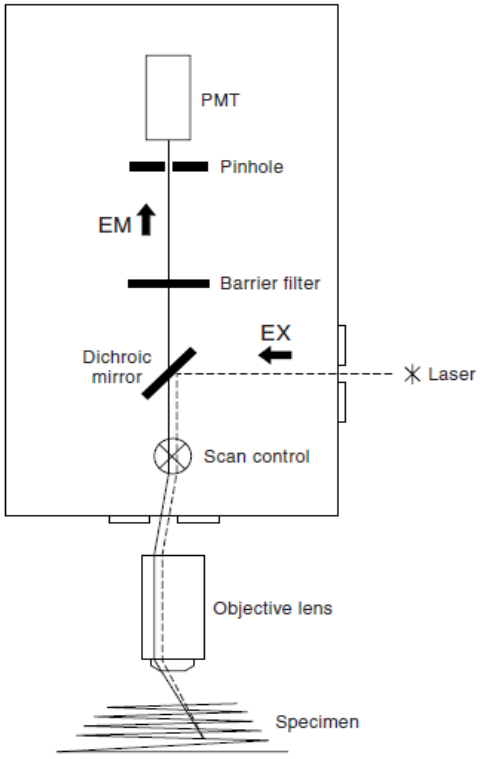

Figure 3.2.6b Optical pathway in a confocal scan head.
EX and EM indicate the paths taken by the excitation and fluorescence emission wavelengths (Douglas B. Murphy)..

A confocal microscope is able to focus in 100nm steps along the z-axis and acquire a stack of images or z-series at different focal planes generating a three-dimensional view of the

sample. Stacks acquired at regular time intervals give the possibility to construct dynamic events in a cell in three dimension using computer software (Ray & Mitra 2017).

Procedure for NPs characterization with Confocal Microscopy

Imaging Chambers CG with microscope slides (8wells chamber, put the company and the cat number) were used in order to characterize the samples using the Confocal Microscope Zeiss LSM 710. After the cell count using the cell counts TC10, 30,000 cells were seeded in each well and the chamber was incubated at 37.0 °in a 5% carbon dioxide (CO2) humidified incubator (Galaxy 1705, New Brunswick, UK) overnight.
The day after, the cells were washed with phosphor-buffered saline (PBS) (-Mg2+, Ca2+) (GIBCOTM,UK) and treated with PI nanoparticles suspension at different concentrations starting from the stock (30mg/ml, 10mg/ml, 3,33mg/ml,1,11mg/ml,0.37mg/ml and 0.12mg/ml). After 24 hours of incubation at 37°C as previously, 400ul of 70% methanol were added to one of the control well for 5 minutes. After PBS wash, 400ul of PI dye previously prepared in PBS (0.4 mg/ml) were added to it and to a second control well. After 1 hour of incubation, all wells were washed with PBS and 200ul of 4% PFA (paraformaldehyde) were added for 10 minutes in the cold room (4°C) for fixation purpose. The cells were then washed with PBS and treated with 200ul of DAPI(Hoechst 33342, trihydrochloride trihydrate16.2mM) /PBS solution for each well for 10 minutes in the incubator. Each well was washed for the last time and replaced with 400ul of PBS before analysis.

3.2.7 Incell Analyser 2000 studies

The IN Cell Analyzer 2000 (*Figure 3.2.7a)* is an automated microscope designed for fast, automated imaging and analysis of fixed and live cells. The primary imaging mode is fluorescence microscopy.

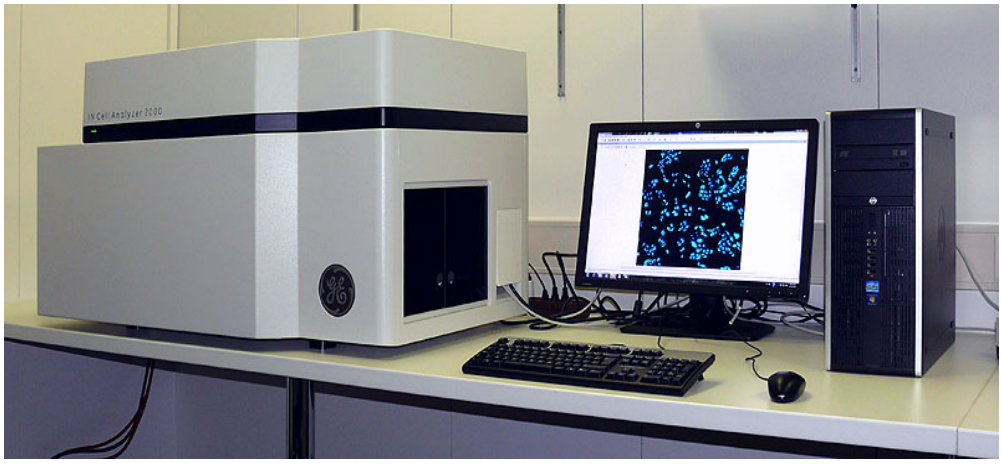

Figure 3.2.7a IN Cell Analyzer 2000 system, UK. A pseudo confocal, high content screening fluorescent microscope with three channel captures was used to capture the stain intensities.

In fluorescence microscopy, the sample, for example a human cell, is usually stained with one or more dyes that bind to certain structures of interest within the sample. During

imaging, the samples is illuminated by light of a specific wavelength and when the dyes are illuminated with a specific wavelength of light, they are designed to fluoresce and the fluorescent light that is emitted is also of a specific wavelength. The fluorescent light emitted by the sample is gathered by an objective lens and various optics are used to direct the light towards a very sensitive camera (in the *IN Cell Analyzer 2000* this is a CCD camera, and in the *IN Cell Analyzer 2200* an sCMOS camera). Thanks to this camera it is possible to visualize the appearance and position of structures in the sample. The workstation is a computer system used for controlling the *IN Cell Analyzer 2000*. The workstation runs software for defining and setting up imaging experiments, conducting experiments, and analyzing the resulting images.

An *IN Cell Analyzer 2000*, includes: a multispectral illumination, excitation filters that excite one fluorophore at a time, polychroic QUAD band mirrors to direct excitation light up though the objectives toward the sample, an objective turret - Fitted with four objectives including up to two objectives containing automated spherical aberration collars, a laser autofocus module. A laser beam is directed through the objective and is focused on the target. While the Z-axis is moved, a photo sensor monitors the reflected beam to determine the exact position of the target. This information is fed back to the control computer so that subsequent images taken of the sample are in the best plane of focus. Furtheromore there is a stage; a carrier plate where the sample is placed in and it is moved over the optics to image different areas of the sample. The carrier plate rests on a smooth stage plate to ensure consistent motion. Emission filters are used to select particular colors of light to allow the emitted light from only one fluorophore to reach the camera and a cooled sCMOS camera is used to capture the light and create images. The imager contains an on board computer and multiple custom circuit boards to receive commands from the workstation and convert those commands into motion and images and the imager is enclosed with cover pieces to keep out light and dust.

Procedure for Incell Analyzer 2000 characterization

Propidium Iodide, as an example of hydrophobic drug, was also encapsulated in Pluronic F127 nanoparticles to confirm the stability of this delivery system. A 12 well cell culture plate was used in order to characterize the samples using the Incell Analyzer 2000 system. 25000 cells in 3ml volume were seeded in each well and the chamber incubated at 37.0 °in a 5% carbon dioxide (CO2) humidified incubator (Galaxy 1705, New Brunswick, UK) overnight. The day after, the cells were washed with phosphor-buffered saline (PBS) (-Mg2+, Ca2+)(GIBCOTM,UK) and treated with PI nanoparticles suspension at different concentrations starting from the stock (30mg/ml, 10mg/ml, 3,33mg/ml,1,11mg/ml,0.37mg/ml and 0.12mg/ml). Two controls wells were left with only cells. After 24 hours of incubation at 37°C as previously, 1ml of 70% methanol were added for 5 minutes to a well containing. This well was washed with PBS and then, 1ml of PI dye previously prepared in PBS (0.4mg/ml) were added to it and to the second control well. After 1 hour of incubation, all wells were washed with PBS and 500ul of 4% PFA (paraformaldehyde) were added for 10 minutes in the cold room (4°C) for fixation purpose. The cells were then washed with PBS and treated with a solution previously prepared with 8ml of PBS and 1uL of DAPI

(Hoechst 33342, trihydrochloride trihydrate,16.2mM). A volume of 500ul of DAPI/PBS solution was added in each well and kept for 10 minutes in the incubator. Each well was washed for the last time and replaced with 400ul of PBS before analysis.

3.2.8 Dialyses release method

A static dialysis bag system is usually created to study the release and diffusion of a component in an other solution. The model formed by two compartiment divides two different environments and due to the osmotic pressure part of the first component cross the semi-permeable membrane by reaching the second acqueous solution in order to simulate the release of the drug (*Figure 3.2.8).*

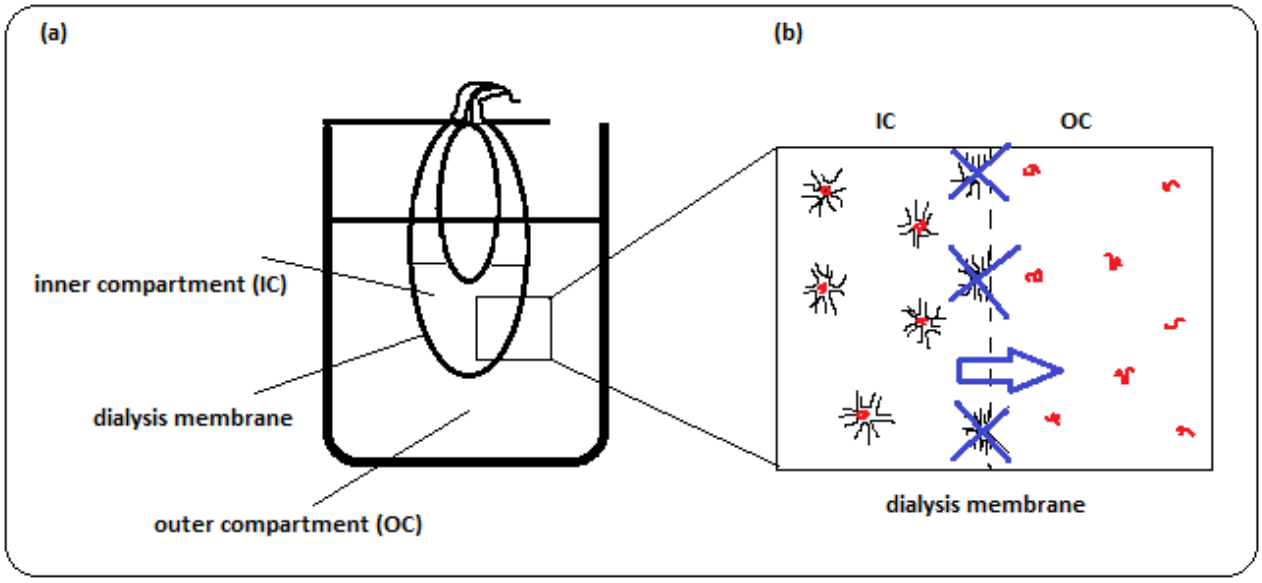

Figure 3.2.8 Schematic illustration of the two-compartment static dialysis bag model over 96 hours (a) and the hypothesized release of Saha drug (b).

To measure the release profile of Saha from nanoparticles, 5mL of Saha Nps solution at a concentration of 100μM was inserted into a pre-hydrated dialysis bag with a molecular weight cut-off of 2 kDa (Pierce, Rockford, IL, USA) and subjected to dialysis against 50 mL of phosphate-buffered saline (PBS) with gentle stirring at 37°C. At the indicated times – every hour for the two first days and every 3 hours the 3rd and last day – 0.2 mL of solution was removed and mixed with an equal volume of DMSO to dissolve the NPs. The samples were analyzed with Fluo Star Omega Spectrophotometer (FLUOstar Omega, BMGLabtech) by measuring the absorbance at 284nm (37°C) placing a 96 well-plate in the Fluo Star Omega Spectrophotometer (FLUOstar Omega, BMGLabtech). The measurements were taken in triplicate, a standard curve was created diluiting Saha drug in PBS at different concentration and PBS (phosphate buffered saline) and DMSO (Dimethyl Sulfoxide) were used like controls.

3.3 Cell culture - Endometrial epithelial cancer cell lines (EEC)

3.3.1 EECs origin

Ishikawa and Hec50 were cultured and used to establish a basal in vitro cell line. Derived from a well differentiated endometrial adenocarcinoma, Ishikawa cells are the best characterised of all endometrial cell lines (Nishida et al.1985). Ishikawa cells have a doubling time of up to 36hrs, display mixed characteristics of glandular and luminal epithelium and express functional steroid receptors for progesterone and estrogen (Albitar et al. 2007)(Croxtall et al. 1990; Boehme et al. 2009). Considered a good model for receptive human endometria, Ishikawa cells have been shown to facilitate adhesion of embryo derived cells (Heneweer et al. 2005). Originally isolated from a metastatic lesion in the peritoneal cavity, in a patient with advanced disease, Hec50 cells form sheets of undifferentiated cells in culture with a much more rapid doubling time than Ishikawa cells (Albitar et al. 2007). Hec50 are PR negative and lack an estrogen response (Davies et al. 2004). This may be due to structural or functional alterations in the ER protein resulting in a loss of its capability to undergo the estrogen-directed conformational changes required for biological activity (Kassan et al. 1989).

3.3.2 EEC cell lines and mediums

Commercially available Ishikawa and Hec50 EEC cell lines were obtained from the American Type Culture Collection (ATCC). All cell culture work was undertaken utilizing appropriate aseptic techniques in ventilated tissue culture hoods (Scanlaf, Mars Safety Class II). Cell lines were maintained in commercially available DMEM/F- 12 (Dulbecco's Modified Eagle Medium/Nutrient Mixture F-12) + Glutamax™ full media (GIBCO™,UK) supplemented with 10% fetal bovine serum (FBS) and 1% antibiotic-anti-mycotic solution in Sigma® plastic culture flasks (GIBCO, UK; 25cm^2, 75cm^2, 125cm^2) at 37.0 °C and 5% CO_2 incubator (Nuaire). For some experiments (Real-Time Glo, Western Blot) the use of DMEM/F-12 without phenol-red (GIBCO™,UK) was required. Cells were supplemented with free, full serum media every 2 days and passaged when confluent. Cells were sub-cultured a minimum of two passages prior to treatment, to ensure reproducibility. Prior to each treatment cells were serum starved in their relevant stripped media containing 10% dextran-coated charcoal-treated fetal bovine serum (DCC-FBS) for 24 hours.

3.3.3 Passage of EEC cell lines in culture

Cells were passaged when confluent (minimum 80% confluency) according to inverted light microscope observation (Primo Vert, Zeiss). All media were thawed and storage in the 37°C water bath and the tissue culture hood and each reagents were properly clean with methanol in order to avoid every possible infection during the passage of the cell lines. The Media

was removed and cells were washed with phospho-buffered saline (PBS) (-Mg^{2+},-Ca^{2+}) (GIBCOTM,UK) to remove residual medium. PBS and residual media was then aspirated and cells were incubated in 2.5ml Trypsin-EDTA (0.25%) C and for 5 minutes (or until the cells appeared rounded and detached) at 37.0 °in a 5% carbon dioxide (CO_2) humidified incubator (Galaxy 1705, New Brunswick, UK) . Trypsin cleaves E-cadherin and other adhesion proteins freeing the cells from plastic surface of the culture flask. Culture flasks were agitated to allow cells to detach and visualized using an inverted light microscope (Primo Vert, Zeiss). 10ml of media was added to neutralize the trypsin inhibiting its action and the resulting cell suspension was split into two centrifuge tubes and centrifuged at 1000 rpm for 5 minutes. The supernatant culture media was then aspirated and the pellet was resuspended in 8ml of pre-warmed DMEM/F-12 + GlutamaxTM media (GIBCOTM) in order to achieve a uniform distribution of the cells (Cell and media suspension). According to the required dilution for confluency in a required number of days, the ratio of cell and media suspension was mixed in 10ml of fresh full serum media and added to a new clean T75 flask.

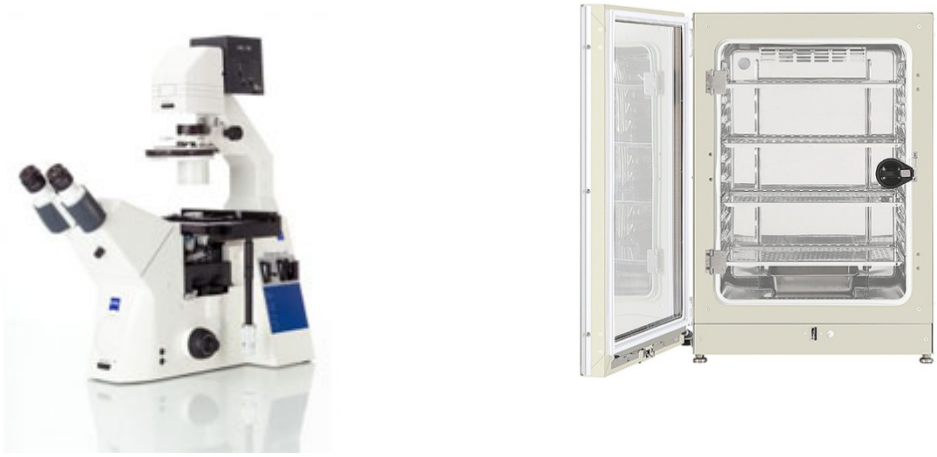

Fig.3.3.3 inverted light microscope observation (Primo Vert, Zeiss) on the left and a 5% carbon dioxide (CO_2) humidified incubator (Galaxy 1705, New Brunswick, UK) on the right.

3.3.4 Cell treatments

Cell treatments for RTM Glo study	Concentration of Nps solutions (µM)
Free Saha	2.5
F127 Saha Nps	2.5
F 127 SS Saha Nps	1.25 – 2.5
F 127 SS HA Saha Nps	1.25 – 2.5
F 127 SS HA empty Nps	1.25 - 2.5 – 6.25 – 25

Cell treatments for Western Blot study	Concentration of Nps solutions (μM)
Free Saha	2.5
F 127 Saha Nps	2.5
F 127 empty Nps	2.5
F 127 SS Saha Nps	1 – 2.5
F 127 SS HA Saha Nps	1 – 2.5
F 127 SS HA empty Nps	1 – 2.5
F 127 SS HA empty	2.5

Table 3.3.4 Cell treatments. This table summarize all the nanoparticles solutions at different concentrations used to treat the cells (Hec50 and Ishikawa) for Real Time Glo analyses and for Western Blot studies.

Saha was purchased in powder form from Sigma, UK, catalogue number. Lyophilized powder was reconstituted in DMSO to a stock concentration of 10mM, aliquoted and stored at -20°C until needed. For Saha-encapsulated nanoparticle fabrication, Saha powder was directly employed; stored at -20°C. Cells, when confluent, were separately treated with either Saha free drug, F 127 empty nanoparticles, F 127 Saha nanoparticles, F 127 SS Saha nanoparticles and F127 SS HA Saha nanoparticles . A control with non-treated cells was always required. Cells were processed for further downstream applications like protein analysis (Western Blot) and cytotoxicity evaluation (Real-Time Glo assay), and they were put in a 6-well plate or in a 96-well plate (Costar, Corning Incorporated). For Western Blot applications, cells at a concentration of 50,000cells/ml were treated with 2.5μM of free Saha, 2.5μM of F 127 empty nanoparticles, 2.5μM of F 127 SS HA Saha-encapsulated nanoparticles, 2.5μM of F127 Saha-encapsulated nanoparticles in Stripped Media, 1 μM and 2.5μM of F 127 SS Saha-encapsulated nanoparticles and 1 μM and 2.5μM of F 127 SS HA Saha-encapsulated nanoparticles. The treatment was left on the cells for 48h (3ml of cells and media suspension per well), after which proteins were extracted and quantified (view *Section **3.4***).

For Real Time Glo applications, cells when confluent, were re-suspended in Stripped Media and plated in a 96-well plate at a concentration of 500 cells/well and a volume of 100ul: they were then incubated in a cell culture incubator at 37°C and 5% CO_2 for 24 hours. After this step, different sets of micro-molar concentrations of free drug and nanoparticles (see Results section) were added and left over a period of maximum 96h (measurements were taken at 0h, 24h, 48h, 72, 96h).

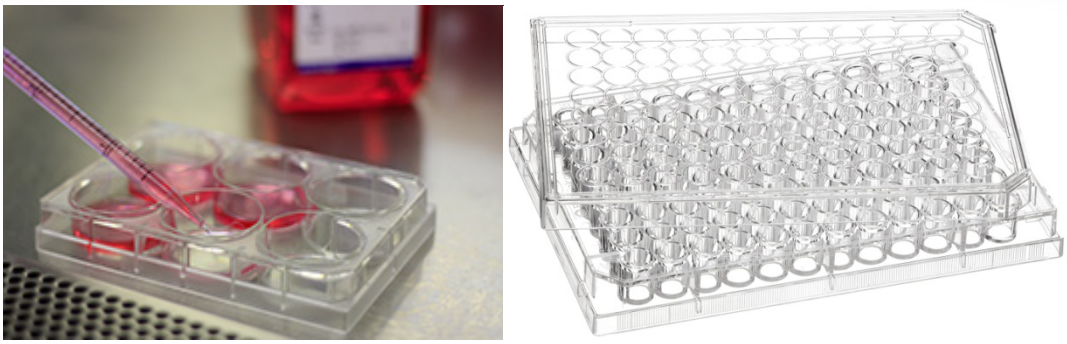

Fig.3.3.4 Example of a 6-well plate on the left and a 96-well plate in the right.

3.4 Western Blot

Western blot is a fundamental technique used in cellular and molecular biology, used for identifying the presence of a specific protein in a complex mixture of polypeptides extracted from cells. This procedure is based on 3 key elements:

protein extraction and quantification, protein separation using an SDS-PAGE (*Sodium Dodecyl Sulphate Polyacrylamide Gel Electrophoresis*); protein transfer on a PVDF membrane followed by specific protein identification using antibodies. More than one antibody can be used. Proteins are then visualized as bands, using a detecting instrument called ChemidocTM MP System.

3.4.1 Protein Extraction and Quantification

Cells treated with the free drug (Saha) or with the empty/encapsulated nanoparticles were washed 3 times in PBS (3ml per well) and each well was then treated for 10 minutes with 60µl of lyses buffer: it is kept on ice and it is composed of RIPA buffer (Sigma Aldrich) mixed with a cocktail of protease and phosphatase inhibitors, which lead to cellular lysis. Each well with the cells and the buffer was then vigorously scraped prior to solution collection into a 1.5ml Eppendorf tube and left for 30min in agitation on ice: during this period, they were vortexed every 5min. The tubes in which cells were collected were then centrifuged for 10min at 10000rcf in a pre-cooled centrifuge (4°C). The supernatant was then collected and stored at -80°C and the pellet discarded.

The following step was protein quantification, using *BioRad DCTM Protein Assay*: 8 different dilutions of BSA from a stock of 300µg/ml were used to build a standard curve and proteins were diluted 1:5 in ddH2O. In each of a 96-well plate, the following amounts were put in order: 5ul of proteins/BSA dilutions/water (blank), 25ul of Reagent AS (Bio-Rad, made of reagents S and A in a 1:50 ratio) and 200µl of Reagent B (BioRad). Each measure was taken in triplicate. The reagents were mixed thoroughly by gently agitation and the plate was left in the dark for 15 minutes before being placed in the Flu Star Omega Spectrophotometer. The absorbance was read at 750nm using a Spectrophotometer

(FLUOstar Omega, BMG Labtech) (*Figure 3.4.1).* The protein concentration was obtained from the standard curve and used to calculate the amount needed for the following stages.

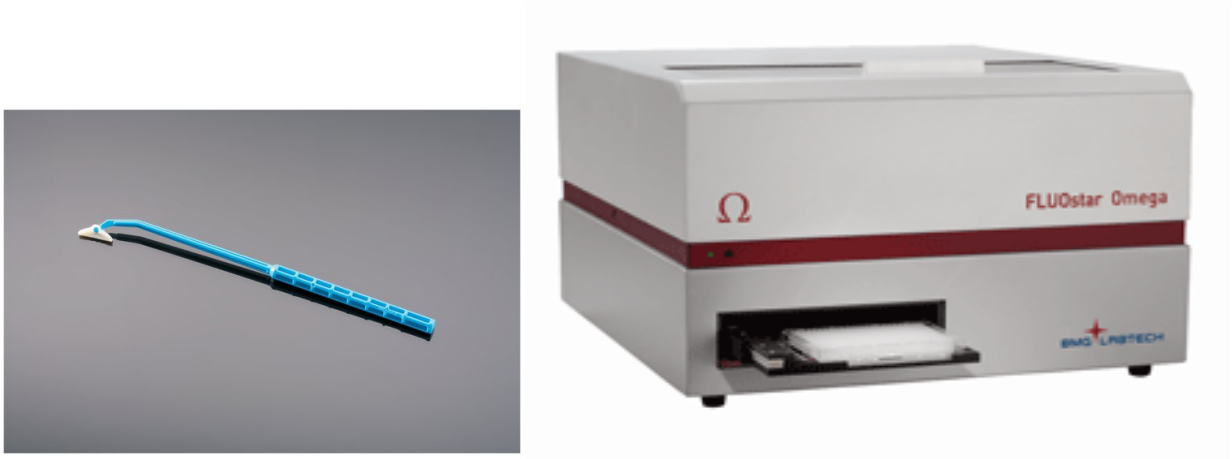

Figure 3.4.1 Example of cell scaper used for protein extraction on the left and the Spectrophotometer FLUOstar Omega used for protein quantification on the right.

3.4.2 Protein Separation by Gel Electrophoresis

After quantification, proteins were separated through Sodium Dodecyl Sulphate Polyacrylamide Gel Electrophoresis (SDS-PAGE). A precast MINI-PROTEANÒ TGX Stain-FreeTM 4- 20% gel was used. To prepare the protein samples for gel electrophoresis (gel running), 10ug of the extracted proteins were mixed with Laemmeli 2X solution (made up of β-mercaptoethanol and Laemmeli 2x in a ratio 1:20) and RIPA Buffer in order to obtain a final volume of 20µl. Laemmeli 2x buffer contains glycerol and bromophenol blue: glycerol causes the samples to sink to the bottom of the gel's well and bromophenol blue is a tracking dye which migrates through the gel first and provides a good indication of how far the proteins have travelled. Laemmeli buffer also contains SDS detergent, which fully denatures proteins and removes all higher ordered structures as well as causing the protein to become uniformly negatively charged, allowing it to migrate towards the positive electrode during the electrophoresis process. Beta mercaptoethanol reduces disulfide bridges of proteins.
After the addition of these components, the samples were then spun in the Galaxy Ministar to ensure the solution was mixed thoroughly and incubated at 95°C for 5min in a Thermal Cycler to denature proteins. The program was set to the Proximo program on the thermal cycler. Only 200µL tubes were used since they are the only ones able to fit in the Thermal Cycler (*Figure 3.4.2).* The sample was then heated at 95°C for 6 minutes and rapidly cooled at 12 °C so that the protein becomes denatured in the Thermal cycler.

Figure 3.4.2 Thermal cycler machine

3.4.3 Protein transfer to Membrane

After the electrophoresis process, the gel with the separated proteins were transferred to polyvinylidene fluoride (PVDF) membrane (Trans-BlotR Turbo™ Mini PVDF Transfer Packs, Biorad) using a Transblot turbo machine (Transfer System Bio-Rad) (*Figure 3.4.3a)*. The Transfer Packs used include an optimized buffer, membrane, and filter paper combination that provides superior blot transfers when paired with the Trans-Blot blotting

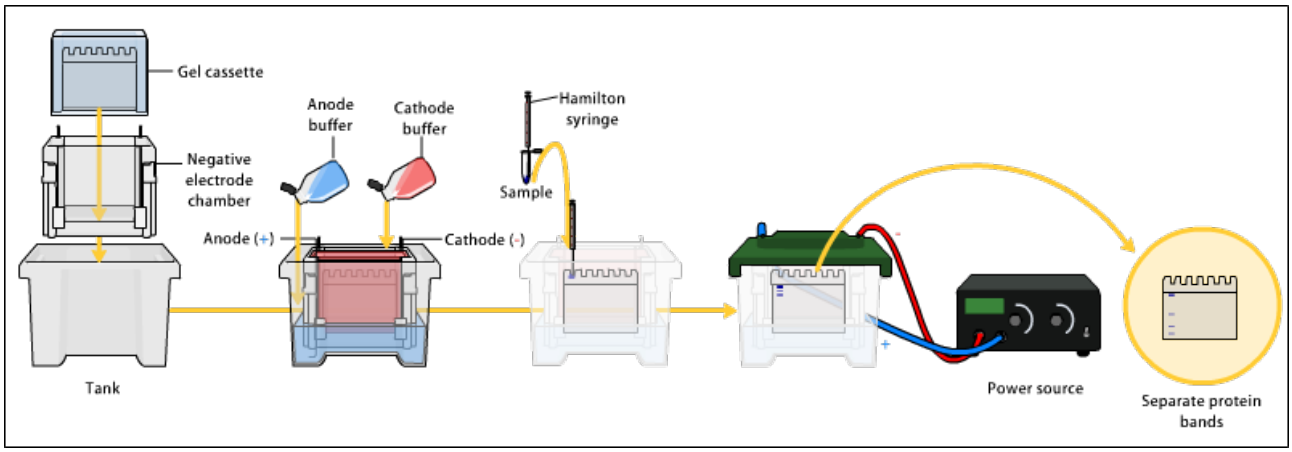

Figure 3.4.3a Procedure for protein separation using an SDS-PAGE (Sodium Dodecyl Sulphate Polyacrylamide Gel Electrophoresis); protein transfer on a PVDF membrane. (Anode buffer and Cathode buffer are the same).

apparatus *(Figure 3.4.3b)*. Immuno-Blot PVDF has a strong binding capacity of 150–160 µg/cm^2, which is roughly twice that of nitrocellulose. The gel was taken out from the running system, put directly on the Transfer pack and programmed to run for 3 minutes at 2.5A and 25V, in order for the proteins to be transferred from the gel onto the membrane.

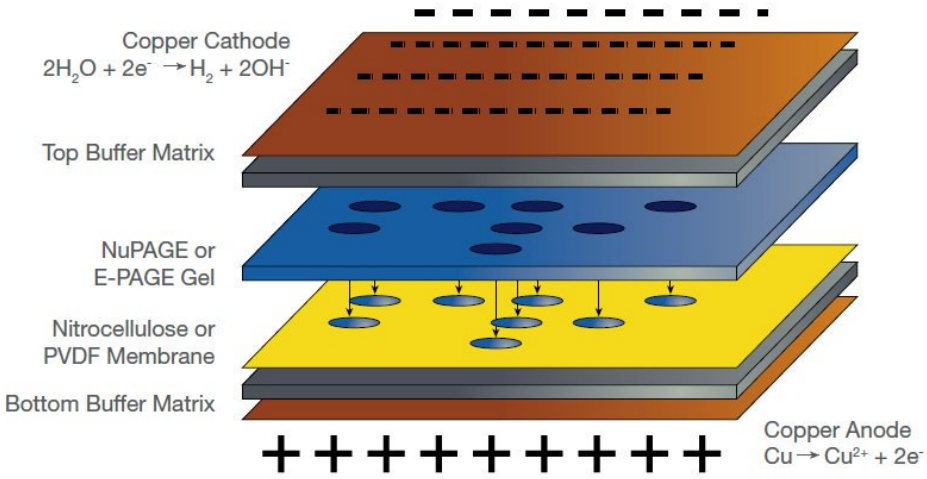

Figure 3.4.3b Layout of components for Protein Transfer from Electrophoresis Gel to PVDF membrane

3.4.4 Protein Detection

After proteins had migrated from the gel to the membrane it was possible to cut the membrane depending on the molecular weight of the proteins of interest. The membranes were then placed in individual trays and submerged in 3ml of Blocking Buffer (*Table 3.4.4*) made of 5% BSA in 1X TBS/T Wash Buffer for 1 hour on a seesaw rocker at 30osc/min. The BSA blocking buffer is used to prevent unspecific binding. The membranes were then submerged in 3ml of primary antibody in blocking buffer overnight at 4°C on a rocking table at 25 oscillations per minute (osc/min). The antibodies employed and their concentrations are described in *Table A*. Following incubation, the membrane was washed 3 times with 3ml of TBS/T 1X, and it was then incubated with secondary antibody (Anti-rabbit and anti-mouse IgG HRP, *Table A*) for at minimum 1 hour at room temperature rocking slowly on rocker machine at 30osc/min. The membranes were then washed with TBS/T 1X every 5 minutes, 3 times at room temperature and a fast rocking rate.

Antibody Name	Manufacturer	Species	Final Concentration
GAPDH	Santa Cruz sc-25778	Mouse	1:1000
N-cadherin	Abcam ab12221	Mouse	1:1000
E-cadherin	Abcam ab1416	Mouse	1:1000
p 21	Cell Signaling #2497	Rabbit	1:1000
p 53	Cell Signaling #9282	Rabbit	1:1000
Anti-mouse IgG HRP	Ge Healthcare NA931V	Sheep	1:2000
Anti-rabbit IgG HRP	GE Healthcare NA934V	Donkey	1:2000

Table 3.4.4 Antibody Name, Manufacturer, Species of origin and Concentration used for Western Blot reactions

The membranes were then taken to the ChemiDoc machine to observe the protein composition of the sample. The membranes were covered with approximately 1000 microliters of each of the two Clarity Western ECL substrates (Bio-Rad; 170-5060 and 170-5061) and incubated for 1 min at room temperature in Biorad enhanced Chemiluminescence (ECL) stain. The secondary antibodies used are coupled with horseradish peroxidise (HRP) label, and the ECL stain contains the substrate luminal which is oxidized by HRP to produce light. The light emitted from this reaction produces a protein band, which was visualized using a ChemidocTM MP imaging system (Biorad) after placing the membranes on the surface of the ChemiDoc and adjusting accordingly to be fully observed.

Figure 3.4.4 ChemiDoc machine for Western Blot analyses (Biorad).

3.4.5 Western Blot Data Analysis

Fluorescent bands were analysed using ImageLab software (Biorad). The volume rectangle tool was used to draw around bands and background, and to quantify band intensity by calculating signal intensity/area mm^2. The housekeeping protein, GAPDH, was run against all samples and quantified in the same way, and its density was used as a reference to normalise protein concentrations. The volumes were then plotted on a Microsoft Excel graph.

3.4.6 Solutions for Western Blot

The different buffers used for these experiments were the following (*Table **B***): *Tris/Glycine/ SDS 10X* solution (also Running Buffer 10X) was made of 30.3g of Tris Base, 144.1g of glycine, 50ml of SDS 20% and added of ddH2O to 1L. The *Running Buffer 1X* solution was made adding 100ml of Running Buffer 10X solution to 900ml of ddH2O. *TBS/T Wash Buffer 1X* was made of 950ml ddH20, 30ml of NaCl 5M, 20ml of Tris 1.5M at pH 7.5 and 1ml of Tween 20 100%. *BSA Blocking Buffer 5%* solution, used for blocking unspecific antibodies from binding to the membrane and also to dissolve the antibodies in, was made of 250ml of TBS/T Buffer solution and 12.5g of BSA.

Reagent Name	Component	Quantity
Tris/Glycine/SDS 10X (Running Buffer 10X)	Tris Base	30.3g
	Glycine	144.1g
	SDS 20%	50ml
	ddH2O	950ml
Running Buffer 1X	Running Buffer 10X	100ml
	ddH2O	900ml
TBS/T Wash Buffer 1X	ddH2O	950ml
	NaCl 5M	30ml
	Tris 1.5M pH 7.5	20ml
	Tween 20 (100%)	1ml
BSA Blocking Buffer 5%	TBS/T Wash Buffer 1X	250ml
	BSA	12.5g

Table 3.4.6 Buffer reagents, Components and Quantities used in Western Blot

3.5 Real-Time GloTM MT Cell Viability Assay

RealTime-GloTM MT Cell Viability Assay is a non-lytic and bioluminescent method used to measure cell viability in real time. This kit was used to assess cytotoxicity of SAHA free drug and different nanoparticle formulations on endometrial cancer cells.

3.5.1 Assay mode of action

This kit assesses the number of viable cells in culture by measuring their reducing potential and thus metabolism (MT). It involves adding to culture cells a luciferase enzyme (NanoLucR) and a cell-permeant pro-substrate, (the MT Cell Viability Substrate): active and viable cells will process the pro-substrate and generate a substrate for NanoLucR luciferase, which diffuses from cells into the surrounding medium and it is used by the NanoLucR Enzyme to produce a luminescent signal. The signal directly correlates with the number of viable cells, making the assay well suited for cytotoxicity studies. The mechanism involved in this process is shown in *Figure 3.5.1.*

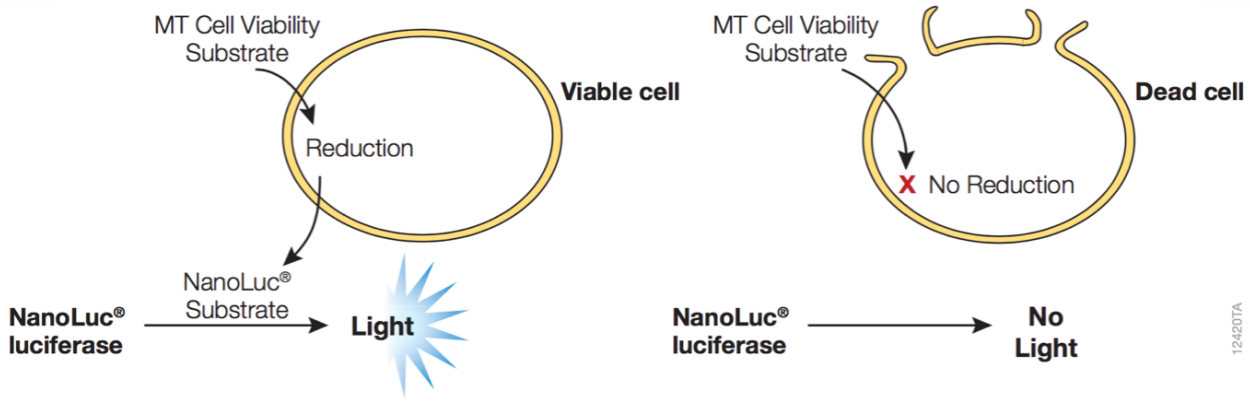

Figure 3.5.1Mechanism of Real-Time GloTMMT Cell Vianility Assay (RealTime-GloTM MT Cell Viability Assay)

This assay presents a variety of advantages over other cytotoxicity assays, including a superior sensitivity and flexibility, the possibility of doing Real-time measurements, and the non-lytic format which allows to perform downstream assays consequently.

3.5.2 Protocol Description for Real-Time Glo

Cells, when confluent, were re-suspended in Stripped Media and plated in a 96-well plate at a concentration of 500 cells/well and a volume of 100ul: they were then incubated in a cell culture incubator at 37°C and 5% CO_2 for 24 hours. The number of cells were calculated by first obtaining the concentration per milliliter by using the TC20TM Automated Cell Counter (1450102 Bio-Rad) *(Figure 3.5.2)* and using the equation $\mathbf{C_1V_1=C_2V_2}$ to calculate the volume needed for the specific number of cells.

On the following day, after equilibrating them to 37°C, the MT Cell Viability Substrate (previously melted and mixed properly) and NanoLucR Enzyme (both at a 1000X concentration) were added to stripped medium (in the ratio of 1:500 of media), together with the treatments of interest (free drug or nanoparticles) at a 2X concentration.
This medium was then added to the wells in order to obtain a 1X concentration of the two substrates. The plate was left in the incubator for up to 96 hours. Every 24 hours luminescence was measured using FLUOstarR Omega, a Filter-based multi-mode microplate reader, and the data collected and analyzed using Microsoft Office Excel software. All data were compared with a control consisting of non-treated cells, obtaining the results as a change in cell viability compare to the vehicle control (fold).

Figure 3.5.2 TC20TM Automated Cell Counter

The media and the solvent in which the treatments were resuspended were used as a blank for background removal. It must be noted that the temperature of the plate must be strictly controlled, because the NanoLucR reaction is affected by temperature: therefore, the time lapse between taking out the plate from the incubator and putting it into the plate reader (pre-set at 37°C) must be as brief as possible.

3.6 Statistics

Statistical analysis was performed on each of the datasets produced from the project. For each experiment a minimum of 3 independent biological repetitions (n=3) was required. Following data collection, all data was analyzed for normality of distribution according to the Kolmogorov Smirnov test. Any data significantly ($p<0.05$) different from a normal distribution was treated as non parametric and analyzed using Kruskal-Wallis for whole data variation (ANOVA equivalent) prior to pairwise comparison using Mann Whitney U test. In the case of data sets which were normally distributed, ANOVA statistical analysis was used to assess statistical significance, prior to an appropriate T-test. The data sets compared were assumed to be of equal variance therefore a p value < 0.05 was considered significant (*) p value<0.01 was considered very significant (**) and p value< 0.001 was considered extremely significant (***). All data shown is noted for n number and appropriate test used in the figure legends.

4. RESULTS AND DISCUSSION

4.1 Nanoparticle Fabrication

A targeted delivery system based on the polymeric nanoparticles as a drug carrier represents a marvelous avenue for cancer therapy (Ferrari 2005) (Kim et al.2008). The power of nanoparticles over freely administrated drug molecules or imaging tracers relies on their multi-functionality and engineerability (Falco et al.2015).
Triblock copolymers are used as a vehicle for different drugs and templates for nanoparticles synthesis (Chen et al.2012). Pluronic F-127 is a commonly used polymer in drug delivery systems, due in part, to low toxicity, biocompatibility with cells and body fluids, and weak immunogenic properties (Perry et al.2011). In this project, Pluronic F127 was used to fabricate nanoparticles in the presence or absence of a hydrophobic drug Saha, an HDACi. The thin film hydration method was used here, to produce the F127 pluronic nanoparticle encapsulated SAHA (*Figure 4.1*). Furthermore, hyaluronic acid functionalization was used to see if targeting the nanoparticle formulation to Endometrial cancer cells expressing varying levels of CD44 confers added selectivity and sensitivity, in line with other CD44 targeting modalities used in oncology (Zhao et al. 2016).

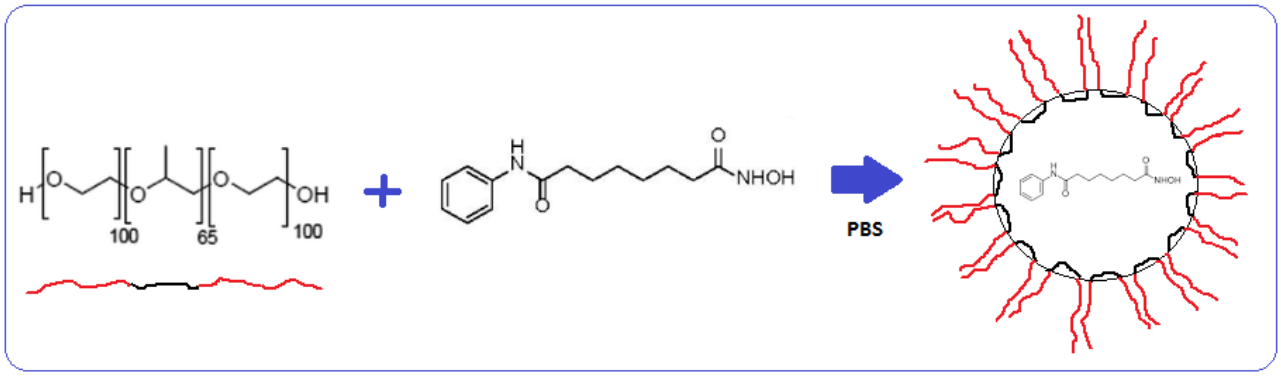

Figure 4.1 Pluronic SAHA Nanoparticle fabrication. *Chemical structure of Pluronic F127 (poly(ethylene oxide)-poly(propylene oxide)-poly(ethylene oxide) (PEO-PPO-PEO) block copolymers) and Saha with mechanism of Saha NPs formation.*

Pluronic F127 is composed of hydrophobic PPO block in the center and two hydrophilic PEO blocks on each side and it possesses a symmetrical structure of (PEO)x(PPO)y(PEO)x, where x and y respectively represent the number of the ethylene oxide and propylene oxide monomers per block (Antonisamy et al. 2016). Depending on the x and y values, (PEO)x(PPO)y(PEO)x can form different self-assembly architectures, which have demonstrated applications in a variety of fields (Basak et al. 2013) (Li et al. 2018). In aqueous media, this amphiphilic copolymer can act as the capping ligand for synthesizing and directing the assembly of colloidal NPs, as utilized in this work. Amphiphilic block

copolymers containing hydrophilic and hydrophobic chains self-assemble into polymeric micelles at or above the critical micelle concentration (CMC). The hydrophobic hydrocarbon chains allow the NPs to assemble with other hydrophobic molecules through hydrophobic-hydrophobic interaction. Furthermore, the driving force for the hydrophobic drug encapsulation phenomenon could be a hydrophobic interaction between carbonyl groups on Saha and methyl groups on Pluronic in order to create a non-covalent nanoparticle system. Additionally, functionalized nanoparticles were prepared by the simple physical mixing of HA-SH and Pluronic S-S pyridyl in aqueous solution (PBS). As a result, functionalized nanoparticles are formed attributed intermolecular interaction between HA-SH and Pluronic S-S pyridyl micelles as shown in *Figure 4.1b.* The inter-micellar crosslinking induced by HA elicited a sustained drug delivery and enhanced the mechanical strength of the nanoparticles (Jung et al. 2016). Furthermore, in the A-B-A tri-block structure, Pluronic S-S pyridyl has a thermo-responsibility in the aqueous solution and can form a self-assembled micelle structure through non-covalent interactions (Jung et al. 2016) (Pathways 2013).

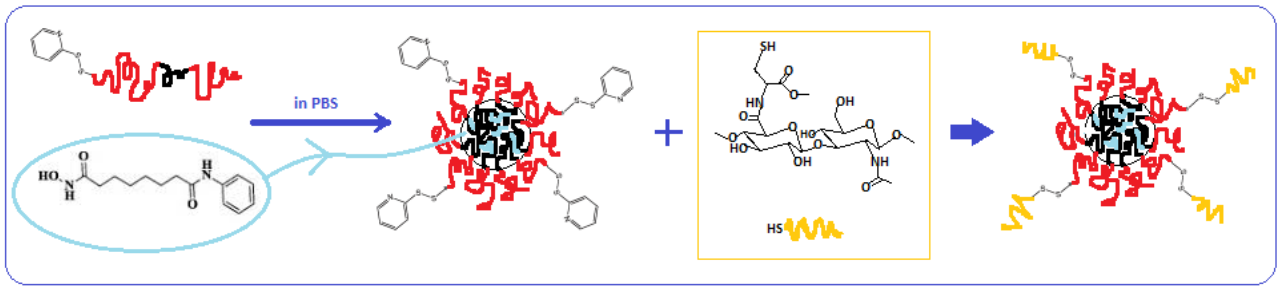

Figure 4.1b Schematic mechanism of functionalized nanoparticles formation. *HA-Pluronic nanoparticles with Saha encapsulated are formed with HA-SH and Pluronic S-S pyridyl.*

4.2 Nanoparticle Characterization

Np physical characteristics have been linked to performance as drug delivery vectors (Cho et al. 2013). The F127 Pluronic based systems described in section 4.1 were subjected to thorough characterization using state of the art methodologies. The nanoparticles were characterized for their size, charge, morphology, encapsulation efficiency and stability. F127-SS nanoparticles and F127/HA coating, which were kindly provided by the laboratory of Dr Varghese in Uppsala University (Sweden), were directly compared with F127 nanoparticles. In addition, an *in vitro* drug release study was performed to assess the utility of the NP based systems compared to free drug effects.

4.2.1 Nanoparticle Size

Nanoparticle size was measured, at room temperature, with a Zeta-sizer (Nano ZS) manufactured by Malvern Instruments Ltd (Worcestershire, UK), in the presence and absence of encapsulated drug. The Polidispersive Index (PdI) is a dimensionless values

from 0 to 1 and it is related to the measure of the width of molecular weight distributions. A smaller value of PdI indicates that the solution is more monodispersed (Malvern instrument 2004). The average nanoparticle size and PdI values are summarized in table 4.2.1 for all particles included in the study.

The mean diameter of the nanoparticles increases with polymer concentration, suggesting a larger micellar aggregate with higher concentration. In the presence of Saha encapsulation, there is no significant difference in the size of Pluronic F127 particles, respectively 22.85±2nm for F127 empty NPS and 23.43±2nm for F127 Saha NPS ($p<0.05$). A more significant difference of Saha encapsulation is shown in the size of Pluronic F127 from Uppsala, in fact, F127 SS empty NPS had a size of 25.17±2nm (PdI 0.256) and F127 SS Saha NPS were 30.48±3nm (PdI 0.229). The F127 pluronic particles exhibited a more increased size distribution following Saha encapsulation compared to the F127 pluronic particles. In addition, F127 PI NPS has a similar size of the other nanoparticles equals to 29.51±3nm (PdI 0.202).

	Size-average (nm)	**PdI**
F127 Saha Nps (2.5uM) in PBS	23.43±2	0.329
F127 Saha Nps (5uM) in PBS	25.73±2	0.354
F127 SS Saha NPs (2.5uM) in PBS	30.48±3	0.229
F127 empty Nps (2.5uM) in PBS	22.85±2	0.243
F127 SS empty NPs (2.5uM)	25.17±2	0.256
F127 PI NPs (2.5uM) in PBS	29.51±3	0.202

Table 4.2.1. ***Nanoparticle Size distribution of Pluronic variants in the presence and absence of Saha.*** *All the nanoparticles were fabricated using the thin film method. The size of the different nanoparticles in the presence or absence of Saha is presented.*

The mean diameter of the nanoparticles increases with polymer concentration, suggesting a larger micellar aggregate with higher concentration. In the presence of Saha encapsulation, there is no significant difference in the size of Pluronic F127 particles, respectively 22.85±2nm for F127 empty NPS and 23.43±2nm for F127 Saha NPS ($p<0.05$). A more significant difference of Saha encapsulation is shown in the size of Pluronic F127 from Uppsala, in fact, F127 SS empty NPS had a size of 25.17±2nm (PdI 0.256) and F127 SS Saha NPS were 30.48±3nm (PdI 0.229). The F127 pluronic particles exhibited a more increased size distribution following Saha encapsulation compared to the F127 pluronic particles. In addition, F127 PI NPS has a similar size of the other nanoparticles equals to 29.51±3nm (PdI 0.202).

Importantly, nanoparticles are in the correct size range (<100nm) to passively target tumor sites due to enhanced permeability and retention (EPR) effect, utilizing the characteristic leaky vasculature in and around the tumor site (Howard et al. 2016).

All of the nanoparticle preparations were observed to be monodispersed solutions, due to the smaller PDI values (PdI 0.202 – 0.354).

4.2.2 Nanoparticle Surface Charge

The charge of both the F127 and F127-SS nanoparticle formulations was determined using the Nanosizer ZS, with all values summarized in table 4.2.2. Consistent with literature findings, the surface charge was negative for all formulations (Frohlich 2012) (Verma & Stellacci 2010).

Cationic particles have been well-known to bind to negatively charged groups on the cell surface and translocate across the plasma membrane. As positively charged particles have the greatest efficiency in cell-membrane penetration and cellular internalization, but other studies have also examined the cellular uptake of negatively charged nanoparticles with different core materials (Verma & Stellacci 2010).The internalization of negatively charged nanoparticles is believed to occur through nonspecific binding and clustering of the particles on cationic sites on the plasma membrane, that are relatively scarcer than negatively charged domains, and their subsequent endocytosis (Verma & Stellacci 2010).

	Zeta potential (mV)
F127 Saha NPs (2.5mg/ml) in PBS	-3.03 ± 3
F127 empty Nps (2.5mg/ml) in PBS	-5.37 ± 4
F127 SS Saha Nps (2.5mg/ml) in PBS	-0.197 ± 150
F127 SS empty Nps (2.5mg/ml) in PBS	-1.13 ± 150

Table 4.2.2 ***Nanoparticle surface charge.*** *Zeta-potential values for different nanoparticle formulations were assessed using Nanosizer ZS.*

Results show that F127 empty nanoparticles are more negative charged than the encapsulated one -5.37 ± 4mV instead of -3.03mV. A similar trend can be seen with F127 SS nanoparticles, where the addition of the drug resulted in a near 5 fold decrease in negative charge. This is due in part to the amine groups present in Saha (pKa 9.2). As the pluronic particles and the drug were formed in aqueous solution, the lower pH could have masked and potentially reduced the nanoparticles negative zeta-potential exposing Saha's ammine positive protons to the outer nanoparticle surface. Kim et al. used a similar approach and induced a pH-dependent zeta-potential modification in the nanostructure's surface, varying the surface charge of silica nanoparticles using differing coating formulations (Kim et al.2014).

4.2.3 Nanoparticle Shape and Size distribution

Atomic force microscopy is not reliant on the wavelength of light and can, therefore, be used to image NP samples at the nanoscale (Scalf et al. 2006). This scanning probe

microscopy techniques were used here to image the particles, as quality control for particle size and topography (Ong. 2007). Following the isolation of spherical shaped nanoparticles on an ideal flat substrate such as mica, their size can be determined easily from the AFM image by measuring the nanoparticle (Canale et al. 2011). These images, for each particle analyzed, are shown in figure 4.2.3 panel A-D and compared to SEM images of the same particle preparations to highlight the physical dimensions, as shown in *Figure 4.2.3* panel E-H. Size data obtained with Dynamic Light Scattering are confirmed by AFM topography. Uniformity and reproducibility were observed through AFM *(Figure 4.2.3)*. F127 Saha NPS, F127 empty NPS and F127-ss Saha NPS exhibit all a rounded shape *(Figure 4.2.3)*. A width dimension around 40nm and a height dimension of around 20nm are shown in F127 Saha nanoparticles *(Figure 4.2.3B)*.

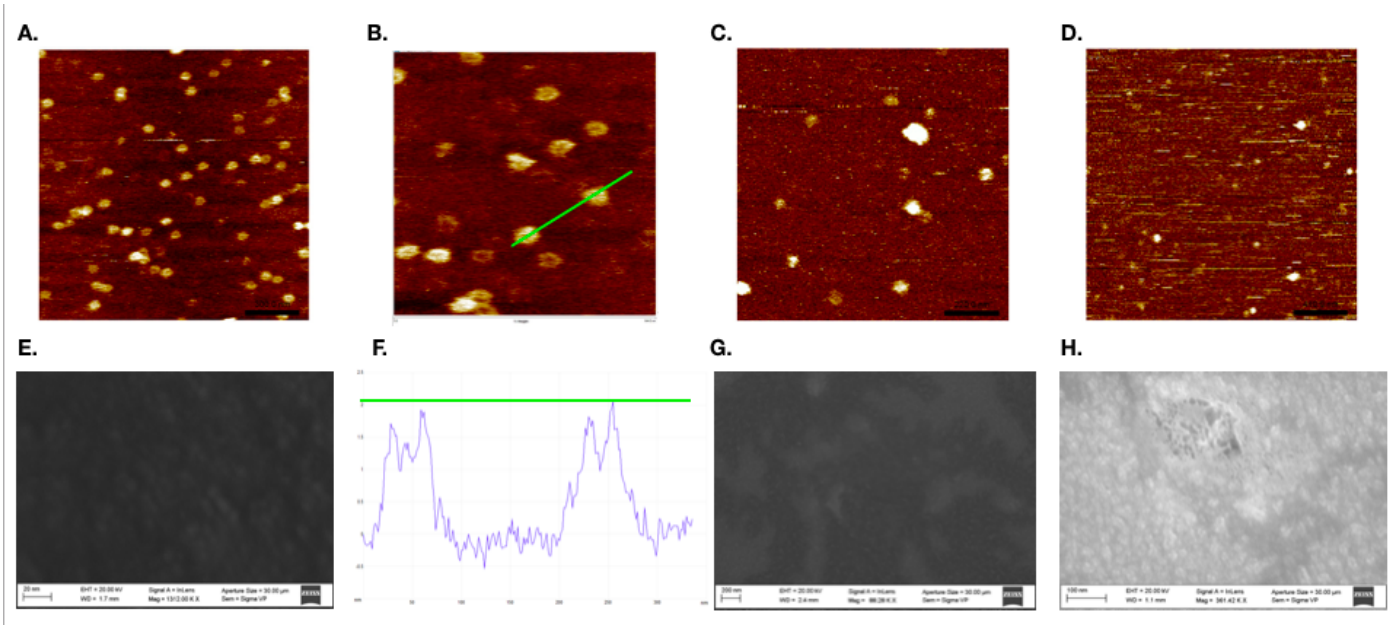

Figure 4.2.3 ***Nanoparticle AFM–SEM topography*** *(analyses were performed at the RBGO laboratories in Swansea and at the Ca'Foscari University). The images at the top were performed using AFM (A-D) and the images at the bottom were performed using SEM (E-H). The topography of F127 Saha nanoparticles (A, B, E), F127 Empty nanoparticles (C, G) and F127 Ss Saha nanoparticles (D, H) were shown. Nanoparticles topography with higher features displayed in a lighter brown. Horizontal green line profile measured along the dotted line in Panel showing F127 Saha particle width around 40nm (F).*

SEM analysis also shows that the particles are mostly spherical in shape and the nanoparticles suspensions are monodispersed solutions *(Figure 4.2.3)*, as shown previously in DLS analyses. Moreover, F127 SS Saha NPS tend to aggregate in order to form several structures of aggregates not homogeneously, this is probably due to the energetic level of stability that they need to achieve when they are forming their structures. For this reason, the functionalized nanoparticles show a heterogeneous shape. Furthermore, the stability of the shape of the particles is improved thanks to the core-crosslinking thiolated Pluronic (Abdullah et al. 2011).

4.2.4 Nanoparticle Encapsulation Efficiency

SAHA is soluble at room temperature in DMSO (Dimethyl sulfoxide) and so was mixed with F127 polymers and incorporated into the fabrication process as shown in figure 4.1b. In order to test the encapsulation efficiency of this reaction, High-Pressure Liquid Chromatography (HPLC) was used, which separates the samples according to their hydrophobicity, characterizing the solution based on differential flow rate and elution time (Terril 2003). The drug encapsulation efficiency is essential to find the amount of drug lost during the fabrication process and how much drug delivered to the target.
Before HPLC analyses, nanoparticles containing Saha was diluted in DMSO in order to break the polymeric structure and release the drug. Subsequently, a standard curve was constructed in order to provide the relative control for comparison and calculation of Saha in a DMSO solution, as shown in figure 4.2.4. The efficiency of detection is shown with a gradient of 0.997.

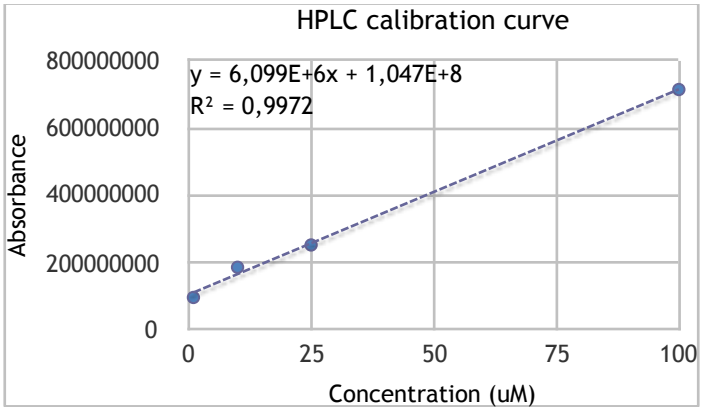

	Quantity of Saha (mg)	Encapsulation Efficiency EE (%)
F 127 Saha Nps	2.5	***0.982863***
F127 Saha Nps	10	***12.016046***
F 127 SS Saha Nps	2.5	***2.450207***
F 127 SS HA Saha Nps	2.5	***2.469151***

F 127 SS HA Saha Nps / *F 127 Saha Nps*	2.51
F 127 SS Saha Nps / *F 127 Saha Nps*	2.49
F127 Saha Nps / *F 127 Saha Nps*	12.23

Fig.4.2.4 ***HPLC analyses.*** *HPLC calibration curve and linear fitting (R2= 0.9972). Saha encapsulation efficiency was calculated relative to a standard curve constructed from increasing Saha concentrations in DMSO solution, measured by HPLC. The nanoparticles*

sample was compared with this calibration curve (A). HPLC values show that Saha is 2.51times more encapsulated in F127 HA Saha NPS than in F127 Saha NPS and 2.49 times in F127 Ss Saha NPS (EE is referred to the Encapsulation Efficiency calculated in %) (B).

F127 Saha nanoparticles reveal a 0.98% encapsulation efficiency (EE), which is lower compared to F127 Saha nanoparticles with a higher quantity of Saha drug, that have 12.02% EE. F127 SS Saha NPS and F127 SS-HA Saha NPS retained only respectively 2.45% and 2.47% of the amount of drug initially loaded, low values of encapsulation efficiency, but these values are higher compared to the encapsulation efficiency of the F127 Saha NPS. In fact, results show that Saha is 2.49 times more encapsulated in F127 SS Pluronic than in our F127 Pluronic.

A fast initial burst release of drug from the nanoparticles could be the cause to explain this low efficiency. The concentration of polymer used during the fabrication is also a possible parameter that can affect the encapsulation efficiency (Yeo & Park 2004). Other parameters such as the polymer solubility, the rate of solvent removal and the interaction between the drug and polymer can be studied to increase encapsulation of the active principle (Boury et al.1997). Furthermore, as shown, the nanoparticle functionalization is probably a solution for enhancing the major retention of the drug after the loading. In fact, is demonstrated that Saha is 2.51 times more encapsulated in F127 SS-HA nanoparticles than in F127 Pluronic.

4.2.5 Nanoparticle Penetration & Stability

Pluronic F127 CMC is 0.26 wt% to 0.8wt% (Sezgin et al.2006). The dissociation of the nanoparticles upon dilution is due to this relatively high CMC. Due to the dilution factor when NP formulations were added to the cells, NP only formulations with propidium iodide (Pi) were fabricated and added to the cells to gauge the stability of the spherical formulations and resultant cell penetration (Neumeyer et al. 2011). Pi is a red-fluorescent nuclear and chromosome counterstain die, which when encapsulated will not release from the pluronic micelle structure and will only penetrate cells that have undergone apoptosis or cell membrane disruption. In fact, propidium iodide is not permeant to live cells, it is also commonly used to detect dead cells in a population thanks to its binding to DNA by intercalating between the bases (Jain et al. 2018). The positive control therefore for Pi penetration was cells cultured over the exact same period prior to fixation with methanol.
The stability of drug nanoparticles remains a very challenging issue during pharmaceutical product development. Stability is affected by various factors such as dosage form, nature of dispersion medium, delivery route, fabrication method and nature of the drug, its size, and charge (Cho 2013). The goal in this experiment was to show that the nanoparticles with Pi encapsulated are able to penetrate the membrane and enter the nucleus demonstrating the pluronic nanoparticle stability when they cross the cell membrane.

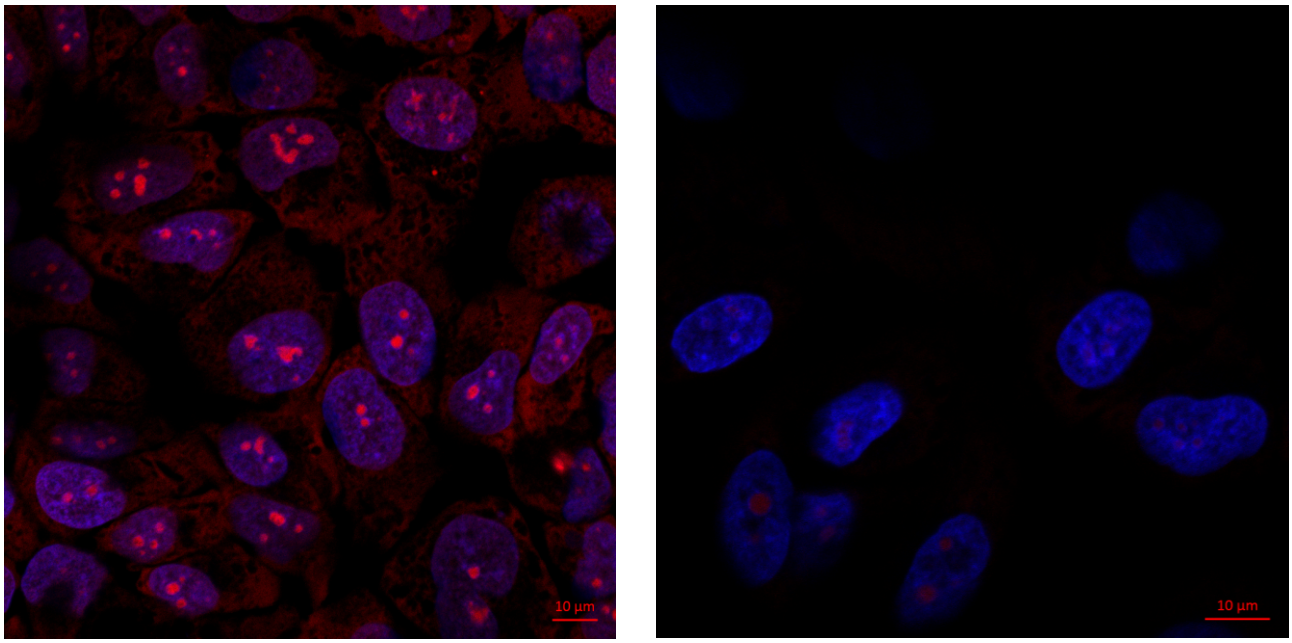

Fig.4.2.5.a ***CLSM images of Ishikawa cells incubated with PI nanoparticles.*** *Images with Ishikawa cells treated with PI nanoparticles at different concentrations (10uM on the left and 0.12uM on the right) demonstrate that at lower concentrations, fewer nanoparticles are able to penetrate into the nucleus.*

Multiple analysis methodologies were used in order to qualitatively and quantitatively analyze PI and NP penetration to the cells. Principally these were based on fluorescence microscopy, using confocal laser scanning microscopy at high, single-cell resolution and z stack analysis as well as In cell microscopy, a pseudo confocal used to analyze PI intensity across the cell population (Douglas 2001). These results are summarized in *Figures 4.2.5.a* and *Figure 4.2.5.b.*

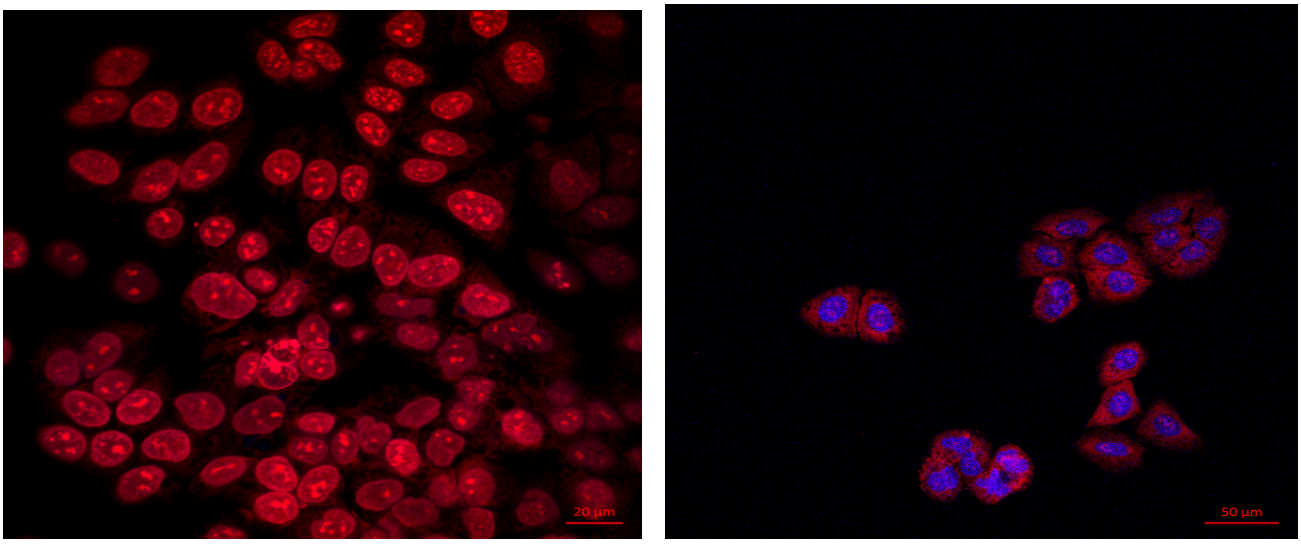

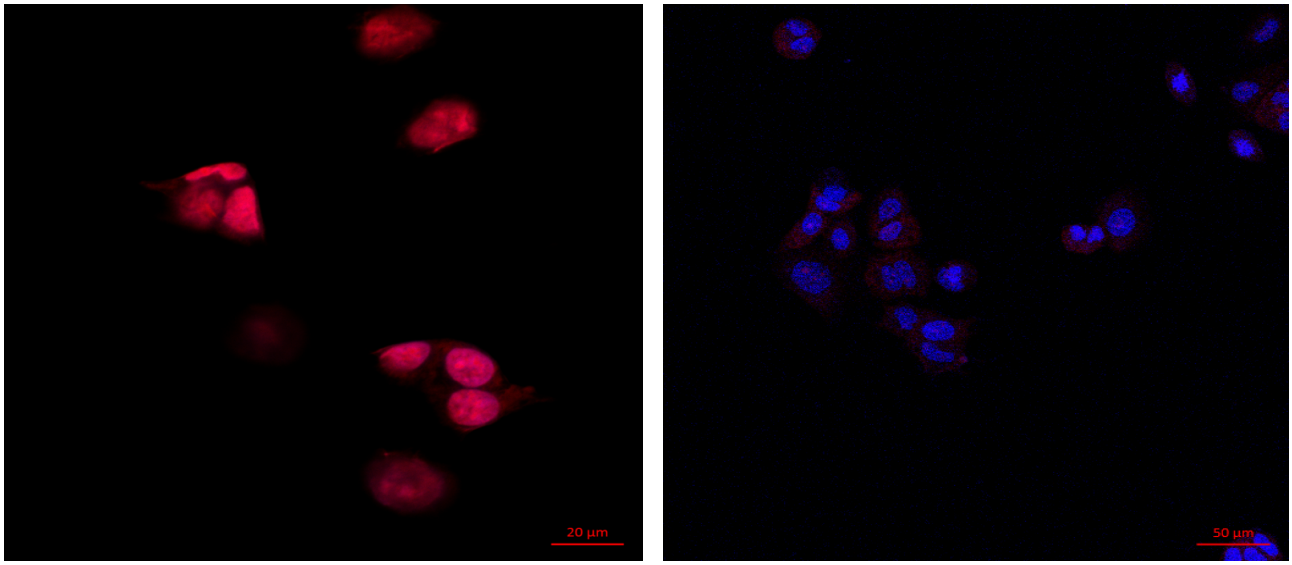

Fig.4.2.5.b ***CLSM images of Ishikawa cells incubated with PI nanoparticles.*** *Images of Ishikawa cells treated with 70% methanol and PI nanoparticles with a concentration of 30µM (on the left) vs Ishikawa cells treated with PI dye (on the right) are shown.*

In this experiment, PI NPs have been studied and synthesized by encapsulating Propidium Iodide inside Pluronic F127 that contain poly(ethylene oxide)-poly(ethylene oxide)-poly(propylene oxide)-poly(ethylene oxide) (PEO-PPO-PEO) block copolymer. Confocal images showed that Ishikawa cell line, when treated with PI nanoparticles (30µM), penetrated the cell membrane and entered the nucleus *(Figure 4.2.5.a)*. Moreover, Z-stacked images were shown in order to demonstrate that the nanoparticles are localized within the cell nucleus at different levels *(Figure 4.2.5c)*.

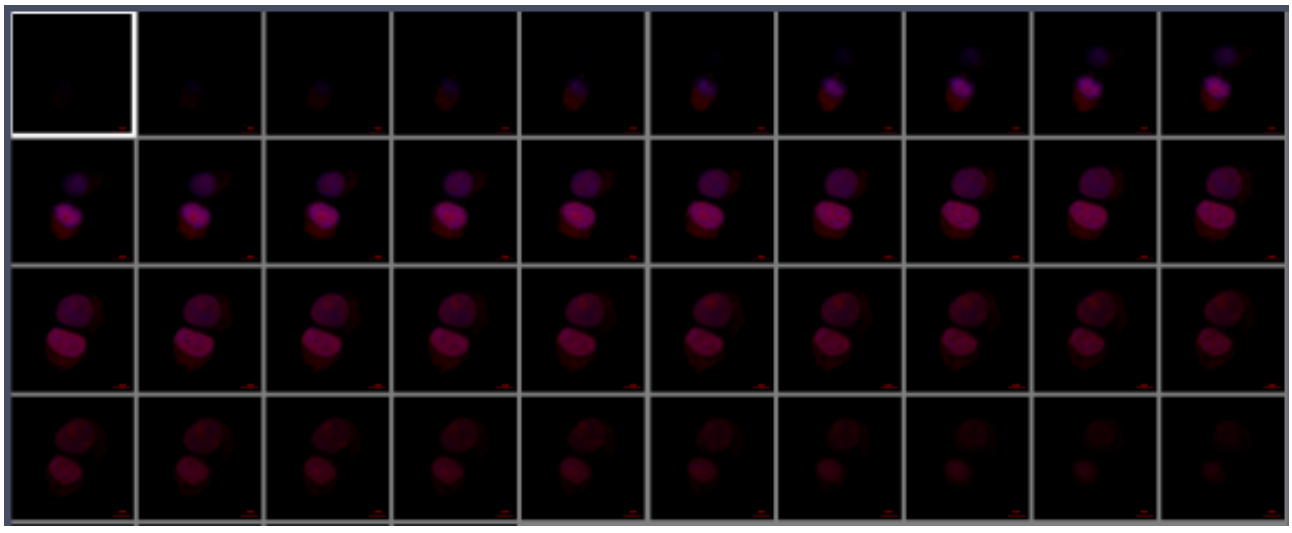

Figure 4.2.5.c ***CLSM images of Ishikawa cells incubated with PI nanoparticles.*** *A series of optical sections were stacked (Z-stacked) by moving the focal plane of the instrument step-by-step through the depth of the cell. The Z-stacked images clearly reveal that the nanoparticles are localized within the cell nucleus.*

The dye was successfully encapsulated in the triblock polymer, the binding ability was investigated using dynamic light scattering study and the hydrodynamic diameter of the nanoparticles was 29.61nm. The formation of PI NPs has been characterized using Incell Analyser 2000 *(Figure 4.2.5d)* and Confocal Microscopy *(Figure 4.2.5a, b and, c)*. These data suggest that PI was an appropriate dye for encapsulation to F127 Pluronic to show its stability in the culture and its ability to remain intact and cross the cell membrane. All this data suggest that Pluronic F127 is an appropriate polymer which gives stability to NPs delivery system for endometrial cancer. Z-stacked images demonstrate that the nanoparticles are localized within the cell nucleus *(Figure 4.2.5c)*. Additionally, these experiment showed that if the concentration of dye nanoparticles is higher there is more possibility for the dye to cross and penetrate the membrane of the cells *(Figure 4.2.5d)*. Furthermore, the images demonstrate that the cells when treated with methanol remaining died, PI penetrate the membrane and remain inside even after the washing with PBS *(Figure 4.2.5b, images on the left)*. In the contrary, the addition of PI on the cells not treated with methanol does not allow the penetration *(Figure 4.2.5b, images on the right)*. Quantitatively analyses to measure PI and NP penetration to the cells were performed using In Cell analyzer 2000 *(Figure 4.2.5d)*.

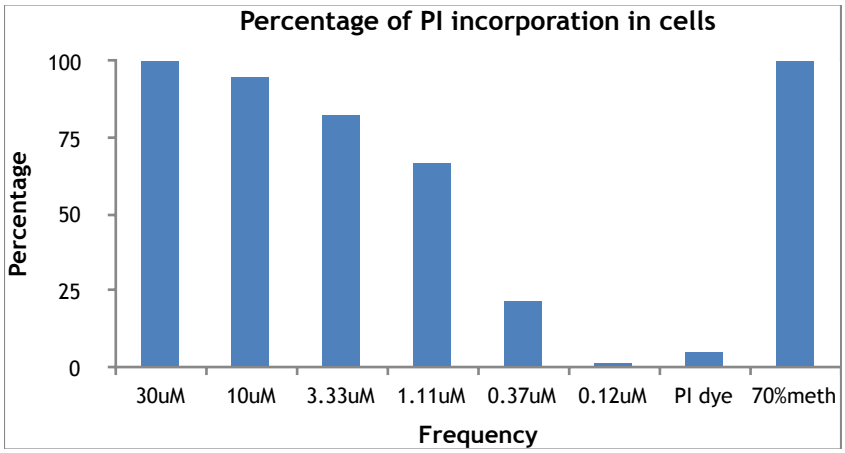

	30uM Freq	10uM Freq	3.33uM Freq	1.11uM Freq	0.37uM Freq	0.12uM Freq	Ctrl Freq	Meth Freq
Nucleus	98	1133	1300	1242	1330	1216	137	184
PI dye	105	1070	1069	832	288	16	7	274
percentage	107,14	94,44	82,23	66,99	21,65	1,32	5,11	148,91

Figure 4.2.5d ***Incell Analyzer 2000 analyses.*** *F127 PI nanoparticles were analyzed on Ishikawa cells at different dilutions. A treatment with PI dye on Ishikawa cells was used as control. A treatment with 70% methanol followed by F127 PI Nps was carried out. The percentage was calculated as follow: PI dye frequency/ Nucleus frequency*100.*

Incell Analyzer results demonstrate that the percentage of PI inside the cells decreases with the effect of the dilution. Is demonstrated that a small number of nanoparticles penetrate the cells at a concentration of 0.12µM *(Figure 4.2.5d)*. Moreover, these results demonstrate that after the cell treatment with 70%methanol, PI penetrate the membrane and remain inside the nucleus even after the washing with PBS as shown in confocal images. The Incell analyses reveal a percentage of frequency equal to 100% of PI incorporation in the cells. The positive control, which is PI dye on Ishikawa cells not treated with methanol demonstrates that PI

doesn't penetrate the cells, in fact, his percentage of frequency is low compared with the percentage of frequency of the methanol treatment. PI uptake after methanol treatment is high due to the "killer effect" of the methanol through the cells.

4.2.6 Drug release Testing

In order to assess the release profile of Saha from the F127 NP formulations, a standard dialysis experiment was set up in line with those used previously (Hua 2014). A dialysis bag with a molecular cut off of 3500Da was used (supplier). NP encapsulated Saha particles were then loaded into the dialysis bag and incubated for 96 hrs, sampling to test the Saha concentration in surrounding media every hour. Saha concentration was then assessed quantitatively using a FluoStar Omega instrument.

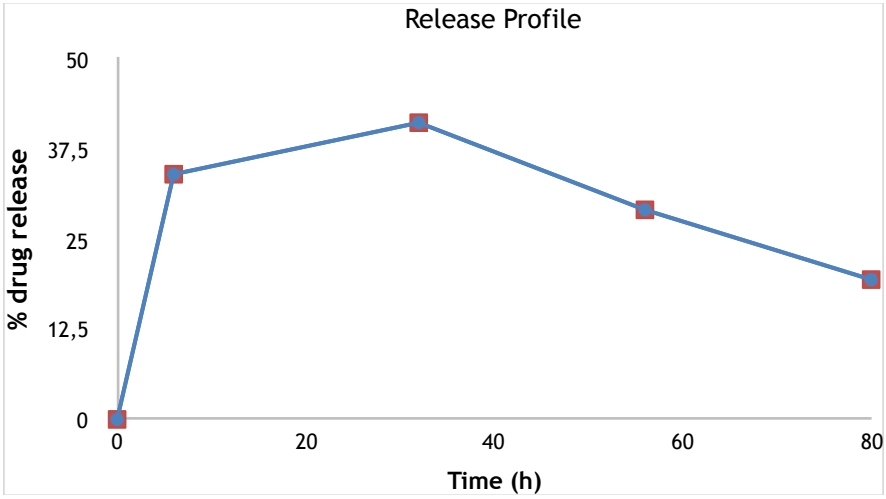

Figure 4.2.6 ***Drug Release Profile graph.*** *The release of Saha drug was measured using FluoStar Omega and the Maximun release of Saha was calculated after about 32 hours.*

The in vitro Saha release results clearly showed the sustained drug release behavior of the F127 Saha nanoparticles: Saha was released within 96 hours with a maximum release after about 36 hours followed by a sustained release of the remaining drug for 3 days. In this experiment, the release profile of the nanoparticles shows a rapid burst release of 34% and a maximum release of 41% after 3 hours *(Figure 4.2.6).* This study demonstrates that the thin film method used for the fabrication of SAHA nanoparticles provide the release of SAHA drug within 96 hours allowing adequate drug release for the treatment of Endometrial Cancer.

An interesting way to study the drug release profile and the drug diffusion through the cell could be with the calculation of the diffusion equation using the mathematical methods for physicists (Arfken & Weber 2005). Moreover, drug concentration, drug solubility, shape and size of the nanoparticles are important considerations when conducting a drug release study using the dialyzes method (Hua 2014).

4.2.7 Summary of Characterization Data

There are many methods to characterize the physical dimension and properties of the particles (Robertson et al. 2016). In this project, the hydrodynamic diameter and the charge were determined using the Dynamic Light Scattering. The morphology of the nanoparticles was visible with Atomic Force Microscopy images and Scanning Emission Miscope images and the stability of the nanoparticles with the dye encapsulated on the cells was characterized by the Incell analyzer followed by the Confocal Laser Scanning Microscopy. Furthermore, thanks to the high-performance liquid chromatography and finally, using the dialyzes method was investigated the drug release in a biological environment. A summary of the NPs characterization techniques is reported in *Figure 4.2.7*.

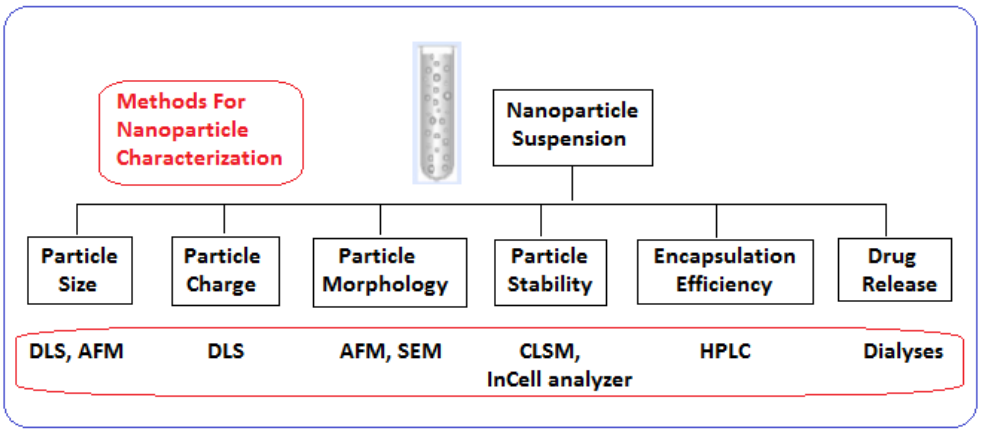

Figure 4.2.7 ***Methods for nanoparticles characterization.*** *In this figure are summarized the methods used in "Pluronic copolymer nanoparticles as an exemplar for epidrug delivery in Endometrial Cancer" for characterize nanoparticles fabricated using the Thin Film Method.*

Each particle was compared with the others observing the different parameters for the characterization *(Table 4.2.7)*. The first important observation is that nanoparticles are in the correct size range (<100nm) and are monodispersed. The mean diameter of the nanoparticles increases with polymer concentration and in the presence of Saha encapsulation, there is no significant difference in the size of Pluronic F127 particles. A more significant difference of Saha encapsulation is shown in the size of F127 SS empty NPs and F127-SS SAHA NPS. The F127 Pluronic particles exhibited a more increased size distribution following Saha encapsulation compared to the F127 Pluronic particles and F127 PI NPs show a similar size of the other nanoparticles. Regarding the charge, F127 empty nanoparticles and F127 SS empty nanoparticles have a similar trend because the addition of the drug resulted in a near 5 fold decrease the negative charge. Moreover, AFM and SEM topography show that the particles are mostly spherical in shape and F127 SS SAHA NPs tend to aggregate. HPLC values show that Saha is 2.51times more encapsulated in F127 HA SAHA NPs than in F127 Saha NPs and 2.48 times in F127 SS SAHA NPs. Finally, SAHA

was released with a maximum release after about 36 hours followed by a sustained release of the remaining drug for 3 days.

	Size (nm)	Charge (mV)	Shape	Stability	Encapsulation efficiency (%)	Drug Release (hours)
F127 Saha Nps (2.5uM)	23.43±2	-3.03 ± 3	Spherical		*0.982863*	*release of Saha after about 36 hours*
F127 Saha Nps (5uM)	25.73±2					
F127 SS Saha NPs (2.5uM)	30.48±3	-0.197 ± 150	Spherical		*2.450207*	
F127 SS-HA Saha NPs (2.5uM)					*2.469151*	
F127 empty Nps (2.5uM)	22.85±2	-15.37 ± 4	Spherical			
F127 SS empty NPs (2.5uM)	25.17±2	-1.13 ± 150				
F127 PI NPs (2.5uM)	29.51±3			*PI remains intact and cross the cell membrane*		

Table *4.2.7* ***Summary of the results for nanoparticles characterization.*** *NPs fabricated for EC treatment, were characterize by size, charge, shape, stability, encapsulation efficiency and drug release.*

4.3 Endometrial Cancer and encapsulated epidrug efficacy

Ishikawa and Hec50 endometrial epithelial adenocarcinoma cell lines were adopted as an in vitro model of EC subtypes, an established approach within the RBGO group in Swansea University. EC is divided into two distinctive subcategories, based on histological differences and clinical outcomes. The Ishikawa cell line is representative of Type I tumors, the most frequent, commonly low cellular grade adenocarcinoma where estrogen receptors are expressed. Alternatively, the Hec50 cell line is representative of Type II tumors which are estrogen independent and not associated with hyperplasia (Murali et al. 2014). These two in vitro models were chosen and studied at multiple concentrations of Pluronic encapsulated SAHA, compared to both empty nanoparticles and free drug treatments, with a view to evaluating the efficacy of both polymer-based nanoparticle delivery systems in Endometrial Cancer.

4.3.1 Cytotoxicity of Empty Pluronic nanoparticles

Pluronic F127 is commonly used polymer for the demonstration of nanoparticle formulation efficiency in drug delivery systems. Pluronic F127 has been shown to exhibit low cellular toxicity previously (Zhang et al. 2011). Ishikawa and Hec50 cellular viability were tested in the presence and absence of increasing concentrations (1.25uM to 25uM) of Pluronic nanoparticles over 96 hours. Furthermore, the two types of cells were tested in the presence and absence of F127 SS-HA nanoparticles over 96 hours. It has been demonstrated in other scientific works (Subtypes 2013) that the novel self-assembled supramolecular HA nanoparticles can prolong drug release the target site and simultaneously minimize toxicity by reducing off-target accumulation, that is highly desirable for cancer therapy. Biopolymers such as hyaluronic acid (HA) possess biocompatibility and biodegradability properties. Their target specific delivery is generally achieved by hijacking cell surface receptor-ligand interactions. In fact, many of the effects of HA are mediated through cell surface receptors, CD44 results to be the principal HA receptor and the chemical modification of HA in the nanoparticles increases the blood circulation time (Huang et al. 2016). Ishikawa (Type I EC cells) expresses low amounts of CD44 while Hec50 (type II E cells) lines show significantly increased expression (Tempferl et al.1998).

The Real-Time Glo (RTGlo) assay (RT-GloTM MT Cell Viability Assay, Technical Manual), a more sensitive and more rapid than other current viability assays (Promega 2016), was used to assess cell viability and cytotoxicity respectively in Ishikawa and Hec50 cell lines. Real-Time Glo kit is offering real-time analyses of the samples under test. Values of cytotoxicity obtained were normalized to non-treated control to obtain a fold value and then plotted against the assay time points, over 96hours. Three biological replicates were performed.

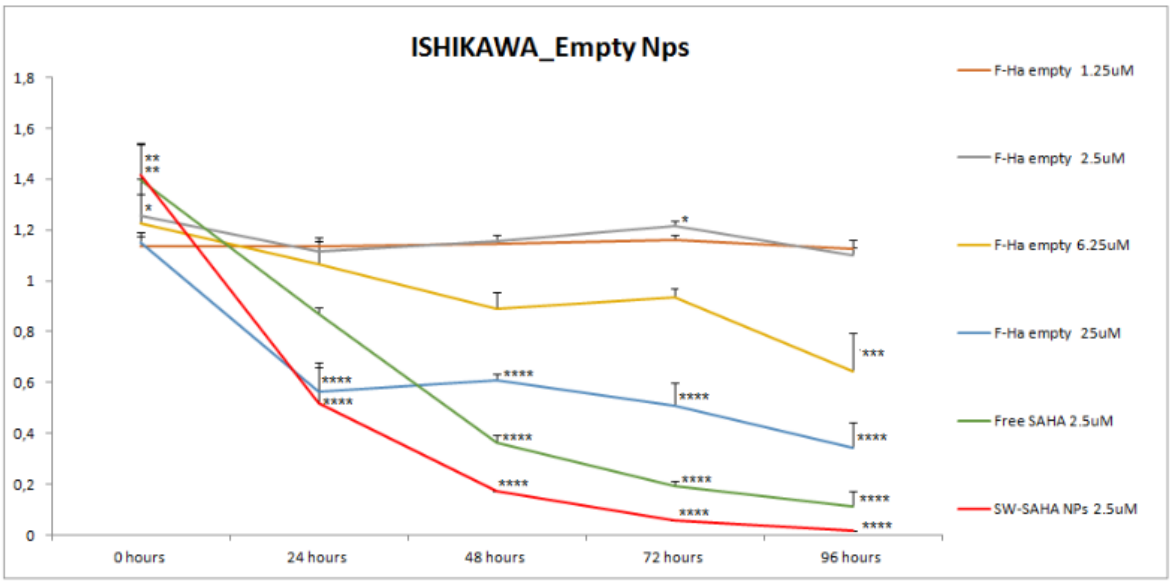

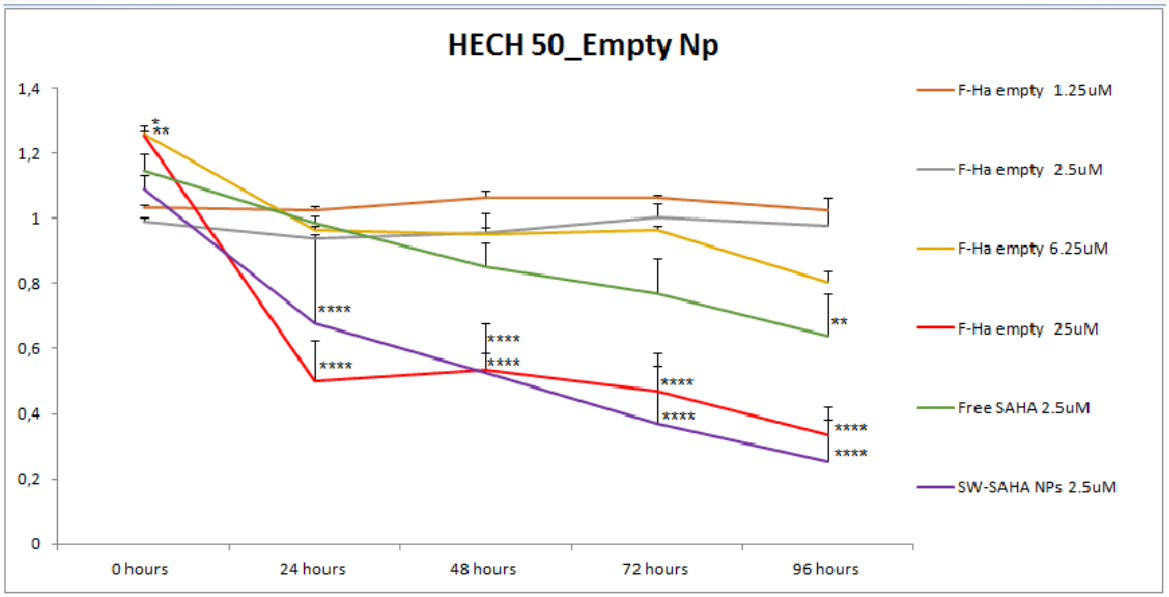

Figure 4.3.2 ***F127 nanoparticle cytotoxicity in an in vitro model EC****. (F= nanoparticles fabricated with Pluronic F127 SS, SW = nanoparticles fabricated in Swansea con Pluronic F127). Both Hec50 (first graph) and Ishikawa (second graph) cells were treated over 96 hours with different concentration of F127 HA-empty nanoparticles, with free Saha (2.5uM) and with F127 Saha nanoparticles. Real-Time Glo data were normalized to the untreated control cells, the standard deviation of a minimum of three independent biological repeats was measured and cellular viability was assayed. Two-Way ANOVA model (Dunnett Test for multiple comparisons) was used for statistical analyses comparing "Type of Treatment" and "Time of Treatment", the two variables of the experiment.*

After found out that F127 nanoparticles in absence of the drug don't kill the cells at the concentration of interest, was demonstrated that also F127 nanoparticles functionalized with Hyaluronic acid and in absence of Saha, at the concentration of 1.25uM and 2.5uM, aren't toxic for the cells. In *Figure 4.3.1* is shown the cytotoxicity of increasing concentrations of empty nanoparticles in Ishikawa (panel A) and Hec50 (panel B) cells, over a period of 96 hours. In this section, it has been demonstrated that F127 SS-HA empty nanoparticles at lower concentration (1.25uM and 2.5uM) are not toxic for Ishikawa and Hec50 cell lines, whereas at higher concentrations they become killers. No significant decrease in cellular viability over 96hrs was observed in both type I and type II cells at 1.25uM of F127 SS-HA empty nanoparticles compared to the untreated control ($p>0.05$). Above 2.5uM concentration, cytotoxic effects were clearly observed, in both cell lines, with a significant decrease in cell viability when compared with the untreated control ($p<0.05$). Therefore, Ishikawa cells and Hec50 show a similar trend after the different nanoparticles treatments because in both cases F127 SS-HA empty particles at 1.25uM and 2.5uM let the cells live, whereas F127 SS-HA empty particles at the 6.25uM start to kill the cells over a 96hr period. Furthermore, it must be noticed that the best killer for both types I and type II cells is F127 Saha nanoparticles at 2.5uM. Despite this, Hec50 cells were seemingly more resilient to these treatments compared to Ishikawa cells.

4.3.3 Encapsulated nanoparticles analyses and comparison with Free Saha drug

In this section, after identifying a dose at which empty nanoparticles weren't toxic, encapsulated nanoparticles were analyzed. The Real-Time Glo assay was also performed for Saha-nanoparticles with Pluronic F127 SS in the absence or presence of HA at two different concentrations, respectively 2.5uM and 1.25uM. Statistical significance was studied comparing the Saha-nanoparticles with a treatment of Free Saha (2.5uM) over a 96 hours treatment period using Anova Two-Way test for multiple comparisons. Free SAHA drug efficacy has previously been assessed by the RBGO research group, in both Type I and types II cell lines (data not shown, statistical significance assessed by ANOVA Two Way and T-test analysis), therefore these results were confirmed in this experiment and three biological replicates were performed.

In *Figure 4.3.3* was demonstrated that for both Ishikawa and hec50 cells, F127 SS Saha nanoparticles with or without the functionalization (HA), at a higher concentration (2.5uM), resulted to be the best killer. Moreover, when these NPS were compared to the Free drug, they clearly exposed a significant cytotoxicity effect ($p<0.05$). When the concentration decreased (1.25uM), the nanoparticles became less cytotoxic as was shown for F127 SS-HA Saha NPS and F127 SS Saha NPS ($p>0.05$). Time-dependent effects, in Type I and Type II cells, were also observed and once again, type II Hec50 cells were more resilient to these treatments. In Ishikawa cell line, it has been shown a significant decrease between 0 and 48 hours, while Hec50 cell line presented a more constant trend over the 96hours period compared to the previous cells.

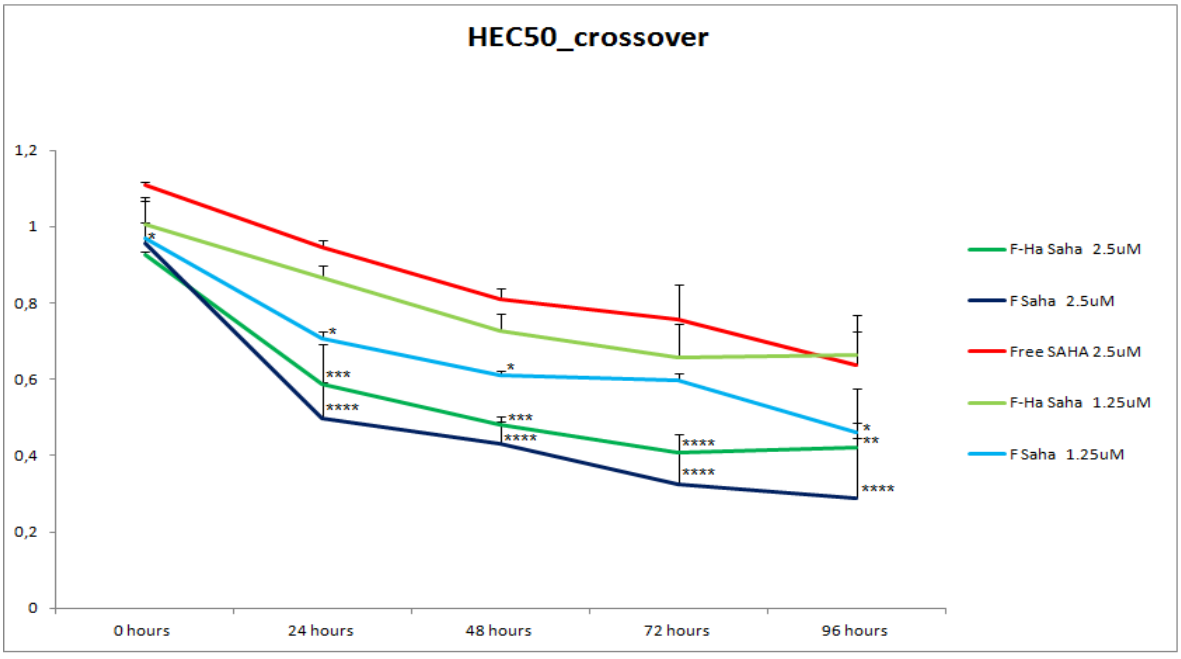

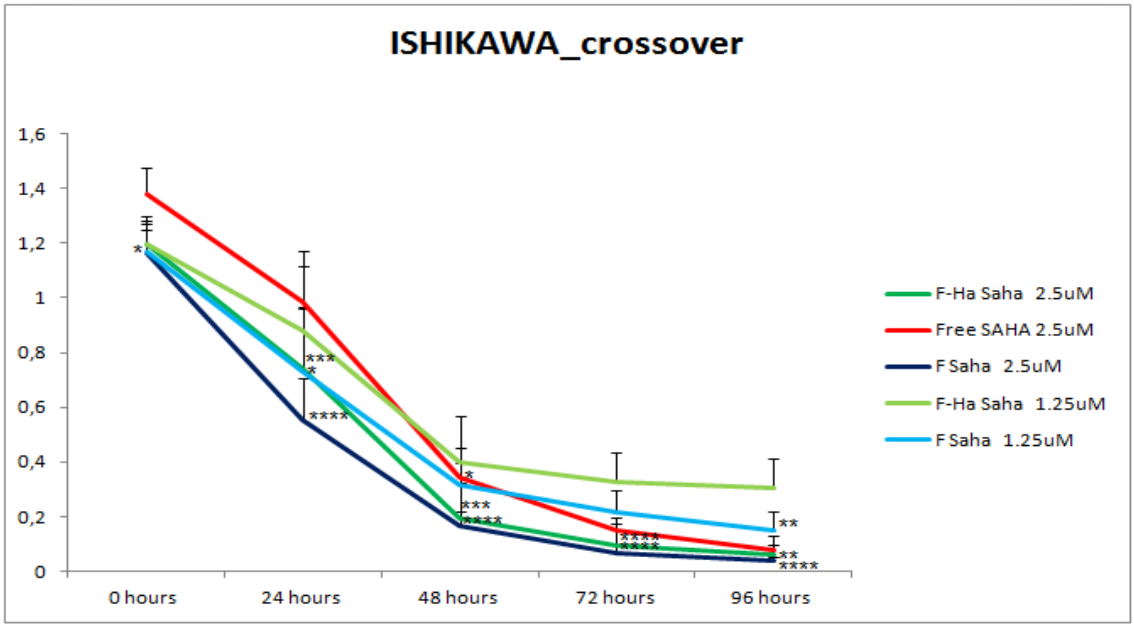

Fig.4.3.3 ***F127 nanoparticle cytotoxicity in a vitro model EC.*** *(F= nanoparticles fabricated with Pluronic F127). Both Hec50 (first graph) and Ishikawa (second graph) cells were treated over 96 hours with different concentration of F127 Saha nanoparticles, in the presence or absence of HA, and with free Saha (2.5uM). Real-Time Glo data were normalized to the untreated control cells, the standard deviation of a minimum of three independent biological repeats was measured and cellular viability was assayed. Two-Way ANOVA model (Dunnett Test for multiple comparisons) was used for statistical analyses comparing "Type of Treatment" and "Time of Treatment", the two variables of the experiment.*

There are many factors that can be relevant for the effect of the encapsulated drugs, such as the release profile of the drug, the encapsulation efficiency, the concentration of the polymer and burst release mechanism. For this reason, it's difficult to directly compare results with other studies that are already present in the literature. Nevertheless, with these results it has been demonstrated that concentration at 2.5uM of Saha-F127 SS and Saha-F127 SS-HA particles, were able to significantly decrease both types I and type II cell lines viability when compared to the control.

As final analyses on the cytotoxic effects of Saha encapsulated nanoparticle formulations, all the nanoparticles showed remarkable efficacy in encapsulating the drug and their effect on type I and type II cell lines in endometrial cancer cell viability. This effect was generally shown after 24hours of treatment. Both F127 SS Saha and F127 SS-HA Saha exhibited a cytotoxic activity. Further analysis is required, using a drug release test with these specific nanoparticles and using an in vivo model, in order to study the mechanism of cellular interaction and the delivery process to the tumor site.

4.3.4 Molecular mechanisms of SAHA drug effects in EC & Cell cycle arrest

SAHA is known to exhibit potent apoptotic and anti-proliferative effects in both types I and type II human endometrial cancers, modifying the expression of specific genes related to the insulin-like growth factor I (IGF-I) receptor signaling pathway (Yang et al. 2014). This synthetic hydrophobic moiety binds to histone deacetylase (HDAC) enzymes and inhibits deacetylation. Through subsequent histone hyperacetylation and the up-regulation of the cyclin-dependent kinase p21, Saha

inhibition can lead to altered cellular phenotypes. The mechanism of action of Saha drug was previously performed by the RBGO Group in Swansea in order to study the role of Saha in the regulation of endometrial cancer cell cycle progression and associated changes in cellular phenotype.

In this section, nanoparticles fabricated with Pluronic F127, in the presence or absence of SAHA, with or without HA conjugation, were added on an in vitro model of EC. Type I and Type II cells were cultured over a period of 48 hours. After this period of time, the efficacy of Saha nanoparticles significant decreased cellular viability. For normalization, GAPDH was used as a housekeeping protein and ImageLab software used to analyze band intensities obtained. Changes in band intensities of the antibody (E-Cadherin, N-Cadherin, P-21, and P53) were observed.

Figure 4.3.4a shows that in Hec50 cells there was not an expression of E-cadherin at the protein level because type II are aggressive, metastatic cells with a mesenchymal phenotype. They also present a p53 mutation, therefore in this experiment p53 was not detected by the antibody. Additionally, an increase in the levels of N-cadherin and p21 was observed after treatment with Free Saha F127 Saha nanoparticles (*Figure 4.3.4a*). If F127 empty nanoparticles are compared with the untreated control, no significant variation of protein levels of N-cadherin is observed ($p>0.5$). In Hec50 cell line, after treatment with F127 SS HA-Saha nanoparticles (1uM), it has been observed a significant increase in the levels of N-cadherin (Panel B) compared to the untreated control. p21 levels also significantly increased after F127 SS-HA Saha nanoparticles (1uM) treatment on Hec50 cells. Moreover, the maximum expression of the levels of p21 on these cells is given by F127 SS-HA Saha nanoparticles (2uM) treatment over 48 hours of treatment. Empty nanoparticles fabricate with the different polymers (F127, F127 SS and, F127 SS-HA), presented a similar behavior in the expression of the molecular level of N-cadherin and p21 on EC cell line (Type II).

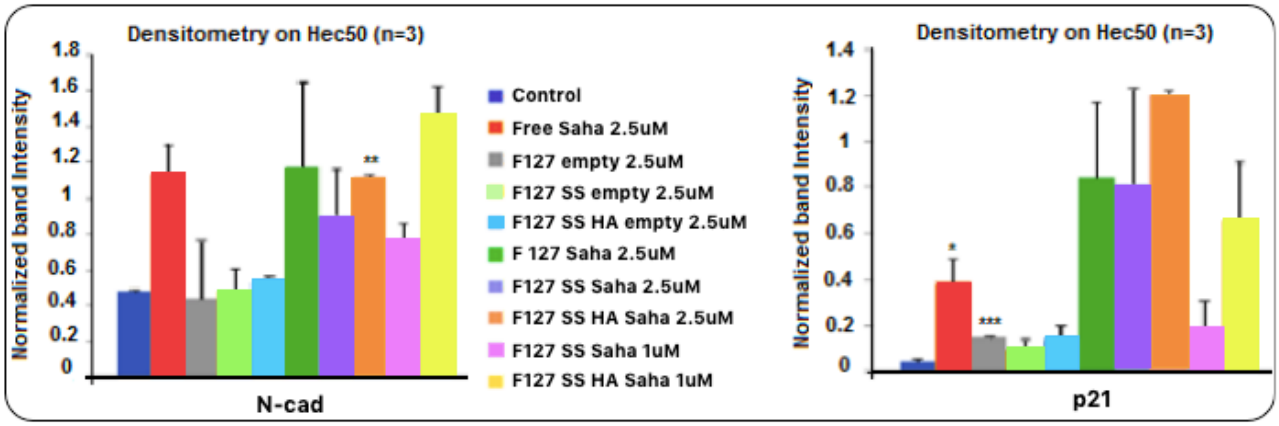

Figure 4.3.4a ***Effect of different NPs treatments on EC cell line (Type II) cycle progression and molecular phenotype.*** *Protein density of different treatments effects on cell cycle arrest markers p53 and p21 as well as molecular phenotype markers E and N cadherin was conducted on Hec50 cells. A minimum of three independent biological repeats was performed and the average and the standard deviation were calculated. A 2-tailed T-test was used for the pairwise comparisons. Previous analyses performed by RBGO Group in Swansea were compared to these results.*

Figure 4.3.4b shows that, in Ishikawa cells, after treatments with F127 Saha NPS (2.5uM), there is an increase in N-cadherin expression levels compared to the untreated control. F127 Saha NPS and free Saha determined a significant increase in the p21 levels. F127 SS-HA Saha nanoparticles determined high expression in N-cad on Ishikawa cell line after their treatment over a period of time of 48 hours. After F127 SS-HA Saha NPS (2.5uM), it was observed a significant increase in the p53 levels compared to the untreated control.

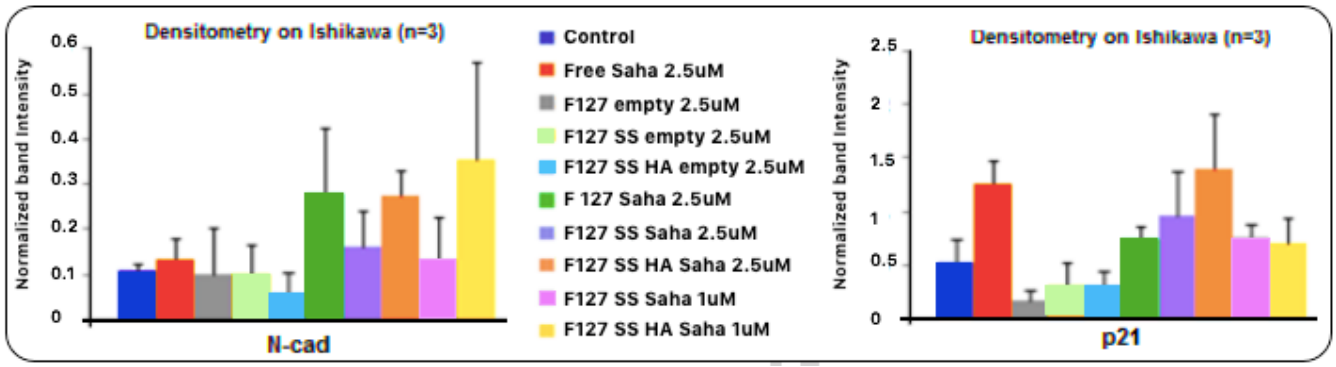

Fig.4.3.4b ***Effect of different NPS treatments on EC cell line (Type I) cycle progression and molecular phenotype****. Protein density of different treatments effects on cell cycle arrest markers p21 as well as molecular phenotype markers N-cadherin was conducted on Ishikawa cells. A minimum of three independent biological repeats was performed and the average and the standard deviation were calculated. A 2-tailed T-test was used for the pairwise comparisons. Previous analyses performed by RBGO Group in Swansea were compared to these results.*

Ishikawa cells (Type I EC), differently from Hec50 (TypeII EC), expressed E-cadherine at the protein level and p53 was detected by the antibody. Type II EC cells were in fact described as an aggressive, metastatic cell type with a mesenchymal phenotype.

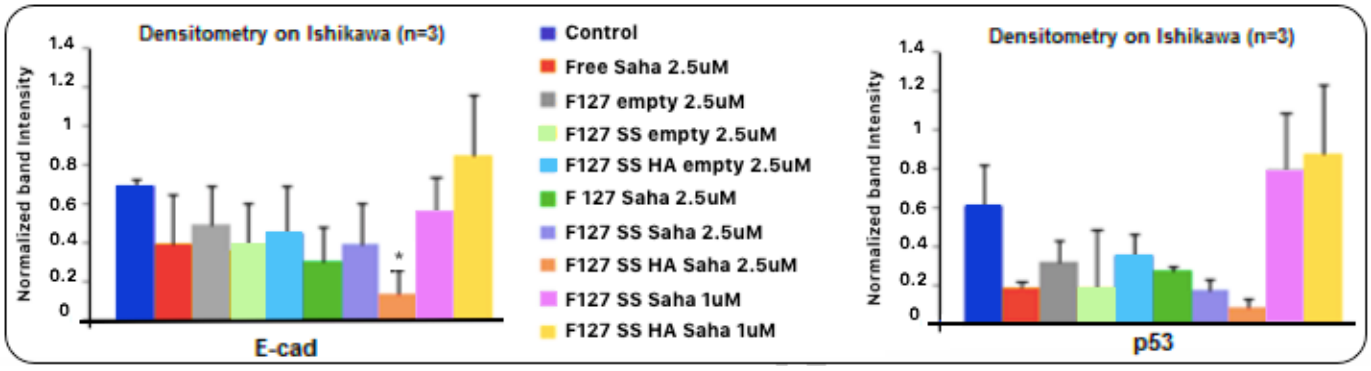

Figure 4.3.4c ***Effect of different NPS treatments on EC cell line (Type I) cycle progression and molecular phenotype****. Protein density of different treatments effects on cell cycle arrest markers p53 as well as molecular phenotype markers E-cadherin was conducted on Ishikawa cells. A minimum of three independent biological repeats was performed and the average and the standard deviation were calculated. A 2-tailed T-test was used for the pairwise comparisons. Previous analyses performed by RBGO Group in Swansea were compared to these results.*

Figure 4.3.4c shows that in Ishikawa cells the levels of E-cadherins and p53 decreased after treatments with free drug and with F127 Saha NPs over 48 hours. In contrast, a significant increase in E-cadherins and p53 levels were observed after treatments with F127 SS-HA Saha NPs (1uM). F127 SS-HA Saha nanoparticles determined the maximum expression in E-caderin and p53 on Ishikawa cell line after their treatment over a period of time of 48 hours. On the contrary, after F127 SS-HA Saha NPS (2.5uM), it was observed a significant decrease in the E-cadherin and p53 levels compared to the untreated control.

F127 Saha nanoparticles treatment and free drug treatment decreases significantly protein levels of E-cadherin in endometrial cancer cell lines, Ishikawa cells. As assumed by Uchida et al., cell migration could be induced by HDAC inhibitors in some adenocarcinoma cell lines. This could explain why Saha nanoparticles increased protein levels of N-cadherin and this could suggest a possible differentiation toward a mesenchymal phenotype.

The effect of this treatment was monitored at the protein level, using western blotting to characterize changes in protein expression linked to cellular characteristics important in cancer cell proliferation and differentiation. P21 and P53 are proteins that regulate the cell cycle and proliferation of cell and induce apoptosis (Muraki et al, 2009; Hajra & Fearon, 2012). E (epithelial) and N (mesenchymal) cadherin are two relevant markers for EMT, which is involved in cancer cell metastatic progression (Hajra & Fearon, 2012) and they are studied to determine the effect of epidrug SAHA on cell phenotype. Western blotting results were also compared with previous results of experiments performed by the RBGO Group in Swansea (Figure 4.3.4d).

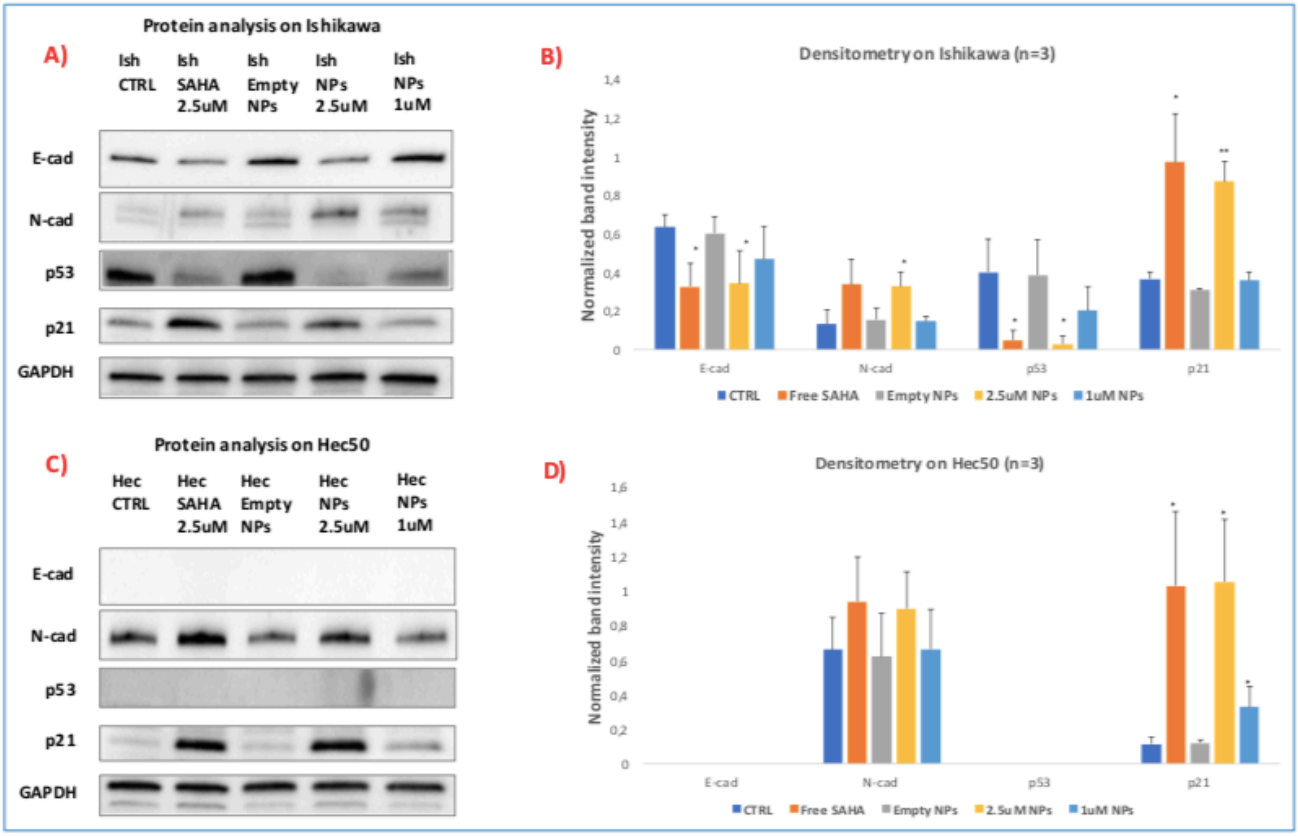

Fig.4.3.4d ***Effect of SAHA on EC cell line cell and molecular phenotype****. Protein analysis of SAHA effects on cell cycle arrest markers p53 and p21 as well as molecular phenotype markers E and N cadherin was conducted on Ishikawa (A) and Hec50 (C) cells, followed by protein density analysis (Panels B and D respectively). *All data shown is average and standard deviation, from a minimum of three independent biological repeats. Pairwise comparisons were done using a 2-tailed T test (RBGO Group, Swansea).*

Comparison with these RGBO results confirmed some data. First of all, Hec50 cells did not express E-cadherin and p53, differently from Ishikawa cells. On Hec50 cells, there were an increase of N-cadherin and p21 levels after treatment with free drug (Saha) and F127 Saha NPs (2.5uM) compared to the untreated control. Also on Ishikawa cells, an increase of N-cadherin and p21 levels ($p<0.05$) after these two treatments was observed. SAHA-NPs increased protein levels of N-cad suggesting a possible differentiation toward a mesenchymal phenotype. HDAC inhibitors could induce cell migration in some adenocarcinoma cell lines and this effect on cell migration and invasion is thought to depend on the type of targeted cells and/or HDACIs used (Uchida et al. 2007).

Moreover, on Type I cell lines, E-cadherin and p53 presented a decrease after free drug (Saha) and F127 Saha NPs (2.5uM) treatments, compared to the control. Saha treatment can affect the ration between E and N cadherin and the subsequent morphological differentiation of type I EC cell lines. There was no significant effect observed in the empty NP control, compared to the untreated control samples ($p>0.05$) and, once again, no meaningful variation was observed with empty NPs ($p>0.05$). Furthermore, on type II cells, no significant variation of protein levels of N-cad and p21 was observed when comparing empty NPs to the untreated control ($p>0.05$), and no significant increase ($p>0.05$) in the levels of N-cad was observed after treatment with free drug and SAHA-NPs. A significant increase in p21 levels for both the treatments occurred ($p<0.05$).

SAHA used in EC cancer cell line treatment increases protein levels of E-cad (Takai et al. 2004). These results differ slightly to what has previously been observed in the published literature, as experiments performed in this thesis project and by RBGO group, showed a significant decrease in Ishikawa cell E-cad levels, after treatment with both free drug and encapsulated nanoparticles.

5. CONCLUSIONS

Gynecological cancers can be traced with epigenetic drugs, one of them is suberoylanilide hydroxamic acid (SAHA), a histone deacetylase (HDAC) inhibitor which is already being used in the clinic. Targeting cancer specific epigenetic mechanisms, is the key to reverse the cancer cell phenotype as the epigenetic modifications occur during cancer differentiation are reversible, differently from genetic events. With this aim, have been approved 4 specific compounds that can be used in drug development programs for human cancers (TT et al. 2013).

The efficacy of SAHA for Type I and Type II EC cell models have been evaluated by RBGO researches in Swansea University. The drug encapsulation in order to improve the delivery represents an important issue in this research. Specific delivery vehicles have been studied thanks to nanomedicine approaches used for gynecological cancer treatment. Some of them include antibody conjugates (ACDs), nanoparticles as liposomes and polymeric particles that are useful for different treatment approaches (Kamaly et al. 2016). These nanomedicine systems have the role to avoid biological barriers achieving the target and reducing drug dose requirements (Howard et al. 2016).

In this thesis project, the epidrug SAHA was encapsulated in pluronic triblock-copolymers which has useful characteristic, bioavailability, and biodegradability (Khattak et al. 20015). NPs were also functionalized by adding hyaluronic acid (HA) to F127 Pluronic S-S pyridyl previously prepared by Swedish collaborators in Uppsala University research center. Nanoparticles were then characterized by size, shape, surface charge, encapsulation efficiency, stability and, release profile exhibiting properties compatible with their downstream application on biological studies. NPs showed a compatible behavior with the EPR effect as they size measured around 25nm and their negative charge favored the interaction mechanism with the cell membrane. NPs stability was gauged using propidium iodide (PI) dye, an example of a hydrophobic drug, which demonstrated that NPs have the capacity to penetrate the membrane cell and enter the nucleus. Additionally, the release profile showed that the maximum release occurs after 36 hours and there is a sustained release of the remaining drug for 3 days.

Real-Time Glo assay was used to proven non-toxicity of empty NPs at 1.25uM to 25uM concentration for EC cell lines. HA NPs can reduce toxicity by reducing off-target accumulation. F127 SS-HA Saha NPS at lower concentration (1.25uM) is less toxic, the drug encapsulated exploits a dose and time-dependent effect.

At molecular level occur specific mechanisms due to SAHA action influencing the expression ration of N and E cadherin on the cell cycle and cancer cell morphology. SAHA, after released from the NPs, demonstrated a molecule effect on Type I EC and Type II EC cells. In this contest, the encapsulation approach becomes a viable alternative to the free drug treatment in order to improve potentially delivery method through the EPR effect. In this work is demonstrated that HDAC inhibitor drug inhibits HDAC activity on one side, but on the other side increase p21 levels inducing a G1 phase arrest. Additionally, N-cad and E-cad levels are studied as they are involved in the epithelial-to-mesenchymal transition mechanism. RBGO group in a previous experiment have focused on combinatorial treatments modifying drug efficacy issues in gynecological cancers showing that DNA Methyl Transferase (DNMT) Inhibitor, 5-AzaC-D, with the HDAC inhibitor SAHA at different rates, significantly increased levels of p21 and E-cadherins, together with decreased levels of p53. Encapsulation efficiencies values, drug concentrations, drug release profile must always be considered as they explain important considerations for the EC phenotype effects. The natural evolution of this thesis will implicate the gene profile analysis of the mechanisms involved in SAHA’s action and the collaboration with other centers (Houston Methodist, Oommen laboratory in Uppsala) in order to proceed with *in vivo* assessment of the efficacy of these systems through murine models. The final goal is to use and translate this novel therapeutic approach to patient and increase the number of women lives suffering the endometrial cancer disease.

My experience was "Nano"

A flight from Venice to Bristol, a train through Cardiff and I arrived in Swansea. After a visit to the old castle in the city center, a nice and relaxing walk along Swansea beach I arrived in Malborough Road where I rented a room and where I could share a house with other students and a funny family.

I couldn't wait to start my practical training in the Centre of Nano Health (CNH) in the Institute of Life Science and I knew from inside of myself that something magical was happening...I was so excited!

"Hi, Veronica, nice to meet you! Would you like to get a coffee?"

From the first day, I met very nice people, helpful when I needed, a welcoming environment and, I learned that coffee makes the world go around:D I still want to thank them because they were able to make me feel like part of a big family. The Reproductive Biology and Gynaecological Oncology (RGBO) Research Group in Swansea; a multidisciplinary team focused on female infertility and gynecological cancers, translating fundamental research to patient benefit through novel diagnostic and therapeutic mechanisms, taught me a lot. They showed me how to share our ideas and opinions during all the science meeting, how to face a problem, how to study it in order to solve it. Good cooperation between resources and the union of biology, engineering, and chemistry are necessary to get the best results.

I had the possibility to get into the heart of the nanotechnology with a very interesting theme that it made me think and dream. The drug delivery field is a complex field, full of new concepts, many issues but offers new solutions to solve different diseases such as gynecological cancer. I think that Nanotechnology is the key to the future.

The term 'Nano' indicates the scale of the nanometers, things that are small enough…in the nanometer size range! But in reality 'Nano' for me is something not small, something interesting with useful properties. There is an infinitive new world in everything, a world made of determinant processes that could be the solution for difficult problems apparently impossible to solve.

I was lucky to discover and touch this Nanoworld. The human mind can do much for humanity and for mother earth, improving health every day.

My experience was simply 'Nano', was so big and amazing in every respect.

I brought home not only a professional experience but an opportunity for personal growth and meeting with new people from all over the world gave me understand and know other cultures. I won't forget that marvelous lunch where everybody brought the typical meal from the place of origin. It was one of the best cooking lessons of my life.

REFERENCES

Abdullah, A. N. Et al., 2011. Development of Disulfide Core-Crosslinked Pluronic Nanoparticles as an Effective Anticancer-Drug-Delivery System. Macromolecular Bioscience. https://doi.org/10.1002/mabi.201100083.

Abu-Lail, N.I. & Camesano, T.A., 2003. Polysaccharide properties probed with atomic force microscopy. Journal of Microscopy, 212(3), pp.217–238.

Ai, X. et al., 2014. Thin-film hydration preparation method and stability test of DOX- loaded disulfide-linked polyethylene glycol 5000-lysine-di-tocopherol succinate nanomicelles. Asian Journal of Pharmaceutical Sciences, 9(5), pp.244–250.

Albanese, A., Tang, P.S. & Chan, W.C.W., 2012. The Effect of Nanoparticle Size, Shape, and Surface Chemistry on Biological Systems. Annual Review of Biomedical Engineering, 14(1), pp.1–16.

Albitar, L. et al., 2007. Models representing type I and type II human endometrial cancers: Ishikawa H and Hec50co cells. Gynecologic oncology, 106(1), pp.52– 64.

Allis, C.D., Jenuwein, T., Reinberg, D., and Ca- parros, M.L., eds. (2007). Epigenetics (Cold Spring Harbor, NY: Cold Spring Harbor Labora- tory Press).

Amant, F., Moerman, P., Neven, P., Timmerman, D., Limbergen, E.V. & Vergute, I., (2005). Endometrial Cancer. Lancet Vol 366 pp 491-505

Antonisamy, J. D., Swain, J., & Dash, S. (2016). Study on binding and fluorescence energy transfer efficiency of Rhodamine B with Pluronic F127-gold nanohybrid using optical spectroscopy methods. SAA. https://doi.org/10.1016/j.saa.2016.09.002.

Asadollahi, R., Hyde, C.A.C. & Zhong, X.Y., 2010. Epigenetics of ovarian cancer: From the lab to the clinic. Gynecologic Oncology, 118(1), pp.81–87.

Azzopardi, E. A., 2016. Polymer therapeutics in surgery: the next frontier. Journal of Interdisciplinary Nanomedicine ISSN 2058-3273.

Basak, R., & Bandyopadhyay, R. (2013). Encapsulation of Hydrophobic Drugs in Pluronic F127 Micelles : E ff ects of Drug Hydrophobicity , Solution Temperature , and pH. https://doi.org/10.1021/la304836e.

Beral, B.E. et al. (2003). Breast cancer and hormone replacement therapy in the million women study. Lancet Vol 362 pp 419-427.

Binnig, G., Quate, C. & Gerber, C., 1986. Atomic Force Microscope. Physical Review Letters, 56(9), pp.930–933.

Blanco, E., Shen, H. & Ferrari, M., 2015. Principles of nanoparticle design for overcoming biological barriers to drug delivery. Nature biotechnology, 33(9), pp.941–951.

Body, N., De Kerdaniel, O., Lavoué, V., Leblanc, M., Henno, S., & Levêque, J. (2016). Cancer de l'endomètre au stade précoce: ganglion sentinelle ou curage pelvien Gynecologie Obstetrique et Fertilite, 44(4), 239–243. https://doi.org/10.1016/S0140-6736(15)00130-0.

Boehme, K., Simon, S. & Mueller, S.O., 2009. Gene expression profiling in Ishikawa cells: a fingerprint for estrogen active compounds. Toxicology and applied pharmacology, 236(1), pp.85–96.

Bokhman, J. V., 1983. Two pathogenetic types of endometrial carcinoma. Gynecologic Oncology, 15(1), pp.10–17.

Booth, F.W., Robert, C.K. Laye, M.J. (2012). Lack of Exercise is a Major Cause of Chronic Diseases, Comprehensive Physiology. Vol 2, pp 1143-1211

Boury, E, Marchais, H., Proust, J. E., and Benoit, J. P., Bovine serum albumin release from poly(alpha-hydroxy acid) microspheres: effects of polymer molecular weight and surface properties. J. Controlled Release, 45, 75-86 (1997).

Brinton LA, Felix AS, McMeekin DS, et al. Etiologic heterogeneity in endometrial cancer: evidence from a Gynecologic Oncology Group trial. Gynecol Oncol 2013; 129: 277–84.

Brown, T.A., 2002. Genomes. In Genomes.

Cabral, H. et al., 2011. Accumulation of sub-100 nm polymeric micelles in poorly permeable tumours depends on size. Nature Nanotechnology, 6(12), pp.815– 823. Available at: http://dx.doi.org/10.1038/nnano.2011.166.

Canale, C., Relini, A., & Gliozzi, A. (n.d.). Chapter 6 Atomic Force Microscopy of Ex Vivo Amyloid Fibrils, 736, 81–95. https://doi.org/10.1007/978-1-61779-105-5.

Cancer Research UK. Uterine cancer statistics. http://info. cancerresearchuk.org/cancerstats/types/uterus/ (accessed Jan 23, 2014).

Chen, M.Y. et al., 2011. Decitabine and suberoylanilide hydroxamic acid (SAHA) inhibit growth of ovarian cancer cell lines and xenografts while inducing expression of imprinted tumor suppressor genes, apoptosis, G2/M arrest, and autophagy. Cancer, 117(19), pp.4424–4438.

Chen, L., Zang, F., Wu, H., Li, J., Xie, J., & Ma, M. (2018). Nanoscale Using PEGylated magnetic nanoparticles to describe the EPR e ff ect in tumor for predicting therapeutic e ffi cacy of micelle drugs †. https://doi.org/10.1039/c7nr08319j.

Chicklore S, Gnanasegaran G, Vijayanathan S, Fogelman I. Potential role of multislice SPECT/CT in impingement syndrome and soft-tissue pathology of the ankle and foot. Nucl Med Commun 2013; 34: 130–39.

Cho, E. J., Holback, H., Liu, K. C., Abouelmagd, S. A., Park, J., & Yeo, Y. (2013). Nanoparticle Characterization : State of the Art , Challenges , and Emerging Technologies. https://doi.org/10.1021/mp300697h.

Clark, L.H. et al., 2016. Adjuvant treatment and clinical trials in elderly patients with endometrial cancer: a time for change? Int. J. Cancer 26 (2016) 282-289.

Clinic, M. 2018. Endometrial cancer Risk factors, 1–3.

Collier, M. A., Bachelder, E. M., & Ainslie, K. M. (2017). Electrosprayed Myocet-like Liposomes : An Alternative to Traditional Liposome Production. Pharmaceutical Research, 419–426. https://doi.org/10.1007/s11095-016-2072-4.

Colombo, N. Et al., 2016. ESMO-ESGO-ESTRO consensus conference on endometrial cancer: diagnosis, treatment and follow-up, Ann. Once. 27 (2016) 16-41.

Consortium, I.H.G.S., 2001. Initial sequencing and analysis of the human genome. Nature, 409(6822), pp.860–921.

Cramer, S. a, Adjei, I.M. & Labhasetwar, V., 2015. Advancements in the delivery of epigenetic drugs. Expert opinion on drug delivery, 5247(April), pp.1–12.

Croxtall, J.D., Elder, M.G. & White, J.O., 1990. Hormonal control of proliferation in the Ishikawa endometrial adenocarcinoma cell line. Journal of steroid biochemistry, 35(6), pp.665–9.

Taylor, S.M. & Jones, P.A., 1979. Multiple new phenotypes induced in 10T 1 2 and 3T3 cells treated with 5-azacytidine. Cell, 17(4), pp.771–779.

Cust, A.E. et al., 2007. Metabolic syndrome, plasma lipid, lipoprotein and glucose levels, and endometrial cancer risk in the European Prospective Investigation into Cancer and Nutrition (EPIC). Endocrine-Related Cancer, 14(3), 755–767. https://doi.org/10.1677/ERC-07-0132.

Davies, S. et al., 2004. Identification of a novel mechanism of NF-kappaB inactivation by progesterone through progesterone receptors in Hec50co poorly differentiated endometrial cancer cells: induction of A20 and ABIN-2. Gynecologic oncology, 94(2), pp.463–70.

Decuzzi, P. et al., 2009. Intravascular delivery of particulate systems: Does geometry really matter. Pharmaceutical Research, 26(1), pp.235–243.

Dupont, C., Armant, D.R. & Brenner, C.A., 2009. Epigenetics: Definition, Mechanisms and Clinical Perspective Cathérine. Seminars in Reproductive Medicine, 27(5), pp.351–357.

Egger, G. et al., 2004. Epigenetics in human disease and prospects for epigenetic therapy. Nature, 429(6990), pp.457–63. Available at: http://www.ncbi.nlm.nih.gov/pubmed/15164071.

Fader, A. N., Arriba, L. N., Frasure, H. E., & Gruenigen, V. E. Von. (2009). Gynecologic Oncology Endometrial cancer and obesity : Epidemiology , biomarkers , prevention and survivorship. Gynecologic Oncology, 114(1), 121–127. https://doi.org/10.1016/j.ygyno.2009.03.039.

Falco, D., Matematica, D., Milano, P., Bonardi, V., Taffetani, M., Falco, C. De, ... Ambrosi, D. (2015). Biomechanical modelling in nanomedicine : multiscale approaches and future challenges Biomechanical modelling in nanomedicine : multiscale approaches and future challenges, (15).

Farace, C. et al., 2016. Immune cell impact of three differently coated lipid nanocapsules : pluronic , chitosan and polyethylene glycol. Nature Publishing Group, pp.1–14. Available at: http:// dx.doi.org/10.1038/srep18423.

Febbraro, T., Lengyel, E. & Romero, I.L., 2014. Old drug, new trick: Repurposing metformin for gynecologic cancers? Gynecologic Oncology, 135(3), pp.614–621.

Ferlay, J. et al., 2015. Cancer incidence and mortality worldwide : Sources , methods and major patterns in GLOBOCAN 2012, 386. https://doi.org/10.1002/ijc.29210.

Ferrari, M. (2005). Cancer nanotechnology: opportunities and challenges, 5(March). https:// doi.org/10.1038/nrc1566.

Fisher, R., Pusztai, L. & Swanton, C., 2013. Cancer heterogeneity: implications for targeted therapeutics. British journal of cancer, 108(3), pp.479–85.

Fukuchi, T. et al., 1998. Catenin mutation in carcinoma of the uterine endometrium. Cancer Research, 58(16), pp.3526–3528.

Gajjar et al., 2012. Symptoms and Risk Factors ofOvarian Cancer: A Surveyin Primary Care Ketan. International Scholarly Research Network. doi:10.5402/2012/754197.

Gan, Y., 2009. Atomic and subnanometer resolution in ambient conditions by atomic force microscopy. Surface Science Reports, 64(3), pp.99–121.

Gélinas, V. & Vidal, D., 2010. Determination of particle shape distribution of clay using an automated AFM image analysis method. Powder Technology, 203(2), pp.254–264.

Goldgerg, A.D., Allis, C.D., & Bernstein, E. (2007). Essay Epigenetics: A Landscape Takes Shape, 635-638. Https://doi.org/10.1016/j.cell.2007.02.006.

Gründker, C., Günthert, A.R. & Emons, G., 2008. Hormonal heterogeneity of endometrial cancer. Advances in Experimental Medicine and Biology, 630, pp.166–188.

Hajra, K.M. & Fearon, E.R. (2002). Cadherin and catenin alterations in human cancer. Genes Chromosomes Cancer. Vol 34pp 255-268

Hansma, P. et al., 1989. The scanning ion-conductance microscope. Science, 243(4891), pp.641–643.

He, C. et al., 2010. Effects of particle size and surface charge on cellular uptake and biodistribution of polymeric nanoparticles. Biomaterials, 31(13), pp.3657–3666.

Heneweer, C. et al., 2005. Molecular mechanisms in uterine epithelium during trophoblast binding: the role of small GTPase RhoA in human uterine Ishikawa cells. Journal of experimental & clinical assisted reproduction, 2(1), p.4.

Hill, E.K. & Dizon, D.S., 2012. Medical therapy of endometrial cancer: Current status and promising novel treatments. Drugs, 72(5), pp.705–713.

Horcas, I. et al., 2007. WSXM: A software for scanning probe microscopy and a tool for nanotechnology. Review of Scientific Instruments, 78(1).

Howard, D. Et al., 2016. Antibody – drug conjugates and other nanomedicines : the frontier of gynaecological cancer treatment.

Howlader, N., et al. 2011. SEER cancer statistics review, 1975–2008, [http://seer.cancer.gov/csr/1975_2008/, National Cancer Institute, Bethesda, MD.

Huang, X. & Brazel, C.S., 2001. On the importance and mechanism of burst release in matrix controlled drug delivery systems. Journal of Controlled Release, 73, pp.121–136.

Hu Q et al., 2012. 5-aza-2'-deoxycytidine improves the sensitivity of endometrial cancer cells to progesterone therapy. Int J Gynecol Cancer.

Hua, S. (2014). Comparison of in vitro dialysis release methods of loperamide-encapsulated liposomal gel for topical drug delivery, 735–744.

Jain, A. K., Singh, D., Dubey, K., & Maurya, R. (2018). Models and Methods for In Vitro Toxicity. In Vitro Toxicology. Elsevier Inc. https://doi.org/10.1016/B978-0-12-804667-8.00003-1.

Jemal, A. et al., 2011, "Global cancer statistics", CA: a cancer journal for clinicians, vol. 61, no. 2, pp. 69-90.

Jiang, W. et al., 2008. Nanoparticle-mediated cellular response is size-dependent. Nature nanotechnology, 3(3), pp.145–50. Available at: http://www.ncbi.nlm.nih.gov/pubmed/18654486.

Jokerst, J. V et al., 2011. Nanoparticle PEGylation for imaging and therapy. Nanomedicine (London, England), 6(4), pp.715–728.

Kamaly, N. et al., 2016. Degradable Controlled-Release Polymers and Polymeric Nanoparticles: Mechanisms of Controlling Drug Release. Chemical Reviews, 116(4), pp.2602–2663.

Khattak, S.F., Bhatia, S.R. & Roberts, S.C., 2005. Pluronic F127 as a cell encapsulation material: utilization of membrane-stabilizing agents. Tissue Eng., 11(5–6), pp.974–83.

Kassan, S., Mechanick, J.I. & Gurpide, E., 1989. Altered estrogen receptor system in estrogen-unresponsive human endometrial adenocarcinoma cells. Journal of steroid biochemistry, 33(3), pp. 327–33.

Kim E. Sapsford, W. Russ Algar, L.B., 2013. Functionalizing Nanoparticles with Biological Molecules: Developing Chemistries that Facilitate Nanotechnology. American Chemical Society, 113(3), p.1904−2074.

Kumar, B., Jalodia, K., Kumar, P., & Gautam, H. K. (2017). Recent advances in nanoparticle-mediated drug delivery. Journal of Drug Delivery Science and Technology, 41, 260–268. https://doi.org/10.1016/j.jddst.2017.07.019.

Kwon, M.J. & Shin, Y.K., 2011. Epigenetic regulation of cancer-associated genes in ovarian cancer. International Journal of Molecular Sciences, 12(2), pp.983–1008.

Lackner, M.R., Wilson, T.R. & Settleman, J., 2012. Mechanisms of acquired resistance to targeted cancer therapies. Future Oncology, pp.999–1014.

Li, Y., Luca, R. De, Cazzamalli, S., Pretto, F., Bajic, D., Scheuermann, J., & Neri, D. (2018). display of multiple chemical elements on a, 10(April).

Liu, L. et al., 2012. Bioconjugated pluronic triblock-copolymer micelle-encapsulated quantum dots for targeted imaging of cancer: In vitro and in vivo studies. Theranostics, 2(7), pp.705–713.

Malvern instruments, 2004. Zetasizer Nano Series User Manual. Department of Biochemistry Biophysics Facility , University of Chambridge, (2), p.207.

Michail, G. D., & Michail, G. D. (2015). International Journal of Clinical Therapeutics and Diagnosis (IJCTD) ISSN 2332-2926 Endometrial Cancer - Diagnosis Endometrial Cancer In Peri & Postmenopausal, 17–27.

Moghimipour, E. & Handali, S., 2012. Utilization of thin film method for preparation of celecoxib loaded liposomes. Advanced Pharmaceutical Bulletin, 2(1), pp.93–98.

Mohamed, E. A., Zhao, Y., Meshali, M. M., Remsberg, C. M., Borg, M., Foda, A. M. M., Ave, C. (2016). HHS Public Access, 101(10), 3787–3798. https://doi.org/10.1002/jps.23265.Vorinostat.

Möller, C. et al., 1999. Tapping-mode atomic force microscopy produces faithful high- resolution images of protein surfaces. Biophysical journal, 77(August), pp.1150– 1158.

Morice, P. et al., 2015. Endometrial cancer. The Lancet, 6736(15), pp.1–15. Available at: http://dx.doi.org/10.1016/S0140-6736(15)00130-0.

Murali, R., Soslow, R. A., & Weigelt, B. (2014). Classifi cation of endometrial carcinoma : more than two types. Lancet Oncology, 15(7), e268–e278. https://doi.org/10.1016/S1470-2045(13)70591-6.

Muraki, Y. et al., 2009. Epigenetic DNA hypermethylation: Clinical applications in endometrial cancer. Oncology Reports, 22(5), pp.967–972.

Mutter, G.L. et al., 1999. K-ras mutations appear in the premalignant phase of both microsatellite stable and unstable endometrial carcinogenesis. Molecular pathology : MP, 52(5), pp.257–62.

Negmeldin, A. T., & Pflum, M. K. H. (2017). Bioorganic & Medicinal Chemistry Letters The structural requirements of histone deacetylase inhibitors : SAHA analogs modified at the C5 position display dual HDAC6 / 8 selectivity. Bioorganic & Medicinal Chemistry Letters, 27(15), 3254–3258. https://doi.org/10.1016/j.bmcl.2017.06.033.

Neumeyer, A., Bukowski, M., Veith, M., Lehr, C., & Daum, N. (2011). Propidium iodide labeling of nanoparticles as a novel tool for the quantification of cellular binding and uptake. Nanomedicine: Nanotechnology, Biology, and Medicine, 7(4), 410–419. https://doi.org/10.1016/j.nano.2010.12.007.

Nishida M, Kasahara K, Kaneko M, Iwasaki H, H.K. & Zasshi, N.S.F.G., 1985. Establishment of a new human endometrial adenocarcinoma cell line, Ishikawa cells, containing estrogen and progesterone receptors. Nihon Sanka Fujinka Gakkai Zasshi., 37(7)(Jul), pp.1103–11.

Nogami, Y. et al., 2013. Current status of molecular-targeted drugs for endometrial cancer (Review). Molecular and clinical oncology, 1(5), pp.799–804.

Oh, N. & Park, J.H., 2014. Endocytosis and exocytosis of nanoparticles in mammalian cells. International Journal of Nanomedicine, 9(SUPPL.1), pp.51–63.

Ong, Q. K., & Sokolov, I. (2007). Attachment of nanoparticles to the AFM tips for direct measurements of interaction between a single nanoparticle and surfaces, 310, 385–390. https://doi.org/10.1016/j.jcis.2007.02.010.

Perry, C. et al., 2007. Iron oxide nanoparticles as drug delivery agents in MIA PaCa-2 pancreatic cells. Proceedings of SPIE, 6441, p.64411T–64411T–9. Available at: https://proceedings.spiedigitallibrary.org/proceeding.aspx?doi=10.1117/12.70175 4.

Pitto-barry, A., Barry, N. P. E., & Barry, N. P. E. (2014). and clinical advances, 5(10). https://doi.org/10.1039/c4py00039k.

Ponta H, Sherman L, Herrlich PA. CD44: from adhesion molecules to signalling regulators. Nat Rev Mol Cell Biol 2003;4:33–45.

Prabhu, R., Patravale, V. & Joshi, M., 2015. Polymeric nanoparticles for targeted treatment in oncology: current insights. Intern Journ of Nanomed, 10, pp.1001– 1018.

Prince HM, Dickinson M. Romidepsin for cutaneous T-cell lymphoma. Clin Cancer Res. 2012;18:3509–3515.

Ramirez, P.T. et al., 2004. Hormonal therapy for the management of grade 1 endometrial adenocarcinoma: A literature review. Gynecologic Oncology, 95(1), pp.133–138.

Rauh-Hain, J.A. et al., 2015. Management for elderly women with advanced-stage, High-Grade Endometrial Cancer, Obstet. Gynecol. 126 (2015) 1198-1206.

Reading, A., & Chapter, T. (2015). Chapter 5. https://doi.org/10.1016/B978-0-12-800511-8.00005-8

Ray, A., & Mitra, A. K. (2017). Nanotechnology in Intracellular Traf fi cking , Imaging , and Delivery of Therapeutic Agents. Emerging Nanotechnologies for Diagnostics, Drug Delivery, and Medical Devices. Elsevier. https://doi.org/10.1016/B978-0-323-42978-8.00008-5.

Riehemann, K. et al., 2014. Nanomedicine – challenge and perspectives. NIH Public Access, 48(5), 872–897. https://doi.org/10.1002/anie.200802585.Nanomedicine.

Risinger, J.I. et al., 1997. PTEN/MMAC1 mutations in endometrial cancers. Cancer Research, 57(21), pp.4736–4738.

Robertson, J. D., Rizzello, L., Avi, M., & Gaitzsch, J. (2016). Purification of Nanoparticles by Size and Shape, 1–9. https://doi.org/10.1038/srep27494

Ross, S.J., 2001. Decreased CD44 Standard Form Expression Correlates With Prognostic Variables in Ovarian Carcinomas. American Society of Clinical Pathologists. Am J Clin Pathol 2001;116:122-128.

Salman MC, Bozdag G, Dogan S, Yuce K (2013) Role of postmenopausal bleeding pattern and women's age in the prediction of endometrial cancer. Aust N Z J Obstet Gynaecol 53(5): 484-8.

San-miguel, F., Richardson, P. G., Laubach, J. P., & Moreau, P. (2015). Panobinostat for the Treatment of Multiple Myeloma, 4767–4774. https://doi.org/10.1158/1078-0432.CCR-15-0530.

Sarfstein, R. et al., 2011a. The mechanism of action of the histone deacetylase inhibitor vorinostat involves interaction with the insulin-like growth factor signaling pathway. PLoS ONE, 6(9), pp.1–12.

Scalf, J., et al. 2006. Part I: Introduction to Nanoparticle Characterization with AFM. Pacific Nanotechnology, Inc.

Sezgin, Z., Yüksel, N., & Baykara, T. (2006). Preparation and characterization of polymeric micelles for solubilization of poorly soluble anticancer drugs. European Journal of Pharmaceutics and Biopharmaceutics, 64(3), 261–268. https://doi.org/10.1016/j.ejpb.2006.06.003.

Sorosky, J.I., 2012. Endometrial Cancer, 120(2), 383–397. https://doi.org/10.1097/AOG.0b013e3182605bf1.

Strahl, B.D. & Allis, C.D., 2000. The language of covalent histone modifications. Nature, 403(6765), pp.41–45.

Subtypes, H., 2012. Molecular characterization of kidney cancer: association of hyaluronic acid family with histological subtypes and metastasis cancer. 2012 May 1; 118(9): 2394–2402. doi: 10.1002/cncr.26520.

Sundar, S., Kundu, J. & Kundu, S.C., 2010. Biopolymeric nanoparticles. Science and Technology of Advanced Materials, 11(1), p.14104.

Szoka, F. (1978). Procedure for preparation of liposomes with large internal aqueous space and high capture by reverse-phase evaporation Biochemistry :, 75(9), 4194–4198.

Takai, N. & Narahara, H. (2009). Histone Deacetylase Inhibitor Therapy in Epithelial Ovarian Cancer. Journal of Oncology. Vol 2010 pp 1-6.

Taylor, S.M. & Jones, P.A., 1979. Multiple new phenotypes induced in 10T 1 2 and 3T3 cells treated with 5-azacytidine. Cell, 17(4), pp.771–779.

Tempferl, C., Haeusler, G., Kaider, A., Hefler, L., Hanzal, E., Reinthaller, A., ... Kainz, C. (1998). The prognostic value of CD44 isoform expression in endometrial cancer, 77, 1137–1139.

Torchilin, V., 2011. Tumor delivery of macromolecular drugs based on the EPR effect. Advanced Drug Delivery Reviews, 63(3), pp.131–135. Available at: http://dx.doi.org/10.1016/j.addr.2010.03.011.

Truong, P.T. et al., 2005. The effects ofage and comorbidity on treatment and outcomes in womenwith endome- trial cancer, Am. J. Clin. Oncol. 28 (2005) 157–164).

TT, Y. et al., 2013. 5-Aza-2'-deoxycytidine may influence the proliferation and apoptosis of cervical cancer cells via demethylation in a dose- and time-dependent manner. Genetic Molecular Research.

Uchida, H. et al. (2007). Histone deacetylase inhibitors stimulate cell migration in human endometrial adenocarcinoma cells through up-regulation of glycodelin. Endocrinology. Vol 148 pp 896-902.

Ven, A. L. Van De, Mack, A., Jr, K. D., Ferrari, M., & Serda, R. E. (2012). Cellular Associations of Silicon Logic-Embedded Vectors. Nanomedicine: Cancer, Diabetes, and Cardiovascular, Central

Nervous System, Pulmonary and Inflammatory Diseases (1st ed., Vol. 508). Elsevier Inc. https://doi.org/10.1016/B978-0-12-391860-4.00001-X.

Verma, A. & Stellacci, F., 2010. Effect of surface properties on nanoparticle-cell interactions. 6(1), pp.12–21.

Weichert, W. et al., 2008. Expression of class I histone deacetylases indicates poor prognosis in endometrioid subtypes of ovarian and endometrial carcinomas. Neoplasia (New York, N.Y.), 10(9), pp.1021–7.

Wojciechowski, M. et al., 2014. CD44 expression in curettage and postoperative specimens of endometrial cancer. Archives of Gynecology and Obstetrics, pp.383–390.

Xiong, X.Y., Tam, K.C. & Gan, L.H., 2005. Release kinetics of hydrophobic and hydrophilic model drugs from pluronic F127/poly(lactic acid) nanoparticles. Journal of Controlled Release, 103(1), pp.73–82.

Yeo, Y. & Park, K., 2004. Control of encapsulation efficiency and initial burst in polymeric microparticle systems. Archives of pharmacal research, 27(1), pp.1– 12.

Yoo, C.B., and Jones, P.A. (2006). Nat. Rev. Drug Discov. 5, 37–50.

Silva, S., Almeida, J., & Vale, N. 2019. Combination of Cell-Penetrating Peptides with Nanoparticles for Therapeutic Application : A Review. https://doi.org/10.3390/biom9010022.

Zhang, W. et al., 2011. Multifunctional Pluronic P123/F127 mixed polymeric micelles loaded with paclitaxel for the treatment of multidrug resistant tumors. Biomaterials, 32(11), pp.2894–2906.

Zhang, X., Jackson, J.K. & Burt, H.M., 1996. Development of amphiphilic diblock copolymers as micellar carriers of taxol. International Journal of Pharmaceutics, 132(1–2), pp.195–206.

Zhao, L. et al., 2012. Curcumin loaded mixed micelles composed of Pluronic P123 and F68: Preparation, optimization and in vitro characterization. Colloids and Surfaces B: Biointerfaces, 97, pp.101–108. Available at: http://dx.doi.org/10.1016/j.colsurfb.2012.04.017.

Zununi, S., Salehi, R., Davaran, S., & Shari, S. (2017). Liposome-based drug co-delivery systems in cancer cells, 71, 1327–1341. https://doi.org/10.1016/j.msec.2016.11.073.

ACKNOWLEDGMENTS

This thesis is dedicated to all the women who every year are fighting a gynecological tumor and to all the people who suffer from any tumor or rare disease. My thoughts turn to them, with the hope of improving their living conditions, thanks to the great power of research. Evil can be defeated, but love, faith, and force of fighting with the tools that science puts at its disposal must not be lacking. My thoughts go to all the people who work in Research with passion and perseverance and who have the great opportunity to help those who suffer.

My thesis and all my studies go to all the people who love me and believe in me.

I thank all my teachers because each of them taught me something special, I thank Ca'Foscari and the University of Verona for all the laboratories and the Master Degree in Science and Technology of Bio and Nanomaterials that showed me a new and infinite world. I thank Professor Giuseppe Pezzotti for giving me the opportunity to deepen my studies at the Kyoto Institute of Technologies. I thank Swansea, the department of life sciences where I did my thesis because thanks to this experience I grew up more by learning to solve various problems. I thank my esteemed Professor Patrizia Canton, I thank the great Professor Mauro Ferrari for introducing me to the world of Nanomedicine, I thank the great Professor Steve Conlan for giving me the opportunity to get my degree project at Swansea University, I thank my supervisor Lewis Francis for supporting me and helping me along this path, I thank the post-doc Seydou Yao for his assistance during my experiments, Simone Pisano , David Howard and Andrea Gazze for their advices and all the fantastic staff that constitutes RBGO.

I thank my whole family, starting from the grandkids: Mattia, Chiara, Noemi, Gioele, Elisa and the little creature which will arrive, I thank my brothers: Ismaele, Mosè, Matteo, Damiana, and their families. I thank "Fratelli Feltracco" Company which is a strong example of passion and dedication to the work.
I thank my boyfriend Javier Ivan who has always encouraged me and loving me for my strengths and weaknesses. A truly infinite thank goes to my mother and my father who have taught me seriousness and duty before anything else, and never give up and grit the teeth especially when life makes in front of you difficult things to solve.

Finally, I thank God for all that I have received and for all the challenges that I believe that nothing comes by chance and that each of us has a mission in life, mine has just begun.

Veronica

RINGRAZIAMENTI

Questa tesi è dedicata a tutte le donne che ogni anno combattono un tumore ginecologico e a tutte le persone che soffrono di tumori o malattie rare. Il mio pensiero si rivolge a loro, con la speranza di migliorare le loro condizioni di vita, grazie al grande potere della Ricerca. Il male può essere sconfitto, ma non devono mai mancare l'amore, la fede e la forza di combattere sfruttando gli strumenti che la scienza mette a sua disposizione. Il mio pensiero va anche verso tutte le persone che lavorano nella Ricerca con passione e perseveranza e che hanno la grande opportunità di aiutare chi soffre.

Dedico la mia tesi e tutti i miei studi a tutte le persone che mi amano e credono in me.

Ringrazio tutti i miei insegnanti perché ognuno di loro mi ha insegnato qualcosa di speciale, ringrazio Ca'Foscari e l'Università di Verona per tutti i laboratori e il Corso di Laurea in Scienze e Tecnologie di Bio e Nanomateriali che mi ha aperto ad un nuovo ed infinito mondo. Ringrazio il professor Giuseppe Pezzotti per avermi dato la possibilità di approfondire i miei studi presso l'Instituto di tecnologie di Kyoto. Ringrazio Swansea, il dipartimento di scienze della vita dove ho svolto la mia tesi perché grazie a questa esperienza ho potuto crescere di più imparando a risolvere vari problemi. Ringrazio la mia stimata professoressa Patrizia Canton come relatrice interna, ringrazio il grande professor Mauro Ferrari per avermi introdotto al mondo della Nanomedicina e avermi invitato a Nanogagliato, ringrazio il grande Professor Steve Conlan per avermi dato l'opportunità di conseguire il mio progetto di laurea presso l'Università di Swansea, ringrazio il mio supervisore Lewis Francis per avermi supportato e per avermi aiutato in questo percorso, ringrazio il post-doc Seydou Yao per la sua continua assistenza durante i miei esperimenti e Simone Pisano e David Howard per i loro consigli e tutto lo staff fantastico che costituisce il gruppo di ricerca RBGO di Swansea.
Ringrazio tutta la mia famiglia, a partire dai nipotini: Mattia, Chiara, Noemi, Gioele, Elisa e la piccola creatura che sta per arrivare, i miei fratelli: Ismaele, Mosè, Matteo, Damiana e le loro famiglie. Ringrazio la ditta Fratelli Feltracco che è stata per me un forte esempio di passione e dedizione al lavoro e il mio ragazzo Javier Ivan che mi ha sempre incoraggiato. Ringrazio mia zia Lina che ora non c'è più, ma che sempre rimarrà nel mio cuore.
Un ringraziamento davvero infinito va a chi mi ha dato la vita e mi ha insegnato a vivere, a mia madre e a mio padre perché mi hanno insegnato che la serietà e il dovere vengono prima di ogni altra cosa e a stringere i denti quando la vita ti mette davanti difficile sfide da risolvere.

Infine, ringrazio Dio per tutto ciò che ho ricevuto dalla Vita. Credo che nulla accada per caso e che ognuno di noi abbia una missione nella vita, la mia è appena iniziata.

Veronica

“Real is rare
but brings your Heart everywhere”